

**UNIVERSIDADE FEDERAL DE SANTA CATARINA  
PROGRAMA DE PÓS-GRADUAÇÃO EM  
ENGENHARIA MECÂNICA**

Amir Roberto De Toni Júnior

**EXPERIMENTAL AND CHEMICAL KINETICS  
MODELING INVESTIGATION OF AUTOIGNITION  
OF JET FUEL AND SURROGATES**

Florianópolis

2017



**UNIVERSIDADE FEDERAL DE SANTA CATARINA  
PROGRAMA DE PÓS-GRADUAÇÃO EM  
ENGENHARIA MECÂNICA**

Amir Roberto De Toni Júnior

**EXPERIMENTAL AND CHEMICAL KINETICS  
MODELING INVESTIGATION OF AUTOIGNITION  
OF JET FUEL AND SURROGATES**

Tese submetida ao Programa de Pós-Graduação em Engenharia Mecânica da Universidade Federal de Santa Catarina para a obtenção do grau de Doutor em Engenharia Mecânica.

Orientador: Prof. Amir Antônio Martins de Oliveira Jr. Ph.D.

Coorientador: Prof. Leonel Rincón Cancino, Dr.

Florianópolis

2017

Ficha de identificação da obra elaborada pelo autor,  
através do Programa de Geração Automática da Biblioteca Universitária da UFSC.

De Toni Júnior, Amir Roberto  
Experimental and chemical kinetics modeling  
investigation of autoignition of jet fuel and  
surrogates / Amir Roberto De Toni Júnior ;  
orientador, Amir Antônio Martins de Oliveira Júnior,  
coorientador, Leonel Rincón Cancino, 2017.  
170 p.

Tese (doutorado) - Universidade Federal de Santa  
Catarina, Centro Tecnológico, Programa de Pós  
Graduação em Engenharia Mecânica, Florianópolis, 2017.

Inclui referências.

1. Engenharia Mecânica. 2. Combustível  
aeronáutico. 3. Cinética química detalhada. 4.  
Misturas substitutas. 5. Atraso de ignição. I.  
Oliveira Júnior, Amir Antônio Martins de. II.  
Cancino, Leonel Rincón. III. Universidade Federal de  
Santa Catarina. Programa de Pós-Graduação em  
Engenharia Mecânica. IV. Título.

Amir Roberto De Toni Júnior

**EXPERIMENTAL AND CHEMICAL KINETICS  
MODELING INVESTIGATION OF AUTOIGNITION  
OF JET FUEL AND SURROGATES**

Esta Tese foi julgada adequada para obtenção do Título de Doutor em Engenharia Mecânica e aprovada em sua forma final pelo Programa de Pós-Graduação em Engenharia Mecânica da Universidade Federal de Santa Catarina.

Florianópolis, 14 de julho de 2017.

---

Prof. Jonny Carlos da Silva, Dr.  
Coordenador do Programa de Pós-Graduação em  
Engenharia Mecânica - POSMEC

---

Prof. Amir Antônio Martins de Oliveira Jr., Ph.D.  
Universidade Federal de Santa Catarina - Orientador

---

Prof. Leonel Rincón Cancino, Dr.  
Universidade Federal de Santa Catarina -  
Coorientador



## Banca Examinadora:

---

Prof. Amir Antônio Martins de Oliveira Jr., Ph.D.  
Universidade Federal de Santa Catarina - Presidente

---

Prof. Luís Fernando Figueira da Silva, Dr.  
Pontifícia Universidade Católica do Rio de Janeiro -  
Relator

---

Prof. Rogério Gonçalves dos Santos, Dr.  
Universidade Estadual de Campinas

---

Edimilson Jesus de Oliveira, Dr.  
Centro de Pesquisas e Desenvolvimento Leopoldo  
Américo Miguez de Mello - CENPES -  
PETROBRAS

---

Prof. Giovanni Finoto Caramori, Dr.  
Universidade Federal de Santa Catarina

---

Prof. Edson Bazzo, Dr.  
Universidade Federal de Santa Catarina



*Aos meus pais, Amir e Neiva,  
e à minha amada Juliana*



*For a successful technology, reality must take precedence over public relations, for Nature cannot be fooled.*

Richard Phillips Feynman, 1918-1988



## AGRADECIMENTOS

Aos Professores Amir Oliveira e Leonel Cancino pelos inestimáveis conselhos ao longo deste trabalho e de minha formação como engenheiro e pesquisador. Sou muito grato por compartilharem seu entusiasmo e curiosidade pela Ciência.

Aos membros da comissão examinadora, Professores Luís Fernando Figueira da Silva, Rogério Gonçalves dos Santos, Giovanni Finoto Caramori, Edson Bazzo e ao Dr. Edimilson Jesus de Oliveira pelo interesse e contribuições à tese.

My profound gratitude to the amazing team of the Combustion Chemistry Centre, Professors Henry Curran and John Simmie, post docs Kuiwen Zhang, Yingjia Zhang, Changyoul Lee, Chong-Wen Zhou and Kieran Somers, and fellow students Yang Li, Patrick Meier, John Bugler, Colin Banyon, Cristina Rizzo and Zisis Malliotakis. I don't know half of you half as well as I should like, and I like less than half of you half as well as you deserve. Especially the blue RCM.

Aos amigos e colegas de LabCET Alexandre Schmidt Ferreira, Camilla Rigoni Medeiros, Christian Alexander Jeedi Hoffmann (*in memoriam*), Eduardo Lucas Konrad Burin, Eduardo Morel Hartmann, Gilson Nunes Maia, João Otávio Dourado Monteiro, Jônatas Vicente, Leandro Alves de Oliveira, Luana Ribeiro Carvalho, Marco Antônio Casarin, Marcos Vinício Oro, Nury Audrey Nieto Garzón, Olívia Carolina da Rosa, Renzo Fabrício Figueroa Piña, Ricardo Morel Hartmann, Roberta Brondani Minussi, Sara Dotta Corrêa e William Alexander Carrillo Ibañez pelas discussões científicas, artísticas e sociopolítico-exergoeconômicas e pela espirituosa e salutar companhia.

Ao Conselho Nacional de Desenvolvimento Científico e Tecnológico (CNPq) pelo apoio financeiro (Processo 162440/2013-8), à Coordenação de Aperfeiçoamento de Pessoal de Nível Superior (CAPES) pela bolsa de doutorado-sanduíche no exterior (Processo BEX 6264/15-8) e à Petróleo Brasileiro S.A. pelo apoio financeiro e material ao projeto de pesquisa (Termo de Cooperação 0050.0070218.11.9).



## RESUMO

Diversos processos físicos e químicos que ocorrem em câmaras de combustão afetam a eficiência, durabilidade, confiabilidade e emissões de turbinas aeronáuticas. Além disso, metas globais de sustentabilidade resultaram em novas regulamentações que compelem os produtores de combustível a introduzir biocomponentes em suas formulações. O conhecimento dos efeitos da formulação do combustível no desempenho de turbinas a gás é de suma importância para o desenvolvimento de novos combustíveis *drop-in*. Este trabalho compreende o estudo experimental e a modelagem da oxidação de combustível de aviação e misturas substitutas utilizando mecanismos de cinética química detalhada. Primeiramente, apresenta-se uma extensa revisão das especificações de combustível de aviação, incluindo combustíveis alternativos, e de experimentos recentes, conduzidos para definir ‘*targets*’ e misturas substitutas. Medições do atraso de ignição de uma amostra de combustível de aviação comercial produzido no Brasil (QAV1) foram realizadas em tubo de choque, para temperaturas de 715 K a 1250 K, pressões de 15 bar e 30 bar, e razões de equivalência combustível/ar de 0,3 e 1,0. Uma curva de ajuste para os dados foi obtida e simulações de cinética química detalhada foram conduzidas, utilizando-se o mecanismo para três componentes (n-decano, iso-octano, tolueno), intitulado MURI 1, elaborado por Dooley *et al.* (2010). Em seguida, medições do atraso de ignição de misturas substitutas MURI 1 (n-decano, iso-octano, tolueno) e TRF (n-heptano, iso-octano, tolueno) foram obtidas em máquina de compressão rápida e tubo de choque, para temperaturas de 650 K a 1300 K, razões de equivalência combustível/ar de 0,5 e 1,0 e pressão de 15 bar, com o propósito de reproduzir o comportamento do combustível comercial QAV1. Foram realizadas simulações de cinética química detalhada, empregando mecanismos disponíveis na literatura e mecanismos ainda inéditos, buscando identificar a capacidade dos modelos em reproduzir comportamentos de coeficiente negativo de temperatura (NTC) e ignição em dois estágios. Por fim, uma análise de sensibilidade dos dois mecanismos para a mistura substituta TRF foi realizada para elucidar quais reações químicas eram críticas para que ambos exibissem atraso de ignição similar, porém ignição de primeiro estágio diferente. Não é de conhecimento do autor que estas medições e simulações já tenham sido realizadas para o combustível aeronáutico brasileiro.

**Palavras-chave:** Combustível aeronáutico, Cinética química detalhada, Misturas substitutas, Tubo de choque, Máquina de compressão rápida.



## ABSTRACT

Several chemical and physical processes in the combustion chamber affect the efficiency, durability, dependability, and emissions of aviation turbines. Moreover, global sustainability criteria has resulted in new regulations requiring fuel producers to increase the amount of biofuels in their aviation fuel formulations. The knowledge of the effects of the fuel formulation in the performance of the gas turbine is of paramount importance to the development of new drop-in fuels. This work comprises modeling and experiments on the oxidation of jet fuel and fuel surrogates from a detailed chemical kinetics perspective. First, a thorough review of jet fuel's specification, including alternative fuels, and of recent experiments carried out to define fuel 'targets' and surrogate compositions is presented. Ignition delay time (IDT) measurements for a Brazilian commercial Jet A-1 fuel sample were performed in a high pressure shock tube (ST) spanning a temperature range from 715 K to 1250 K, pressures of 15 bar and 30 bar and fuel/air equivalence ratios of 0.3 and 1.0. An expression fitting the measurements was obtained and a detailed chemical kinetics modeling of the autoignition was carried out using the three-component MURI 1 (n-decane, iso-octane, toluene) mechanism from Dooley *et al.* (2010). Then, the IDT of fuel surrogates MURI 1 (n-decane, i-octane, toluene) and TRF (n-heptane, iso-octane, toluene) was measured both in a shock tube and a rapid compression machine at the temperature range of 650 to 1300 K, fuel/air equivalence ratio of 0.5 and 1.0, and pressure of 15 bar with the intent of reproducing behavior of the Jet A-1 fuel. Detailed chemical kinetics modeling of these experiments was performed employing literature and unpublished mechanisms, aiming at identifying their ability to reproduce negative temperature coefficient (NTC) and two-stage ignition behavior. A sensitivity analysis of the mechanisms for surrogate TRF was carried out in order to elucidate the critical reactions governing an overall similar ignition delay but different first-stage ignition. To the author's knowledge, this is the first time that these measurements and simulations have been performed for the Brazilian Jet A-1 aviation fuel.

**Keywords:** Aviation fuel, Detailed chemical kinetics, Surrogate fuels, Shock tube, Rapid compression machine



## TABLE OF CONTENTS

1	INTRODUCTION	1
1.1	MOTIVATION AND OBJECTIVES	3
1.2	THESIS OVERVIEW	4
2	OVERVIEW OF JET FUEL SOURCES AND PROPERTIES	7
2.1	HISTORICAL BACKGROUND	7
2.2	JET FUEL SPECIFICATIONS	10
2.2.1	<i>Fuel composition and properties</i>	11
2.2.2	<i>Fuel performance and emissions</i>	15
2.3	ALTERNATIVE FUELS	19
2.3.1	<i>Fischer-Tropsch synthetic fuels</i>	20
2.3.2	<i>Biofuels</i>	23
2.4	CONCLUDING REMARKS	29
3	SURROGATE FUELS AND MODELING	31
3.1	GENERAL CONSIDERATIONS	31
3.2	COMPONENTS AND FORMULATIONS OF JET FUEL SURROGATES	33
3.3	EXPERIMENTS WITH REAL FUELS AND SURROGATES	40
3.3.1	<i>Experiments with Jet A POSF 4658</i>	40
3.3.2	<i>Experiments with other conventional fuels</i>	51
3.3.3	<i>Experiments with alternative jet fuels</i>	56
3.3.4	<i>Additional research</i>	64
3.4	CLOSING REMARKS	65
4	EXPERIMENTS	71
4.1	INTRODUCTION	71
4.2	EXPERIMENTS WITH JET A-1 AT IVG - UDE	72
4.2.1	<i>Facility at IVG - UDE</i>	74
4.2.2	<i>Fuel and mixture preparation</i>	76
4.3	EXPERIMENTS WITH SURROGATES AT C3 - NUI GALWAY	77
4.3.1	<i>Rapid compression machine</i>	77
4.3.2	<i>High pressure shock tube</i>	80
4.3.3	<i>Fuel surrogates and mixture preparation</i>	81
4.4	RESULTS	84
4.4.1	<i>Measurements of IDT for Jet A-1</i>	84
4.4.2	<i>Measurements of IDT for MURI 1 surrogate</i>	86
4.4.3	<i>Measurements of IDT for TRF surrogate</i>	90
5	MODELING AND ANALYSIS	95
5.1	MURI MECHANISM	95

5.1.1	<i>Modeling of Jet A-1 ignition delays</i> .....	96
5.1.2	<i>Modeling of surrogate MURI 1 ignition delays</i> .....	98
5.2	MECHANISMS FOR TRF SURROGATE .....	100
5.3	SENSITIVITY ANALYSIS .....	104
5.3.1	<i>Sensitivity analysis of RCM ignition delay</i> .....	105
6	CONCLUSIONS AND RECOMMENDATIONS .....	123
6.1	RECOMMENDATIONS .....	127
	Bibliography .....	129
	Appendix A – Fundamentals of sensitivity analysis .....	141

## LIST OF FIGURES

2.1	Generic transesterification reaction . . . . .	24
3.1	Compilation of POSF 4658 ignition delay times . . . . .	41
3.2	Pressure traces of RCM experiments with Jet A POSF 4658 (top), and surrogate MURI 1 (bottom), showing the absence of first-stage ignition in the latter - Source: Dooley <i>et al.</i> - Combust Flame Vol. 157 (2010) . . . . .	42
3.3	Compilation of POSF 4658 laminar flame speeds as function of equivalence ratio for different unburned gas temperatures . . . . .	47
3.4	Simplified scheme for the primary mechanism of oxidation of alkanes . . . . .	66
4.1	Operation of a shock tube, (a) initial condition, (b) and (c) propagation of incident shock wave, (d) and (e) propagation of reflected shock wave. Source: Cancino (2009)	73
4.2	Distance-time diagram in shock tube. (1) unshocked gas, (2) shocked gas by incident shock, (3) expanded driver gas, (4) unexpanded driver gas, (5) shocked gas by reflected shock. Source: Cancino (2009) . . . . .	74
4.3	Determination of the ignition delay time from the CH* and CH <sub>2</sub> O* chemiluminescence signals. . . . .	75
4.4	Rapid compression machine at C3 - National University of Ireland, Galway. . . . .	77
4.5	Typical RCM pressure trace showing both reactive and nonreactive pressure profiles, with the reactive profile exhibiting two-stage ignition. . . . .	79
4.6	High pressure shock tube at C3 - National University of Ireland, Galway. . . . .	80
4.7	Schematic of the infrared laser diagnostic setup. . . . .	82
4.8	Shock tube measurements of ignition delay times for Jet A-1. . . . .	84
4.9	Pressure-time histories of stoichiometric MURI 1 autoignition in RCM. . . . .	87
4.10	Pressure-time histories of lean MURI 1 autoignition in RCM. . . . .	87
4.11	Measured ignition delay times for surrogate MURI 1. . . . .	89
4.12	Pressure-time histories of stoichiometric TRF surrogate autoignition in RCM. . . . .	90

4.13	Pressure-time histories of lean TRF surrogate autoignition in RCM. . . . .	91
4.14	Measured ignition delay times for surrogate TRF . . . . .	93
5.1	Comparison of measured Jet A-1/air and simulated surrogate ‘B’ ignition delay times. . . . .	97
5.2	Measured and calculated pressure time histories for stoichiometric MURI ignition delays. Nonreactive pressure histories in black, solid lines represent compressed temperature of 660 K, dashed lines 675 K . . . . .	99
5.3	Measured and calculated pressure time histories for lean MURI ignition delays. Nonreactive pressure histories in black, solid lines represent compressed temperature of 675 K, dashed lines 700 K . . . . .	100
5.4	Experimental and computed ignition delay times for surrogate MURI. Solid lines represent constant volume (ST) simulations, dashed lines show simulation with facility effects (RCM). . . . .	101
5.5	Measured and calculated pressure time histories for stoichiometric TRF ignition delays. Nonreactive pressure histories in black, solid lines represent compressed temperature of 675 K, dashed lines 700 K . . . . .	102
5.6	Measured and calculated pressure time histories for stoichiometric TRF ignition delays. Nonreactive pressure histories in black, solid lines represent compressed temperature of 700 K, dashed lines 750 K . . . . .	103
5.7	Experimental and computed ignition delay times for surrogate TRF at stoichiometric condition. Solid lines represent constant volume (ST) simulations, dashed lines show simulation with facility effects (RCM). . . . .	104
5.8	Experimental and computed ignition delay times for surrogate TRF at lean condition. Solid lines represent constant volume (ST) simulations, dashed lines show simulation with facility effects (RCM). . . . .	105
5.9	Measured and calculated pressure time histories for lean TRF ignition delay at compressed temperature of 750 K. . . . .	106
5.10	Computed pressure time histories and fuel depletion for lean TRF ignition delay at compressed temperature of 750 K. Open symbols denote NUIG’s model, half-filled symbols indicate Cancino’s model. . . . .	108

5.11	Sensitivity coefficients for the OH radical at the onset of first stage pressure rise, 1.8 ms for NUIG, 2.7 ms for Cancino. . . . .	108
5.12	Sensitivity coefficients for HO <sub>2</sub> at the onset of first stage pressure rise, 1.8 ms for NUIG, 2.7 ms for Cancino. . . . .	109
5.13	Sensitivity coefficients for n-heptane at the onset of first stage pressure rise, 1.8 ms for NUIG, 2.7 ms for Cancino. . . . .	110
5.14	Sensitivity coefficients for iso-octane at the onset of first stage pressure rise, 1.8 ms for NUIG, 2.7 ms for Cancino. . . . .	111
5.15	Sensitivity coefficients for OH during the first stage pressure rise, 2.3 ms for NUIG, 3.4 ms for Cancino. . . . .	112
5.16	Sensitivity coefficients for HO <sub>2</sub> during the first stage pressure rise, 2.3 ms for NUIG, 3.4 ms for Cancino. . . . .	113
5.17	Sensitivity coefficients for the four heptyl radicals during the first stage pressure rise, 2.3 ms for NUIG, 3.4 ms for Cancino. . . . .	113
5.18	Sensitivity coefficients for the four octyl radicals during the first stage pressure rise, 2.3 ms for NUIG, 3.4 ms for Cancino. . . . .	115
5.19	Sensitivity coefficients for OH when temperature T = 825 K, 3.1 ms for NUIG, 4.9 ms for Cancino. . . . .	116
5.20	Sensitivity coefficients for HO <sub>2</sub> when temperature T = 825 K, 3.1 ms for NUIG, 4.9 ms for Cancino. . . . .	116
5.21	Sensitivity coefficients for the four heptyl radicals when temperature T = 825 K, 3.1 ms for NUIG, 4.9 ms for Cancino. . . . .	117
5.22	Sensitivity coefficients for the four octyl radicals when temperature T = 825 K, 3.1 ms for NUIG, 4.9 ms for Cancino. . . . .	118
5.23	Sensitivity coefficients for OH when temperature T = 850 K, 8.5 ms for NUIG, 15.3 ms for Cancino. . . . .	119
5.24	Sensitivity coefficients for HO <sub>2</sub> when temperature T = 850 K, 8.5 ms for NUIG, 15.3 ms for Cancino. . . . .	120
5.25	Summary of the most sensitive reactions during TRF's ignition delay, in rapid compression machine, at 15 bar, 750 K and $\phi=0.5$ . Reactions in red promote reactivity, reactions in blue decrease reactivity. . . . .	121



## LIST OF TABLES

1.1	Specifications of aircraft piston engines . . . . .	2
2.1	Selected specification properties of jet fuels . . . . .	10
2.2	Average jet fuel compositions, % vol . . . . .	11
2.3	Boiling point and freezing point of representative jet fuel hydrocarbons . . . . .	12
2.4	Density and net energy content (N.E.C.) of representative jet fuel hydrocarbons . . . . .	13
2.5	Potential contribution of each hydrocarbon class to selected jet fuel properties . . . . .	14
2.6	Density, gravimetric energy and volumetric energy content of conventional and alternative fuels . . . . .	20
2.7	Chemical composition of fatty acids in biodiesel feedstocks	26
3.1	Kinetics limitations for jet fuels in gas turbine engines . .	33
3.2	Applicability of components for surrogates of transportation fuels . . . . .	36
3.3	Summary of the composition of surrogate mixtures for jet fuels . . . . .	39
3.4	Available experimental kinetics data for Jet A POSF 4658 since 2007 . . . . .	43
3.5	Available experimental kinetics data for different JP-8 samples since 2007 . . . . .	54
3.6	Available experimental kinetics data for alternative jet fuels since 2007 . . . . .	58
4.1	Properties of the studied Jet A-1 fuel - QAV1 . . . . .	76
4.2	Surrogate compositions, in % mol., investigated at C3 - NUI Galway . . . . .	81
4.3	Measured ignition delay times in ST for stoichiometric and lean Jet A-1/air mixtures . . . . .	85
4.4	Measured ignition delay times in RCM for stoichiometric and lean MURI 1/air/CO <sub>2</sub> mixtures . . . . .	88
4.5	Measured ignition delay times in ST for stoichiometric and lean MURI 1/air mixtures . . . . .	89
4.6	Measured ignition delay times in RCM for stoichiometric TRF/air/CO <sub>2</sub> mixtures . . . . .	91
4.7	Measured ignition delay times in RCM for lean TRF/air/CO <sub>2</sub> mixtures . . . . .	92

4.8	Measured ignition delay times in ST for stoichiometric and lean TRF/air mixtures . . . . .	93
5.1	Composition of proposed Jet A-1 surrogates for autoignition simulations and related <i>a priori</i> targets. . . . .	96
5.2	Nomenclature of the species included in the sensitivity analysis, Cancino / NUIG . . . . .	107

## GLOSSARY

AAFEX	Aircraft Alternative Fuel Emissions Experiment.
AIAA	American Institute of Aeronautics and Astronautics.
ASTM	American Society of Testing & Materials.
CFD	Computational fluid dynamics.
CtL	Coal-to-liquid.
DCN	Derived cetane number.
FAE	Fatty acid ester.
FT	Fischer-Tropsch.
GtL	Gas-to-liquid.
HDS	Hydrodesulfurization.
HEFA	Hydroprocessed esters and fatty acids.
ICAO	International Civil Aviation Organization.
IDT	Ignition delay time.
IPK	Iso-paraffinic kerosene.
KAUST	King Abdullah University of Science and Technology.
LHV	Lower heating value.
LLNL	Lawrence Livermore National Laboratory.
LTO	Landing and take-off cycle.
MCH	Methylcyclohexane.
MURI	Multi University Research Initiative.
NASA	National Aeronautics and Space Administration.
NIST	National Institute of Standards and Technology.
NTC	Negative temperature coefficient.
PAH	Polycyclic aromatic hydrocarbon.
POSF	Properties of Sample Fuel.
PRF	Primary reference fuel.
RCM	Rapid compression machine.
SPK	Synthetic paraffinic kerosene.
ST	Shock tube.
TEL	Tetraethyl lead.
TRF	Toluene reference fuels.
TSI	Threshold sooting index.



## 1 INTRODUCTION

In the early days of aviation, the Wright brothers flew their first Flyer model powered by a four-cylinder water-cooled inline engine fueled with Standard Oil motor gasoline from a boatyard (EDWARDS, 2003). Since then, aircraft propulsion, thereby aircrafts themselves, underwent a fantastic progress towards higher speeds, higher flight ceilings and higher fuel efficiency, with much of this evolution depending on, and also influencing, the quality of available fuel.

Internal combustion engines used in the first cars and boats were too heavy to propel aircrafts so, in order to obtain engines with better power-to-weight ratio, manufacturers devised radial cylinder arrangements that combined increased displacement with shorter and lighter crankshafts. Radial and rotary engines propelled most aircrafts during the First World War but at the end of the conflict further improvements of these designs were limited by metallurgy and fuel issues (GUNSTON, 1989; GUNSTON, 1994).

Meanwhile the popularization of cars was accompanied by the emergence of engine problems like ‘pinging’ or ‘knocking’ that occurred in situations like driving uphill. Soon it was recognized that the cause of knocking was a premature ignition of the gasoline/air mixture and, as a result, significant research effort was channeled to find antiknock additives. Even though ethanol was widely acknowledged as a very effective antiknock agent, General Motors and DuPont pushed the use of tetraethyl lead (TEL) for which the companies held patents. When the octane rating was established in the late 1920’s, TEL was already in widespread use as antiknock additive.

The use of TEL, combined with metallurgic and valve advances, allowed manufacturers to rise engine’s compression ratio, thus greatly increasing specific power, i.e., power per displacement ratio. Table 1.1 presents the evolution of aeronautic engines in terms of compression ratio and specific power. Note that, among the engines listed, the Rolls-Royce Merlin was a V-12 engine while the remaining models were radial or rotary engines. As it can be seen in the table, powerplants produced after 1930 presented a twofold increase in specific power, thereby allowing significant improvement in aircraft’s range and gross weight.

Regardless of the expanded flight envelope provided by high octane fuel, the maximum performance of piston engines was limited by the occurrence of sonic speeds at the propeller’s tip and, in the case

Table 1.1: Specifications of aircraft piston engines

Year	Engine model	Avgas octane rating	Compression ratio	Specific power hp/l
1911	Clerget 7Z	–	4.3	8.0
1923	Wright R-790 Whirlwind	50	5.1	17.0
1929	Bristol Jupiter VIII F	73–77	5.8	19.3
1933	Rolls-Royce Merlin I	100–130	6.85	32.96
1937	Wright R-3350 Duplex-Cyclone	100–130	6.0	40.27
1938	Bristol Centaurus	100–130	7.2	47.05
1941	Nakajima Homare	92 with ADI	8.0	51.70
1944	P&W R-4360 Wasp Major	115–145	6.7	60.19

Sources: Gunston - World Encyclopaedia of Aero Engines (1989); Gunston - Jane's Fighting Aircraft of World War II (1994); Lumsden - British Piston Aero Engines and Their Aircraft (2005)

of radial engines, there was additional limitation related to the large frontal area causing increased aerodynamic drag. At the end of the World War II, multi-row radial engines and their V-12 counterparts were still widely used but the recently introduced turboprops and turbojets offered significant advantages, like fewer moving parts, thus lower maintenance, and higher power-to-weight ratios. Besides these performance and maintenance features, the prominent differences of these new aircraft powerplants were the continuous combustion and the reaction nature of its thrust generation, for which led gasoline soon proved itself unsuitable.

As this brief historical review shows, the development of reciprocating aircraft engines was, in many ways, accompanied by the development of high-performance avgas while the relationship between jet fuels and gas turbines was not as close. Nowadays, developments in jet engines are achieved by employing predictive and efficient computational tools that incorporate turbulent flow, molecular transport and relevant chemical kinetics (COLKET *et al.*, 2007). Yet, significant gaps exist in the current knowledge of these processes and their coupling, including the lack of agreement around what can be considered an adequate chemical kinetics description for aviation fuels.

As noted by Dryer *et al.* (2012), the projected evolution of petroleum-derived and petroleum/alternative-derived blended jet fuels

and emerging propulsion technologies points to an increasing need to understand physical and chemical kinetic fuel property effects on multiphase, gas turbine combustion performance and emissions. Surrogate fuel concepts provide a pragmatic approach for modeling physical and chemical properties of real fuels that vary geographically, seasonally, and historically and that contain hundreds of individual hydrocarbon species. Provided that surrogate fuel formulations can replicate real fuel properties, the models derived for such mixtures can be utilized in engineering design tools to predict fuel effects on new combustion technologies, as well as for screening the compatibility of candidate non-petroleum derived alternative fuels with legacy equipment.

Therefore, comprehensive knowledge of phenomena like low temperature ignition and oxidation of hydrocarbons is of foremost importance to the adequate evaluation of prospective ‘drop-in’ alternative fuels. A drop-in fuel is a substitute for conventional jet fuel, which is fully compatible, mixable and interchangeable with conventional jet fuel thus it does not require any adaptation of the aircraft and of transport and storage infrastructure (IATA, 2016).

## 1.1 MOTIVATION AND OBJECTIVES

In order to assess the potential performance effects of conventional/drop-in fuel blends, the overall goal of this study is the evaluation of the autoignition characteristics of currently produced Brazilian aviation fuel and surrogate mixtures. Thus a series of specific objectives were devised as follows:

- To measure the ignition delay time of a Brazilian Jet A-1 fuel, a three-component surrogate mixture and a toluene reference fuel (TRF), using shock tube and rapid compression machine;
- To simulate the ignition using two newly developed detailed chemical kinetics mechanisms available in the literature;
- To perform sensitivity analysis of the results to identify main reaction paths and important chemical aspects of the ignition phenomena.

## 1.2 THESIS OVERVIEW

The present investigation was developed at the Laboratory for Combustion and Thermal Systems Engineering - LabCET at Universidade Federal de Santa Catarina - UFSC, the Institute for Combustion and Gas Dynamics - IVG at the University of Duisburg-Essen in Germany and at the Combustion Chemistry Centre - C3 at National University of Ireland - NUI in Galway.

This document is divided in six chapters. This introduction is followed by an overview of jet fuel specifications in terms of composition, properties, performance and emissions, accompanied by descriptions of alternative aviation fuels made from natural gas, coal and renewable sources. The third chapter discusses jet fuel surrogates and the modeling efforts, including a review of post-2007 experiments in facilities like flow reactors, shock tubes, rapid compression machines and stabilized flames.

Based on the knowledge presented thus far the fourth chapter is dedicated to the description of the experimental aspects of the present study. Initially a high pressure shock tube study of a Jet A-1 fuel sample was carried out by our collaborators at the IVG - University of Duisburg-Essen, followed by chemical kinetics modeling performed by the author. These results, combined with data from rapid compression machine experiments conducted at the Karlsruhe Institute of Technology, were published in the Proceedings of the Combustion Institute (DE TONI *et al.*, 2017).

The second part of the investigation comprised an experimental and numerical study of the low temperature reactivity and thermal ignition of fuel surrogates. The experiments, employing both rapid compression machine and shock tube facilities, were conducted at the Combustion Chemistry Centre (C3) at the National University of Ireland, Galway. The surrogates investigated were a literature jet fuel surrogate (MURI 1) and a lighter version of MURI 1, which is similar to a low-octane gasoline. The fourth chapter also includes details about fuel mixture preparation and evaporation diagnostics, followed by the presentation of measurements obtained.

A detailed chemical kinetics modeling of the ignition delay times measured at NUI Galway is presented in the fifth chapter, including a comparative sensitivity analysis between an alcohol-containing gasoline model developed by LabCET and IVG (CANCINO, 2009) and an unpu-

---

blished mechanism by C3 - NUI Galway. To conclude, the sixth chapter presents conclusions and recommendations for future work involving fuel surrogates and detailed chemical kinetics, followed by references and appendices.



## 2 OVERVIEW OF JET FUEL SOURCES AND PROPERTIES

This chapter provides an account of the historical development of jet fuel, the current state of its specification, and descriptions of its properties and performance due to each different class of hydrocarbon present. The chapter also presents information about alternative fuels for aviation, describing feedstocks, production processes as well as the test programmes and flight demonstrations carried out in the last fifteen years. The following section is dedicated to the historical development of jet fuel.

### 2.1 HISTORICAL BACKGROUND

The first successful jet-powered aircraft, invented by the German engineer Hans Von Ohain, flew in 1939. Von Ohain chose gasoline as the fuel because ‘it was available at the time’ and was the fuel employed in all piston engine aircraft. Two years later, Sir Frank Whittle used ‘illuminating kerosene’ as the fuel of his turbojet also because it was available (MAURICE *et al.*, 2001). In fact turbojet engines proved to be more tolerant to fuel properties than piston engines and these properties were dictated by fuel system limitations, operation requirements and, ultimately, by refining industry’s capabilities.

According to Maurice *et al.* (2001) avgas and gasoline, the main refinery products at the time, were almost immediately recognized as far from ideal jet fuels since their high volatility would produce engine malfunction at altitude due to ‘vapor lock’. The lighter components in gasoline had poor lubricity thus wearing the metering pumps whilst the octane enhancing additives, which contained lead, resulted in erosion of the hot turbine blades.

On the other hand, the middle distillate fraction of petroleum had little value or use for the refiners and presented some interesting characteristics like higher volumetric heating values and higher hydrogen content thus producing less soot. These features would lead to the production of jet fuel but only after the industry decided that the jet engine ‘had a future’, since there were rumors that it was uncontrollable at higher speeds and, as a consequence, certainly did not seem to have any future in commercial aviation.

The first fuel for aviation gas turbines was specified by the US Army Air Corps in 1944 and identified as Jet Propellant # 1 or JP-1. It had a distillation range roughly between 149–260°C and a freezing point below –60°C, the latter requirement being specially difficult to attain by most refiners. Even with this setback the JP-1 specification took the first step, clearly moving jet fuels from avgas towards the kerosene range. Other early fuel specifications, like JP-2 and JP-3, included a viscosity limit below 1 cSt (1 mm<sup>2</sup>/s) at 38°C thus establishing the jet fuels as blends of gasoline and kerosene fractions. In 1951, four years after the creation of the US Air Force, the JP-4 fuel specification was issued as a result of a collective effort of USAF specialists and fuel suppliers, defining fuel specification based on general characteristics of available crude oil and the recognition that many fuel properties are interdependent.

Like its predecessor, the JP-4 was a mixture of gasoline and kerosene fractions of crude oil, but with strong vapor pressure restrictions to reduce boil-off losses and reduced attention to viscosity, since atomizers had been developed for thicker fuels like diesel. At the time, jet fuels were produced almost exclusively from straight distillation of suitable light crude oil, being a readily available product without major alternative use. The lowest boiling fraction of this fuel contained normal paraffins (straight chain alkanes) that had been removed from regular gasoline because of their low octane ratings (EXXON MOBIL, 2005). The boiling range of JP-4 was 66–149°C which the US Navy considered too dangerous to store in its aircraft carriers, hence, the Navy adopted only the kerosene fraction of JP-4, that presents a 182–260°C distillation range, a flashpoint above 60°C and freezing point specification below –40°C. This fuel was designated JP-5 and was suitable for the lower altitude operation of the Navy aircraft even though its reduced volatility demanded the use of higher energy ignitors.

Thus, within a decade, the definition of jet fuel requirements had matured to a standard close to other liquid fuels but its ability to provide cooling to the engine lubricant was still very limited. Problems with fuel ‘coking’ occurred in fuel injectors and manifolds, albeit the quality control tests presented no indication of excessive deposition in conventional, gasoline-derived gum tests. The phenomenon of coking would be later defined as thermal oxidative stability resulting of a series of liquid oxidation reactions with minor components, like heterocompounds, with oxygen dissolved in the fuel. In the late 1950’s a flow

device was developed to evaluate more realistically the high temperature performance of jet fuels and the success of such effort reinforced the use of jet propulsion.

In the 1960's the availability of feedstock became a concern. Jet fuels were produced primarily from light, low sulfur crude oil, with little or no processing besides atmospheric distillation, thus keeping the prices low. Then, increasing demands for imported light Arabian crudes reduced the offer and the feedstock began to be replaced by heavier crude, high in sulfur and difficult to refine into the existing product slate. At the same time commercial aviation began its expansion into the jet age and a kerosene fuel designated as Jet A by the American Society of Testing & Materials was the baseline fuel for commercial aircraft. Considering passenger safety, Jet A was defined as a pure kerosene fuel, similar to JP-1, with a flashpoint above 38°C and freezing point below -40°C (-47°C for international Jet A-1) (CHEVRON, 2006b).

These specifications endured mostly unaltered since then, except for sulfur content limits. New policies demand a decrease in sulfur content aiming at reducing environmental impact. However, this also affects the fuel's lubricity, since the phenomenon of boundary lubrication (lubrication provided by metal-adhering films) is attributed to trace amounts of sulfur-, nitrogen- and oxygen-containing compounds. Such problem is amended with the use of additives.

It is important to notice that fuel specifications were developed considering crude oil as the only practical feedstock, thus implying the presence of different classes of hydrocarbons in the fuel. In the current and future scenarios, with the development of alternative feedstocks and processes, the most likely near-term solution to meet regulations involves the blending of alternative components into conventional fuel, following the path established during the 1990's with the development of Sasol's synthetic paraffinic kerosene. More details about this alternative fuel will be presented later on.

The following section provides more detailed information regarding fuel properties and composition, the different classes of compounds present in its formulation and the contribution of each one, in trace or bulk amounts, to the overall characteristics of jet fuels.

## 2.2 JET FUEL SPECIFICATIONS

The main properties of commercial jet fuels are presented in Tab. 2.1. As one would expect, these fuel properties are ‘operational’ requirements related to the intended application. The real Jet A and Jet A-1 greatly varies in composition, e.g. typical aromatic content between 8 and 22%, as a result of different quality of crude oil and refiner capability. As pointed out previously, fuel specifications are ‘biased’ since they include implicit assumptions that are met when petroleum is the feedstock, like smooth boiling range distribution and the absence of a specified minimum aromatic content.

Table 2.1: Selected specification properties of jet fuels

Fuel	Jet A	Jet A-1
Specification	ASTM D 1655	DEF STAN 91-91
Acidity, mg KOH/g	0.10	0.015
Aromatics, % vol max	25	25
Sulfur, % mass	0.30	0.30
Distillation, °C, 10% recovered, max	205	205
Distillation, °C, end point	300	300
Flash point, °C, min	38	38
Density, 15°C, kg/m <sup>3</sup>	775–840	775–840
Freezing point, °C, max	−40	−47
Viscosity, −20°C, mm <sup>2</sup> /s, max	8.0	8.0
Net heat of combustion, MJ/kg, min	42.8	42.8
Smoke point, mm, min	18.0	19.0
Naphthalenes, % vol, max	3.0	3.0
Filter pressure drop, mm Hg, max	25	25
Existent gum, mg/100 ml, max	7	7

Source: Chevron - Aviation Fuels Technical Review (2006b)

Table 2.2, reported by Colket *et al.* (2007), presents two average compositions of jet fuels. The World Survey Average is the average composition of 55 jet fuel samples (Jet A, Jet A-1, JP-8 and JP-5) collected from locations worldwide while the Composite Jet A (POSF 4658) is an average fuel obtained by mixing equal volumes of Jet A from five different US refiners.

When studying such a complex mixture of hydrocarbons, one must have in mind the characteristics and roles of different classes of compounds regarding combustion behavior, storage and thermal stabi-

Table 2.2: Average jet fuel compositions, % vol

Compound	World Survey Average	Composite Jet A
paraffins, n- + i-	58.78	55.2
monocycloparaffins	10.89	17.2
dicycloparaffins	9.25	7.8
tricycloparaffins	1.08	0.6
alkyl benzenes	13.36	12.7
indanes + tetralins	4.9	4.9
naphthalene	0.13	<0.2
substituted naphthalenes	1.55	1.3

Source: Colket *et al.* - 45th AIAA Aerospace Science Meeting and Exhibition (2007)

lity, engine performance and emissions, lubricity and others. The development of an appropriate fuel surrogate depends on knowing these relations and these issues are discussed in the following subsections.

### 2.2.1 Fuel composition and properties

As presented in Tab. 2.2, aviation turbine fuel is a mixture of many different hydrocarbons, separated from crude oil by distillation. By this process, it is possible to assure that a kerosene fuel has carbon number distribution between 8 and 16 carbons while for a ‘wide-cut’ jet fuel this distribution is about 5 to 15 carbons.

Most of the hydrocarbons in jet fuels are members of paraffinic, naphthenic (cycloalkane) or aromatic classes and it is important to know how physical and chemical properties vary, for hydrocarbons within the C<sub>8</sub>-C<sub>16</sub> range, as a function of the class. Table 2.3 presents data of boiling and freezing points of some representative hydrocarbons grouped by carbon number.

From Tab. 2.3, it is possible to notice an increase in boiling point for larger hydrocarbons, thus compounds of the middle kerosene range with boiling point around 220°C probably are C<sub>10</sub> aromatics, C<sub>11</sub> naphthenes and C<sub>12</sub> paraffins, with some 5°C variation occurring between linear and branched alkanes of the same carbon number. The freezing point also increases with carbon number within each class but is strongly influenced by molecular shape. Normal paraffins and unsubstituted aromatics crystallize at much higher temperatures than other compounds with the same carbon number since the geometry

Table 2.3: Boiling point and freezing point of representative jet fuel hydrocarbons

Compound	Formula	Class	B.P. °C	F.P. °C
n-octane	C <sub>8</sub> H <sub>18</sub>	n-paraffin	125.7	-56.8
2-methylheptane	C <sub>8</sub> H <sub>18</sub>	i-paraffin	117.6	-109.0
1-methyl-1-ethylcyclopentane	C <sub>8</sub> H <sub>16</sub>	naphthene	121.5	-143.8
ethylcyclohexane	C <sub>8</sub> H <sub>16</sub>	naphthene	131.8	-111.3
o-xylene	C <sub>8</sub> H <sub>10</sub>	aromatic	144.4	-25.2
p-xylene	C <sub>8</sub> H <sub>10</sub>	aromatic	138.4	13.3
cis-decalin	C <sub>10</sub> H <sub>18</sub>	naphthene	195.8	-43.0
tetralin	C <sub>10</sub> H <sub>12</sub>	aromatic	207.6	-35.8
naphthalene	C <sub>10</sub> H <sub>8</sub>	aromatic	217.9	80.3
n-dodecane	C <sub>12</sub> H <sub>26</sub>	n-paraffin	216.3	-9.6
2-methylundecane	C <sub>12</sub> H <sub>26</sub>	i-paraffin	210.0	-46.8
1-ethylnaphthalene	C <sub>12</sub> H <sub>12</sub>	aromatic	258.3	-13.8
n-hexilbenzene	C <sub>12</sub> H <sub>18</sub>	aromatic	226.1	-61.0
n-hexadecane	C <sub>16</sub> H <sub>34</sub>	n-paraffin	286.9	18.2
2-methylpentadecane	C <sub>16</sub> H <sub>34</sub>	i-paraffin	281.6	-7.0
n-decylbenzene	C <sub>16</sub> H <sub>26</sub>	aromatic	297.9	-14.4

Source: Chevron - Aviation Fuels Technical Review (2006b)

of these two hydrocarbon classes allows them to easily pack together into a crystalline structure.

Table 2.4 lists density and energy content of representative jet fuel hydrocarbons. For compounds in the same class density increases with carbon number, while for compounds with the same carbon number density increases by class in the order paraffin, naphthene and aromatic.

For compounds of the same carbon number, energy content increases per unit weight by class, from aromatic, to naphthene to paraffin, clearly matching the different hydrogen to carbon ratio of each class. In a volume basis, the order is reversed and this becomes evident for fuels, e.g., less dense gasoline has higher energy content on a weight basis whereas more dense diesel has higher energy content on a volume basis.

In terms of viscosity, carbon number is more important than hydrocarbon class; for a given carbon number, naphthenes generally present higher viscosity than aromatics and paraffins. Table 2.5 summarizes how the contribution of each class affects the overall jet fuel properties in terms of a beneficial effect (denoted by '+'), neutral or

minor contribution (denoted by ‘o’), or a detrimental effect (denoted by ‘-’).

As it can be seen in Tab. 2.5, the main benefit provided by aromatics in the fuel is a good volumetric energy content, while the main contribution of naphthenes is the reduction of freezing point hence improving the low-temperature fluidity of the fuel. The table also shows that i-paraffins present intermediate properties between aromatics and n-paraffins thus being interesting as a main component of the fuel mixture.

While paraffinic and naphthenic fractions of the jet fuel present largely dispersive intermolecular forces, some aromatic compounds shows polar and hydrogen-bonding character thus increasing the water solubility in the fuel and also causing some types of elastomers used in fuel system to swell (CHEVRON, 2006a), which the industry considers as a safeguard against fuel leaks. This swelling occurs in seals made of nitrile rubber, a copolymer composed of poly(butadiene) and poly(acrylonitrile), the latter presenting a highly polar cyano group ( $-C\equiv N$ ) on adjacent polymer chains. The net negative charge in the cyano group interacts with the electropositive aromatic hydrogens, the-

Table 2.4: Density and net energy content (N.E.C.) of representative jet fuel hydrocarbons

Compound	Class	Density at 20°C, g/cm <sup>3</sup>	N.E.C. at 25°C, MJ/kg	N.E.C. at 25°C, MJ/l
n-octane	C <sub>8</sub> n-paraffin	0.7027	44.42	31.21
2-methylheptane	C <sub>8</sub> i-paraffin	0.6979	44.38	30.97
1-methyl-1-ethylcyclopentane	C <sub>8</sub> naphthene	0.7809	43.57	34.02
ethylcyclohexane	C <sub>8</sub> naphthene	0.7879	43.40	34.20
o-xylene	C <sub>8</sub> aromatic	0.8801	40.81	35.92
p-xylene	C <sub>8</sub> aromatic	0.8610	40.81	35.14
cis-decalin	C <sub>10</sub> naphthene	0.8967	42.62	38.22
tetralin	C <sub>10</sub> aromatic	0.9695	40.52	39.06
naphthalene	C <sub>10</sub> aromatic	1.1750	40.12	47.14
n-dodecane	C <sub>12</sub> n-paraffin	0.7488	44.11	33.03
2-methylundecane	C <sub>12</sub> i-paraffin	0.7458	44.08	32.87
n-hexilbenzene	C <sub>12</sub> aromatic	0.8602	41.80	35.96
n-hexadecane	C <sub>16</sub> n-paraffin	0.7735	43.95	33.99
n-decylbenzene	C <sub>16</sub> aromatic	0.8554	42.23	36.12

Source: Chevron - Aviation Fuels Technical Review (2006b)

Table 2.5: Potential contribution of each hydrocarbon class to selected jet fuel properties

Property	n-paraffin	i-paraffin	naphthene	aromatic
Gravimetric energy content	+	+	o	-
Volumetric energy content	-	-	o	+
Combustion quality	+	+	+	-
Low-temperature fluidity	--	o/+	+	o/-

Source: Chevron - Aviation Fuels Technical Review (2006b)

refore, breaking the polymer–polymer and penetrant–penetrant intermolecular bonds and forming polymer–penetrant intermolecular bonds, thus producing the swelling (GRAHAM *et al.*, 2006).

It is important to notice that the properties evaluated in Tab. 2.5 are bulk properties, so their values, to a first approximation, are close to the weighted averages of the property’s values of the individual components. Properties like energy content, distillation range, fluidity and combustion characteristics are bulk ones, while lubricity and stability are related to trace amounts of certain heterocompounds that may be present in the base fuel as manufactured, additives, or even contaminants.

Regarding lubricity and stability, the molecular structures of these fuels are modified by the process of hydrotreatment or hydrodesulfurization (HDS). According to the DEF STAN 91-91 (MINISTRY OF DEFENCE, 2012), ‘mildly’ hydrotreated components are those petroleum derived hydrocarbons subjected to hydrogen partial pressures below 70 bar while those submitted to hydrogen partial pressures greater than 70 bar are considered ‘severely’ hydroprocessed. Refiners employ this ‘upgrading’, catalytic process to remove sulfur-containing compounds like mercaptans, thiols, thiophenes and organic sulfides, but HDS also promotes saturation of olefins and, in severe conditions, saturation of aromatic rings and consumption of nearly all sulfur and nitrogen heterocompounds. In the absence of these naturally occurring species the use of additives is necessary, mainly for lubricity.

Additives are fuel soluble chemicals added in small amounts to enhance or maintain properties important to fuel performance and handling. Many additives are derived from petroleum-based raw materials and their concentration is in the parts per million range. The use of additives is the main difference between commercial and military jet fuels. International Jet A-1 contains a static dissipator and eventually

an antioxidant while Jet A usually contains no additives or perhaps an antioxidant. Military fuels demand three or four additives, specially regarding thermal stability since high-performance military aircraft place higher thermal stress on fuel.

Regarding antioxidant additives, their use is required in any fuel or fuel blend that has been hydrotreated under Jet A-1 and US military specifications, being optional in non-hydrotreated fuels under these specifications and for Jet A. Approved antioxidants for jet fuels are sterically hindered phenols like 2,6-ditertiary butyl-4-methyl phenol. The addition of antioxidant must occur immediately after the hydrodesulfurization to avoid any initial oxidative reaction in the following steps of processing and storage.

Other important class of additives are corrosion inhibitors and lubricity improvers, since most of the tanks and pipelines in fuel distribution system are made of uncoated steel. Corrosion inhibitors prevent free water and oxygen from rusting and corroding parts whilst lubricity additives are employed to compensate for the poor lubricity of hydro-treated jet fuels. The latter additives contain a polar group, like a carboxylic acid, that adheres to metal surfaces forming a thin film that improves boundary lubrication.

Having discussed the composition of jet fuels in terms of bulk and trace components, the next subsection addresses the effects of the composition in fuel's handling, combustion and emissions.

### 2.2.2 *Fuel performance and emissions*

Since the primary function of aviation turbine fuels is to power the aircraft, energy content, combustion quality and emissions are key fuel performance features. Other significant properties are related to handling such as fluidity, lubricity, stability and so on. The relationship between energy content and soot propensity is one of the major jet fuel performance features deserving careful assessment.

Energy content of hydrocarbons differ, as pointed out in Tab. 2.4, in terms of class and hydrogen to carbon ratio, with more paraffinic fuels presenting lower density, thus higher energy per mass, whereas more aromatic ones presenting higher density, thus higher energy by volume. Usually, a denser, high volumetric energy content jet fuel is preferred, considering that it is typically bought and sold by volume,

unlike some gaseous fuels, sold by heating value.

In terms of combustion behavior, however, higher aromatic fraction is related to increased soot formation propensity which must be minimized for several reasons including radiant heat loss, premature engine failures due to increased combustor liner temperatures and turbine erosion and effects in high altitude atmospheric chemistry (DAGAUT; CATHONNET, 2006). Fuel specifications include three main properties to evaluate fuel's soot tendency: maximum limits for aromatic and naphthalene fractions and smoke point, a measurement of the maximum flame height achieved in a standard wick-fed lamp without smoking. Experimental studies in combustion rigs (LOHMANN; JEROSZKO, 1983; ROSFJORD, 1984) showed that viscosity, surface tension, specific gravity and distillation temperatures also affect soot formation since these properties are related to fuel spray droplet size, hence residence time and rate of vaporization.

Unfortunately changes in fuel may or may not produce interpretable variations in soot production. Fuels with increased aromatic content, from typical 20 % up to 52 %, thus with correspondent H/C ratio decreasing from 1.89 to 1.59, were prepared for NASA's Broad Specification Fuels Technology Program (LOHMANN; JEROSZKO, 1983) and presented unexpected lower viscosity and higher volatility characteristics, producing less soot than Jet A. Since the higher aromatic fuels were prepared mixing Jet A with 'blending stocks' and xylene tower bottoms, the authors attributed the unusual result to these "narrow and unique cuts" of aromatics. On the other hand, if these blends resulted in higher viscosity and lower volatility, therefore, higher soot formation, it is difficult to ascertain which factor was predominant: the greater concentration of carbon and precursors or the degradation in fuel's atomization and distribution that results in fuel-rich regions.

Regarding gaseous emissions, air transportation receives less attention than other sectors since its contribution to global emissions is small compared to ground vehicles and stationary power sources. Some emissions from aircrafts are limited according to the landing and take-off cycle (LTO) defined by the International Civil Aviation Organization (ICAO), that regulates emissions near ground level but indirectly limit them in altitude too. The idle operation of a legacy turbine engine employs rich mixtures to produce low carbon monoxide and unburned hydrocarbon emissions, also resulting in reduced fuel composition sensitivity regarding ignition and relight (LOHMANN; JEROSZKO, 1983).

The disadvantage of this approach is the increase in particulate emissions at idle while in high power levels, during climbout and takeoff, the engine operates in leaner, thus hotter, conditions, which eventually impacts nitrogen oxide emissions.

Carbon dioxide emission in aircraft is a minor concern and its future reduction is linked to engine and airframe improvements as well as the use of biofuels. Water vapor, the other major product of hydrocarbon combustion, forms contrails and aviation-induced cirrus clouds at cruise altitude and their effects on climate change is an area of ongoing research. Sulfur oxides and nitrogen oxides comprise the most hazardous gaseous emissions and their regulation is more stringent. Sulfur oxides are related to trace amounts of sulfur-containing hetero-compounds and their presence in the jet fuels depend on the quality of the crude oil feedstock and the level of hydrotreating employed by the refiner. Even though the specifications allow a maximum of 3000 ppm sulfur the worldwide average appears to be around 500–1000 ppm (CHEVRON, 2006b).

Nitrogen oxides are mostly formed from oxidation of atmospheric nitrogen at very high temperatures in the combustor, with fuel bound nitrogen representing about 2 % of NO<sub>x</sub> total emission. Nitrogen oxides are thought to contribute to the formation of ozone near ground level as well as acid rain. Since thermal NO<sub>x</sub> formation is controlled by maximum temperature, engine design and operating conditions are key factors to ensure complete, fast and uniform combustion thus lowering this emission. This issue becomes more important when burning fuels with higher aromatic content since there is an increase in flame temperature with reduced H/C ratio (LOHMANN; JEROSZKO, 1983).

Regarding fuel stability, most of the problems are related to oxygen-containing compounds, like peroxides and hydroperoxides, that remain dissolved in the fuel and may attack fuel system elastomers. Additional reactions may result in the formation of insoluble particulates and soluble gums, that deposit on surfaces and induce clogging of filter and small orifices. The thermal stability of a jet fuel is of critical importance since the fuel acts as heat exchange medium in many engine and airframe subsystems like hydraulic fluid and air conditioning equipment. The resulting heating of the fuel accelerates the formation of particulates and gums in liquid phase. While the storage stability can be improved with antioxidant additives, they are not usually effective in improving thermal stability.

The jet fuel is also expected to lubricate moving parts in fuel pumps and fuel metering units. The lubrication mechanism is a combination of hydrodynamic lubrication and boundary lubrication. The former is the result of a layer of viscous liquid preventing opposing moving surfaces from contacting each other thus higher viscosity fuels, e.g., those presenting higher naphthenic fraction, provide better lubrication than lower viscosity ones. When the tolerances between surfaces are narrow, boundary lubrication becomes important.

As noted previously, the boundary lubrication is associated with the presence of trace amounts, ca. 10 ppm, of heterocompounds containing oxygen, nitrogen or sulfur. The naturally occurring compounds that provide jet fuel with its intrinsic lubricity can be removed by hydrotreating, the refining process employed to reduce aromatic content. Nevertheless, low sulfur or aromatics level are not necessarily indicative of inadequate lubricity since the boundary lubricity cannot be predicted from bulk physical or chemical properties but it can only be measured in an ASTM designed test apparatus known as Ball-on-Cylinder Lubricity Evaluator (BOCLE).

Another fuel property that plays an important role is the ‘fluidity’, the combination of viscosity and freezing point. Jet fuel specifications place an upper limit in viscosity to prevent excessive pressure drop in the fuel system and specially to assure the formation of a fine spray of droplets that evaporate quickly as they mix with air. More viscous fuels are also more difficult to relight in flight. Regarding freezing point, it is important to note that, being a mixture of hundreds of different compounds the jet fuel does not solidify at one temperature like pure substances. As the fuel is cooled down the hydrocarbons with highest freezing points solidify first forming wax crystals. The freezing point of the jet fuel is defined as the temperature at which the last wax crystal melts. The presence of wax crystals affects fuel ‘pumpability’ and the freezing point is an indicator of this low temperature characteristic. Typically a jet fuel remains pumpable some 4–15°C below its freezing point, thus making the fuel freezing a concern only in special cases, like polar route flights during the winter.

Also related to the fuel handling system is fuel’s volatility, characterized by vapor pressure and distillation curve. A volatile fuel is one that has higher vapor pressure and lower initial distillation temperature. However, a too volatile fuel may cause vapor lock in the fuel system as well as evaporative losses. This fuel property was the major

problem in early fuel formulations and to this day there is still a double standard: the widely used Jet A/A-1, a kerosene-type, relatively non-volatile fuel, and Jet B, a wide-cut fuel, better suited for cold weather applications because it has lower viscosity and freezing point and it is used when evaporative losses are less of a concern.

Taken together, these findings indicate how complex it is to attain desired properties and performance with acceptable emissions in a fuel obtained as ‘straight run’ as possible. Studies like those of Rosfjord (1984) demonstrate the nontrivial relationship between different compounds of the same hydrocarbon class and their effects on several fuel properties like ignition and soot propensity. A compromise between sophisticated combustion control, increased maintenance cost and broad specification fuels is the most likely middle to long term scenario. Moving on, alternative fuels will be discussed in the ensuing section.

## 2.3 ALTERNATIVE FUELS

Petroleum products have always been the preferred transportation fuels since they offer an optimal combination of availability, ease of handling, energy content, performance and, most of all, price. However, since the 1973 oil embargo, concerns about energy security and continued availability prompted government and industry to look at alternative sources.

In the case of aviation fuels the search for an alternative fuel is more complex for several reasons: (i) any alternative fuel must be compatible with conventional fuel so it can be transported and stored within the existing infrastructure; (ii) airlines keep their aircrafts in service for around forty years (BLAKEY *et al.*, 2011) so the alternative fuel must provide safe and reliable operation of engines and airframes with minimal increase in maintenance.

Another major issue is related to the energy content of the alternative fuel. First generation biofuels like alcohols and esters, already adopted in fuel blends for land transportation, contain oxygen which gives no contribution to fuel’s heating value. Table 2.6 presents a comparison of these energy ratings for conventional and alternative fuels.

As it can be seen in Tab. 2.6, Fischer-Tropsch (FT) and ‘hydroprocessed esters and fatty acids’ (HEFA) fuels are the alternatives

Table 2.6: Density, gravimetric energy and volumetric energy content of conventional and alternative fuels

Fuel	Density at 15°C, kg/l	Gravimetric Energy, MJ/kg	Volumetric Energy, MJ/l
Jet A/A-1	0.808	43.2	34.9
Methanol	0.796	19.9	15.9
Ethanol	0.794	27.2	21.6
Biodiesel	0.870	38.9	33.9
Fischer-Tropsch Synfuel	0.759	44.2	33.6
Camelina HEFA	0.751	44.1	33.1
Beef tallow HEFA	0.758	44.1	33.4

Source: Chevron - Alternative Jet Fuels, Addendum 1 (2006a); Corporan *et al.* - Energy & Fuels, Vol. 25 (2011)

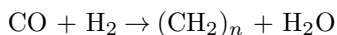
that more closely reproduce gravimetric or volumetric energy contents of conventional fuel. These similarities are not enough to immediately establish them as potential near or mid-term alternative fuels since experimental work by Corporan *et al.* (2011) revealed that alternative paraffinic fuels produced via FT or hydroprocessing of several feedstocks like beef tallow, yellow and brown grease and camelina oil, present inferior lubricity, lesser seal swelling and low density, which impacts aircraft range.

The following subsections discusses production, composition, properties and the tests carried out so far with some alternative fuel components.

### 2.3.1 Fischer-Tropsch synthetic fuels

The Fischer-Tropsch process was first developed by the German chemists Franz Fischer and Hans Tropsch in 1925. The FT process starts with the partial oxidation of the feedstock, usually coal or methane, in the presence of steam, oxygen and a catalyst to produce ‘syngas’, a mixture of carbon monoxide and hydrogen. Methane is the preferred carbon source since its capital cost is around 30% lower and also because in coal gasification the unwanted CO<sub>2</sub> formation is typically close to 50% while in methane reforming this yield is about 20%.

The obtained syngas is then converted into paraffinic hydrocarbons by employing iron or cobalt-based catalysts (DRY, 2002). Today two main FT operating modes are used: a high temperature (300–350°C) process with iron-based catalysts for the production of gasoline and linear, low molecular mass olefins; and a low temperature (200–240°C) process using either iron or cobalt catalysts to obtain high molecular weight linear waxes. The general reaction describing Fischer-Tropsch synthesis is



which occurs in a catalytic site and mostly produces straight chain alkanes, according to the Anderson-Schulz-Flory polymerization model (HUBER *et al.*, 2006). At each stage of growth, the adsorbed hydrocarbon may undergo: (i) hydrogenation followed by desorption thus forming primary FT products; (ii) addition of another CH<sub>2</sub> monomer to continue chain growth; (iii) desorption.

It must be stressed that many detailed mechanisms have been proposed to describe the FT synthesis but the matter remains controversial. Since FT always produces a wide range and amount of olefins, paraffins and oxygenates like ketones, alcohols and aldehydes, these appear to be primary products, even though, at the hydrogen's partial pressure, virtually all olefins should be hydrogenated to paraffins (DRY, 2002). Another important question is the process' selectivity, influenced by temperature, pressure, syngas H<sub>2</sub>/CO ratio, catalyst type and promoters.

According to Dry (2002), a FT plant employing iron catalysts and operating at 340°C is able to produce 40 % straight run, low octane and low aromatic gasoline, with additional 20 % yield of propene and butene that can be oligomerised to produce highly branched, high octane gasoline. However the straight run gasoline demands hydrogenation of its C<sub>5</sub>–C<sub>6</sub> cut while the C<sub>7</sub>–C<sub>10</sub> fraction needs severe reforming with platinum catalysts to enhance octane rating, making FT gasoline production less attractive than the diesel option.

The high linearity and low aromatic content that hamper the production of FT gasoline are very positive for producing high cetane diesel fuel. Using low temperature processes and cobalt catalysts to enhance wax production, 20 % straight run diesel is produced with a post-hydrotreatment cetane number of 75. Heavier than diesel products

account for nearly 50 % yield and, after a mild hydrocracking, a high quality, aromatic free diesel is obtained.

South African company Sasol pioneered the development of a synthetic FT jet fuel, when its iso-paraffinic kerosene (IPK) was included in the DEF STAN 91-91 Issue 3 (1999) as a 50 % by volume component for Jet A-1. According to Corporan *et al.* (2011) this coal-to-liquid (CtL) kerosene is produced via oligomerization of C<sub>3</sub> and C<sub>4</sub> olefins followed by hydrotreating and fractionation, producing a fuel with very high degree of branching. The composition of the Sasol IPK is around 85 % of C<sub>10</sub>–C<sub>14</sub> iso-paraffins, 11 % of C<sub>10</sub>–C<sub>13</sub> naphthenes and 4 % of C<sub>10</sub>–C<sub>12</sub> n-paraffins (EDWARDS *et al.*, 2010; BLAKEY *et al.*, 2011). In 2008, the Issue 6 of DEF STAN 91-91 was published with the certification of a fully synthetic jet fuel also developed by Sasol and, until 2009, Sasol IPK remained the only alternative to Jet A-1 in commercial use, fueling most of the aircraft leaving O.R. Tambo International Airport in Johannesburg.

Since then, Shell, Syntroleum and Rentech also developed FT kerosene fuels but using gas-to-liquid (GtL) processes, a pathway adopted by Sasol in its Oryx plant in Qatar. These GtL kerosenes do not present a naphthenic fraction, with Shell's fuel being close to a 75/25 blend of C<sub>8</sub>–C<sub>12</sub> branched and linear paraffins whilst Syntroleum and Rentech ones are 78 iso-/22 n- mixtures of C<sub>8</sub>–C<sub>16</sub> paraffins.

Even with the certification of Sasol's IPK, a test programme called Aircraft Alternative Fuel Emissions eXperiment (AAFEX) (ANDERSON *et al.*, 2011) was conducted by NASA in 2009 to evaluate gaseous and particulate emissions of standard JP-8, Shell GtL, Sasol CtL and 50/50 blends of each FT fuel with JP-8. The measurements were carried out in two CFM56-2C1 engines of a parked McDonnell Douglas DC-8 owned by NASA's Dryden Flight Research Center (now Neil A. Armstrong Flight Research Center). In the study, it was observed that burning FT fuel did not affect engine performance thus not offering advantage or penalty in terms of fuel economy. However the alternative fuels exhibited higher combustion efficiencies at low power settings, therefore indicating a general trend of being less polluting. When the 50/50 blends were burned, no significant reduction in certification gas emissions was obtained, pointing out a clearly relationship between aromatic content and emissions.

The test also showed that the aromatic-free FT fuels caused fuel-system seals to shrink, resulting in fuel leaks in the aircraft tank and in

the tanker trucks used to store and deliver them. The leaks went away with the addition of JP-8, which presents an intrinsic aromatic fraction. This result is in accordance with previous studies (GRAHAM *et al.*, 2006; CORPORAN *et al.*, 2007; DEWITT *et al.*, 2008) where Syntroleum's GtL fuel and different aromatic solvents were tested regarding material compatibility with nitrile rubber. Other engine performance tests were conducted by the US Air Force to study Syntroleum and Shell GtL fuels, and their blends with JP-8, in several transport and fighter platforms (BLAKEY *et al.*, 2011) with only beneficial impacts being observed with the use of these FT blends.

Considering the several tests reported above, it is safe to assert that alternative FT fuels are suitable as 'drop-in' replacements for conventional Jet A/A-1, once they are corrected for density and heating value, i.e. present a minimum aromatic content that also prevents fuel leaks.

### 2.3.2 Biofuels

Biofuels, as the name implies, are fuels derived from living organisms such as microalgae, plants and animals. Different components in the biomass can be converted in liquid fuels: starch and sugar are converted in alcohol by fermentation; edible and nonedible oils and fats are used to produce fatty acid esters and hydrotreated oils; and new processes for the conversion of lignocellulose are emerging. Although these sources present great energy potential, many problems regarding their production and quality remain unsolved.

As pointed out previously, the adoption of alcoholic biofuels in aviation is unlikely considering their low gravimetric energy content, as seen in Tab. 2.6. Hence, the remaining biofuels to be considered currently are fatty acid esters (FAE) and hydrotreated oils. Fatty acid esters, also commonly referred to as biodiesels, are long chain groups derived from transesterification of triglyceride fats in the feedstock, usually a vegetable oil. The transesterification is the most common way of upgrading vegetable oils (HUBER *et al.*, 2006) to avert their intrinsic disadvantages like high viscosity, low volatility and coking propensity. Figure 2.1 presents a generic transesterification reaction with ethanol.

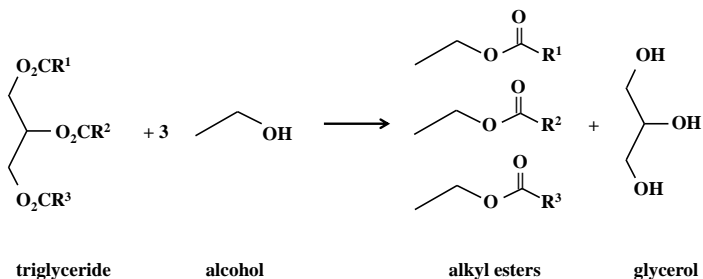


Figure 2.1: Generic transesterification reaction

Figure 2.1 does not show the presence of a catalyst in the reaction but most of the industrial biodiesel plants conduct the transesterification with alkali catalysts, usually sodium methoxide (HUBER *et al.*, 2006), since the uncatalysed reaction only occurs at elevated pressure and temperature, e.g. 120 atm and 350°C, thus being highly energy intensive. There is much ongoing research to develop new catalysts, specially heterogeneous ones, that could be easily removed from the product and recycled.

The composition of the alkyl groups, denoted by ‘R’, in the resulting esters varies according to the feedstock in terms of number of carbons and presence of carbon-carbon double bonds. Table 2.7 shows the chemical composition of fatty acids present in several oil crops.

From the data in Tab.2.7 one can see some of the reasons why vegetable-derived fuels demand further processing to be compatible with conventional jet fuel. Coconut, macaw palm kernels, palm, and olive oils are the only feedstocks that provide significant amounts of fatty acids with carbon chains similar to kerosene, i.e. up to 15 carbons. Most of the vegetable oils are primarily composed by carbon chains with 16 or 18 carbons, much of the latter presenting unsaturations, therefore the preference of using them to obtain biodiesel.

A process like pyrolysis or zeolite upgrading, that could be employed before or after the transesterification, can eliminate the ester group as CO<sub>2</sub> and also promote the cleavage of the long alkyl chain to form smaller paraffins, olefins, naphthenes and aromatics by Diels-Alder reaction (HUBER *et al.*, 2006). Though technically possible, the transesterification followed by an upgrading would hardly be commer-

cially viable.

Regarding test programmes and flight demonstrations, Blakey *et al.* (2011) reports several such initiatives, conducted by airlines, manufacturers and the military during the 2007-2010 span and it is remarkable that the use of FAMEs was restricted to a single test by Virgin Atlantic. In February 23<sup>rd</sup> 2008, during a 45-minute flight between London and Amsterdam, one of the four GE CF6-80C engines of a Boeing 747-400 was fueled with a blend of 80% Jet A-1 and 20% fatty acid methyl ester from coconut and babassu palm oil. Regardless the successful demonstration, Boeing issued a disclaimer stating that the FAME used was the only suitable fuel available at the time and that it did not consider FAMEs a viable option for aviation.

Table 2.7: Chemical composition of fatty acids in biodiesel feedstocks

Oil or fat	fatty acid composition, % weight									
	number of C : C=C bonds									
	8:0	10:0	12:0	14:0	16:0	18:0	18:1	18:2	18:3	22:1
babassu <sup>a</sup>	2.6-7.3	1.2-7.6	40.0-45.0	11.0-27.0	5.2-11.0	1.8-7.4	9.0-20.0	1.4-6.6		
camelina <sup>b</sup>					0.0-6.4	0.0-2.8	14.1-19.5	18.8-24.0	27.0-34.7	0.0-4.0
canola					1.2-6.0	1.0-2.5	52.0-66.9	16.1-31.0	6.4-14.1	1.0-2.0
coconut	4.6-9.5	4.5-9.7	44.0-51.0	13.0-20.6	7.5-10.5	1.0-3.5	5.0-8.2	1.0-2.6	0.0-0.2	
corn				0.0-0.3	7.0-16.5	1.0-3.3	20.0-43.0	39.0-62.5	0.5-13.5	
cotton-seed				0.6-1.5	21.4-26.4	2.1-5.0	14.7-21.7	46.7-58.2		
jatropha <sup>c</sup>					12.1-17.0	2.9-9.7	34.0-50.1	29.1-41.6		
macaw kernel <sup>d</sup>	3.7	2.8	32.6	9.2	8.2	2.2	36.2	3.8		
macaw pulp <sup>d</sup>			0.4	0.4	24.6	1.1	52.6	13.8	2.3	
olive			0.0-1.3	7.0-20.0	0.5-5.0	55.0-84.5	3.5-21.0			
palm		0.0-0.4	0.5-2.4	32.0-47.5	3.5-6.3	36.0-53.0	6.0-12.0			
peanut				0.0-0.5	6.0-14.0	1.9-6.0	36.4-67.1	13.0-43.0		0.0-0.3
rapeseed				0.0-1.5	1.0-6.0	0.5-3.5	8.0-60.0	9.5-23.0	1.0-13.0	5.0-56.0
soybean					2.3-13.3	2.4-6.0	17.7-30.8	49.0-57.1	2.0-10.5	0.0-0.3
sunflower					3.5-7.6	1.3-6.5	14.0-43.0	44.0-74.0		
tallow (beef)				2.1-6.9	25.0-37.0	9.5-34.2	14.0-50.0	26.0-50.0		

Sources: Huber *et al.* - Chem. Rev., Vol. 106 (2006); <sup>a</sup>Hong *et al.* - Chem. Eng. Process: Process Intens., Vol. 74 (2013); <sup>b</sup>Budin *et al.* - J. Am. Oil Chem. Soc., Vol. 72 (1995); <sup>c</sup>Achten *et al.* - Biomass Bioenergy, Vol. 32 (2008); <sup>d</sup>Coimbra & Jorge - J. Food Sci., Vol. 76 (2011)

After this pioneering flight and following the introduction of biodiesel as a blend in conventional diesel for road transport in England, a problem with FAE contamination of jet fuel ensued due to the concurrent transport infrastructure. Since there is a carry through of contaminants, such as metals, from the raw oil into the FAE, the presence of typical contaminants of biodiesel, like zinc, nickel and vanadium, in jet fuel could cause severe damage to the hot end materials in the turbine. According to Blakey, a contamination of 30 ppm of FAE in jet fuel is already accepted and the industry is working towards a 100 ppm limit.

Another type of biofuel is upgraded oil by hydrotreatment. The triglycerides present in oils and fats can be hydrotreated in a way similar to the latter stages of conventional refinery and Fischer-Tropsch processes thus promoting deoxygenation, saturation, hydrocracking and isomerization of the alkyl chains. Many different sources of triglycerides could be harnessed this way, like algae, animal fats, brown and yellow grease, camelina and jatropha. These two plants, camelina and jatropha, play an important role in the near to mid-term development of these HEFA fuels, since camelina is an oil crop well established in some US states like Montana, Idaho and North Dakota for its use in biodiesel production, while jatropha is able to grow under drought conditions and in sandy soils that are otherwise unused for farming, therefore presenting strong sustainability and social responsibility appeal. However many critics are raising doubts about the effective oil yield of jatropha in low-quality soils and the likely competition between food and this oil crop in developing countries.

Although being a technology at a lower readiness level, hydroprocessing was used to produce fuel for many test flights, with the advantage that the resulting fuel looks very similar irrespective of the feedstock. The hydrotreating process branded “Ecofining”, developed by Honeywell’s subsidiary UOP, yields a synthetic paraffinic kerosene (SPK) with around 85 % iso and 15 % n-paraffins in the C<sub>9</sub>–C<sub>15</sub> range, with high amounts of C<sub>10</sub> and C<sub>11</sub> compounds (BLAKEY *et al.*, 2011; CORPORAN *et al.*, 2011). According to Meeks *et al.* (2011), albeit high in iso-paraffins, these are much less branched compared to gasoline or diesel, usually containing only one methyl branch in a long-chain alkane, thus its effect is of little importance.

Regarding hydrotreated oil testing, it is possible to draw a parallel between airline efforts and military/manufacturer work. Tests flights conducted by Air New Zealand, Continental (now United) Air-

lines, Japan Airlines and KLM/Air France favored the use of HEFA fuels made from algae, camelina and jatropha oils. The HEFA fuels were blended with Jet A/A-1, in amounts up to 50 %, and usually fueled one engine of the aircraft, thus allowing the study of engine relight and overall performance parameters such as fuel consumption. The results of these test flights were mostly qualitative, with Air New Zealand claiming a potential fuel saving of 1.2 % with its jatropha HEFA, which is in accordance with the data from UOP showing an energy content of 44.3 MJ/kg for this HEFA compared to 42.8 MJ/kg in Jet A-1 specification.

On the other hand, the US Air Force and US Navy, accompanied by manufacturers Boeing and Pratt & Whitney, elected HEFA fuels made from camelina and animal fats for their tests, that included engine performance, gaseous and particulate emissions (BLAKEY *et al.*, 2011). At first, all HEFA fuels produced less particulate matter, which is expected due to the absence of aromatic compounds. In fuel blends, an increase in aromatic content and molecular weight resulted in a decrease in combustion efficiency, hence increasing carbon monoxide and unburned hydrocarbon emissions. The CO<sub>2</sub> and H<sub>2</sub>O emissions are mostly related to the H/C ratio, hence the heating value, of the fuel, with HEFAs presenting hydrogen to carbon ratio above 2.0 while for conventional jet fuel this value is usually 1.95 or below. Finally, the nitrous oxide emissions, related to a combination of high temperature and residence time, are effectively dependent of the control system that drives the engine to a constant turbine inlet temperature.

Among other emerging process that yield renewable fuel candidates Amyris Biotechnologies has developed a yeast fermentation procedure that converts biomass materials through the isoprenoid metabolic pathway into farnesene isomers (RENNINGER; MCPHEE, 2010). Subsequent hydrogenation produces an entirely pure enantiomeric mixture of farnesane (2,6,10-trimethyl dodecane) which has been used as both an alternative diesel and aviation fuel in mixtures up to 10 %, with certification tests using mixtures up to 20 %.

Blakey *et al.* (2011) concluded that an effective performance comparison between alternative and conventional fuels is hampered by the variable and extensive composition of Jet A/A-1 and JP-8. The authors also emphasize the need for a description of how the ratio of iso, normal and cyclic paraffins affect engine operation and material compatibility, as well as an extension of such model to aromatics.

## 2.4 CONCLUDING REMARKS

This chapter has given an account of the historical development of jet fuel, the current state of its specification, and descriptions of its properties and performance due to each different class of hydrocarbon present. The chapter also presented information about alternative fuels for aviation, describing feedstocks, production processes as well as the test programmes and flight demonstrations carried out so far. Many important conclusions can be drawn from this overview.

Since its origin as avgas and illuminating kerosene, jet fuel evolved from an early definition based on distillation curve and vapor pressure to a complex description involving flash point, freezing point, maximum aromatic and naphthalenic content and so on. Successive developments of jet engines revealed the importance of trace amounts of heterocompounds in phenomena like boundary lubrication, thermal stability and fuel coking while different qualities of crude oil influenced its availability and the development of processes to upgrade the distillate, therefore, affecting the bulk composition and price.

This overview emphasizes the extensive requirements jet fuels are expected to meet. Besides giving off its heat of combustion to propel the aircraft, the fuel must lubricate moving parts in the fuel pumps and fuel metering units as well as provide cooling to engine and airframe lubricants. It cannot be too volatile at room temperature and low pressures due to the risk of vapor lock in the fuel system and also cannot be too viscous in the freezing temperatures of flight altitude. Even before being fueled to the aircraft, it must be safe and stable to transport and to store, and all these requirements influence its composition. Another major conclusion is the trade off between bulk composition, fuel properties and combustion performance, with the relationship between H/C ratio and aromatic content being of crucial importance.

Compared to Jet A, a fuel composed solely of branched paraffins would present higher heat of combustion per unit mass and higher H/C ratio, resulting in less emissions and increased aircraft range, but its volumetric energy content would be poor, thus aircraft range would in fact diminish. A pure aromatic fuel would also decrease aircraft range, since the gravimetric energy content of this hydrocarbon class is lower, and moreover would be very prone to extinction and would produce inadmissible amount of particulate and gaseous emissions. Other fuel properties also affected by bulk amounts of each hydrocarbon class

are freezing point, hence low-temperature fluidity, which is related to naphthenes, and nitrile rubber seal swelling, linked to aromatic content.

Also noteworthy is how the intrinsic complexity of an oil-derived product influences the search for alternative fuels composed by a handful of components, specially regarding combustion performance. The presence of hundreds, if not thousands, of different hydrocarbons in the fuel is responsible for its smooth distillation curve and the interaction between each hydrocarbon class affects kinetics and fluid dynamic phenomena like ignition, lean blow-off and relight. While conventional fuel comprises several isomers of the same compound with different degrees of branching, the specificities of alternative fuel production usually produce only one to three isomers. Moreover, problems emerge when considering substituted aromatics with long alkyl chains, e.g., *n*-decylbenzene, because it is difficult to predict if the kinetic behavior favors its aromatic or aliphatic character.

First generation alternative fuels like biodiesel are composed by long chain fatty acid esters, with esters varying according to the number of carbons and degree of unsaturation, thus being reminiscent of linear paraffins. Hydroprocessed esters and fatty acids (HEFA) fuels, a second generation biofuel, comprise a larger variety of molecules since they include linear and branched paraffins of shorter lengths, therefore being a more likely near and mid-term alternative to conventional jet fuel. Fischer-Tropsch fuels, either from coal or natural gas, are already produced in industrial scale and their composition includes linear, branched and, depending on the hydroprocess, even cyclic paraffins. As of today, these alternative fuels still require a blending with conventional fuel to provide a minimum aromatic fraction that ensures seal swell.

However, a more focused search for alternative fuels has been limited by the lack of an appropriate description of the conventional jet fuel in terms of the role of each hydrocarbon class and expected properties. Therefore, the ensuing chapter will introduce the concept of surrogate fuels and their importance to combustion and chemical kinetics studies.

### 3 SURROGATE FUELS AND MODELING

The previous chapter presented an overview of the specifications of conventional jet fuels, the influence of each hydrocarbon class in its properties and performance, and also descriptions about the production of alternative fuels, namely Fischer-Tropsch products and biofuels. This chapter comprises a brief historical perspective of the development of surrogate fuels followed by a review of experiments and chemical kinetics studies of jet fuels carried out since the publication of an extensive review by Dagaut & Cathonnet (2006) and a “findings and recommendations” article by Colket *et al.* (2007).

#### 3.1 GENERAL CONSIDERATIONS

Earlier experimental studies by Lohmann & Jeroszko (1983) and Rosfjord (1984), conducted with NASA and US Air Force sponsorship, employed test fuels prepared by a combination of some conventional fuel (JP-4, JP-8, Jet A) with specialty petrochemical products like ‘blending stocks’, xylene tower bottoms, decalin, tetralin and iso-paraffinic solvents, in order to assess fuel property effects on combustion. However, unexpected results, such as a decrease in viscosity and distillation temperatures with higher aromatic content, proved this broad analysis of fuels hapless due to the mosaic composition of the starting components. Therefore the need for an adequate description of transportation fuels using ‘surrogates’ emerged.

The term surrogate fuel first appeared in a work by Wood *et al.* (1989) in which complex, 14-component blends of hydrocarbons were used in an attempt to match JP-4 and JP-5 boiling range, atomization quality and combustion behavior. Since then surrogate fuel definition evolved to cover simpler mixtures of hydrocarbons, adequate to computational fluid dynamic (CFD) studies, as well as more elaborate blends to emulate either chemical, physical or combustion properties of real fuels in detailed chemical kinetics and experimental investigations. A surrogate fuel is usually defined in terms of the number of chemicals in its composition and relative to ‘targets’, the kind of measurable that is expected to mimic. There are three main types of targets, in order of increasing complexity: property targets, development targets and application targets (FARRELL *et al.*, 2007).

A property target refers to chemical and physical fuel properties, like hydrogen to carbon ratio and distillation curve, respectively. A one-component surrogate could be able to match overall H/C ratio of a real fuel but other physical properties, like flash point and viscosity, depend on the interaction of different hydrocarbon classes. Matching more than one property target is usually not possible, or even desirable, with less than a handful of components.

Development targets are kinetic and fluid dynamic phenomena important for validating fuel behavior that are typically evaluated in experiments with well controlled conditions like ignition delay time (IDT) in shock tubes (ST), species evolution in flow reactors or multi-component spray vaporization. The controlled conditions of these experiments involve extensive instrumentation and careful handling of reactants and products, thus allowing studies that include effects of pressure, temperature and trace composition. These development targets are closer to the intended application and the phenomena studied usually involves complex interactions between species and molecular-level transport coupling, therefore studies with a simple, one-component surrogate are unlikely.

Application targets are measurements obtained from engine tests in transient and steady-state operation, such as combustion efficiency, gaseous and particulate emissions. These tests are similar to certification protocols with the surrogate going through the entire fuel system to the engine and exhaust, therefore providing conditions such that issues with material compatibility, fuel coking, lubricity and others may arise. These assessments also have a wide scope, considering the very nature of atmospheric conditions such as relative humidity, temperature and pressure.

Among the many possible targets, the Jet Fuel Working Group (COLKET *et al.*, 2007) identified some of the more relevant kinetically-controlled phenomena that, at the time, deserved special attention in near term studies. Table 3.1 shows these high priority objectives and the conditions at which they should be evaluated.

The data in Tab. 3.1 shows temperatures and pressures encompassing a broad domain, considering different jet engine technologies and generations. It must be clear that many experiments, like measurements of burning velocity and extinction strain rates, are conducted at pressures well below those of turbines so facility results need to be extrapolated to engine conditions. The table includes laminar flame

speed tests that are traditionally employed to check high-temperature flame response, but evidences indicate that phenomena governing flame speed and extinction are different (HOLLEY *et al.*, 2006) hence an agreement in laminar flame speed between real fuel and surrogate should not be given too much significance since their extinction response can greatly differ.

Therefore thorough study of surrogate fuels must include testing of individual components for kinetics mechanisms as well as zero-dimensional, e.g. shock tubes and flow reactors, and one-dimensional experiments, e.g. stagnation flow flames, of proposed surrogates. Also, validation data on individual components is necessary to distinguish errors due to ill-conceived surrogate compositions from errors due to mechanistic limitations. Having defined the main purpose and uses of surrogate fuels, the following section discusses which chemical compounds are indicated as relevant to jet fuel surrogate formulations and the amount of information available on their thermophysical properties and oxidation mechanism.

### 3.2 COMPONENTS AND FORMULATIONS OF JET FUEL SURROGATES

According to Colket *et al.* (2007), while gasoline and diesel have ‘standard’ components, chosen regarding their ignition behavior, jet fuels lack such composition reference. This should not be unexpected since gas turbine engines are more tolerant to variations in fuel composition than piston engines. For gasoline, the octane rating, which indicates fuel’s resistance to detonation, is defined based on the ignition

Table 3.1: Kinetics limitations for jet fuels in gas turbine engines

Issue	Experiment or Measurable	Equiv ratio $\phi$	Inlet temp K	Turbine pressure atm
Heat release rate	flow reactor	limits	350–900	0.3–35
Fuel type effect	sensitivity	limits	350–1100	0.3–35
Flame propagation	laminar flame speed	limits	350–1100	0.3–35
Flame stability	extinction strain rate	limits	350–1100	0.3–6.0
Soot formation	PAH	1.5–3.0	600–900	10–35
NOx emission	H/C ratio		450–900	4.0–35

Source: Colket *et al.* - 45th AIAA Aerospace Science Meeting and Exhibition (2007)

properties of n-heptane and 2,2,4-trimethylpentane, also known as iso-octane. For diesel the ignition propensity is evaluated with the cetane number scale, which is gauged with binary mixtures of n-hexadecane, also called n-cetane, and 2,2,4,4,6,8,8-heptamethylnonane, also known as iso-cetane. The definition of distillate reference jet fuels, with firmly controlled physical properties but varying composition, proved to be ill-fated, given their tendency to degrade during long-term storage (BOWDEN; ERWIN, 1983).

Under the auspices of NASA and the US Air Force, a series of tests conducted in the early 1980's (BOWDEN; ERWIN, 1983; LOHMANN; JEROSZKO, 1983; ROSFJORD, 1984) indicated that, for those engines, fuel's physical properties, rather than chemical ones, were dominant factors in most aspects of engine performance. Chemical attributes, like overall H/C ratio and hydrogen content, were deemed important in soot-related phenomena like smoke emissions and combustor liner heating. Also, combustors with very fuel-rich primary zones seemed to be most sensitive to the fuel composition effects on soot, even though the impact on particle size distribution was not studied at the time, an issue that has been addressed in recent works.

New turbine engines are operating closer to fuel's stability limits, thus being likely to exhibit stronger composition sensitivity and the adoption of partial premixing raises concerns regarding stability and auto-ignition characteristics. Some of the composition limitations already present in jet fuels include maximum aromatic content of 25 % vol, maximum naphthalene content of 3 % vol, and for JP-8 there is also a minimum hydrogen content of 13.4 % mass.

In recognition of the great uncertainty in this field, the National Institute of Standards and Technology (NIST) held a workshop on Combustion Simulation Databases for Real Transportation Fuels in September 2003 (TSANG *et al.*, 2003). Following the event, three working groups, for gasoline, jet fuel and diesel respectively, were created to draw coherence to the effort of defining a palette of surrogate compounds. Four years later these groups reported their advances in three conference papers (PITZ *et al.*, 2007; COLKET *et al.*, 2007; FARRELL *et al.*, 2007) from which it is possible to recognize hydrocarbons that are relevant to each fuel and the amount of information available regarding thermophysical and transport properties as well as understanding their oxidation chemical kinetics. Table 3.2 presents this information in qualitative terms as follows:

- ‘A’ denotes high relevance to the fuel; detailed and validated mechanism over a wide range; dependable thermophysical and transport properties data in terms of correlations or equations of state (density within .3 %, viscosity and thermal conductivity 5 %).
- ‘B’ denotes reduced yet important relevance to the fuel; mechanism validated with modest limitations; sufficient thermophysical and transport properties data for model (density within 3 %, viscosity and thermal conductivity 5-10 %).
- ‘C’ denotes possible but not crucial component; mechanism reported with major limitations; limited thermophysical and transport properties data for model.
- ‘D’ denotes no mechanism reported; extremely limited or no experimental thermophysical and transport properties data, only predictive model.
- ‘F’ denotes no relevance to the fuel; no thermophysical and transport properties data or predictive model available.

Table 3.2: Applicability of components for surrogates of transportation fuels

Compound	Relevance to real fuel			Understanding of mechanism		Property information	
	gasoline	jet fuel	diesel	low & mid temp	high temp	thermophysical	transport
n-heptane	A	B	B	A	A	A	A-
n-decane	F	A	B	B	A-	A	A
n-dodecane	F	A	B	B	B	A	A
n-tetradecane	F	A	B	B	B	B+	B
n-cetane	F	B	A	C	C	B+	B
i-octane	A	B	C	A-	A	B+	B
i-cetane	F	B	A	C	C	B-	C+
methylcyclohexane	C	B	C	C	C	B+	B
propyl/butylcyclohexane	C	A	B	D	D	B	C
decalin	F	B	B	D	D	B	B-
toluene	A	C	A	C	C	A	B+
propyl/butylbenzene	C	A	B	C	C	B	B
1-methylnaphthalene	C	B	C	C	C	B	C

Sources: Pitz *et al.* - 2007 SAE World Congress (2007); Colket *et al.* - 45th AIAA Aerospace Science Meeting and Exhibition (2007)

It can be seen from the data in Tab. 3.2 that, as late as 2006, only linear alkanes and one branched alkane received sufficient study to allow reliable modeling of their combustion, while mechanisms for naphthenic and aromatic compounds lack wide validation. The amount of data regarding paraffins showed broad behavior variation between isomers, e.g., branched alkanes are much more difficult to ignite than linear ones while soot formation follows the opposite trend, with normal paraffins having the lowest tendency to produce particulates.

Colket *et al.* points out some issues regarding the definition of the representative compounds listed on Tab. 3.2. Odd numbered alkanes larger than n-heptane are usually not listed, specially since the amount of experimental data on such molecules is very scarce, even though an odd alkane may yield a greater number of odd carbon fragments that could affect soot formation pathways. Also relevant are recent results (SHAFER *et al.*, 2006; MOSES, 2008; DOOLEY *et al.*, 2012b; WON *et al.*, 2014) indicating that jet fuel is better approximated by alkanes with one or two branches, instead of highly-branched molecules like iso-cetane. However, highly-branched alkanes and linear ones are much more affordable as surrogate compounds since the price of pure weakly-branched molecules is around one dollar per milligram.

Another important question is related to the use of prevaporized fuel in the studies, which presumes surrogate efforts focused on chemical rather than physical properties like boiling range. The prevaporized approach allows the definition of simpler surrogate blends of fewer components, for which both mechanisms and validation limits could be reasonably established, thus meeting ‘property’ and ‘development’ targets. However, such course of action is unlikely to yield a surrogate to meet ‘application’ targets as indicated in previous studies. Colket *et al.* highlight that the relaxation of the boiling range constraint may prove to be an important simplifying assumption to allow near term progress on the development of reaction kinetics models.

Since the earlier studies with surrogate fuels, it was common practice to select one or more ‘reference fuels’ from each hydrocarbon class and adjust its proportions to match desired real fuel properties. In such fashion, many surrogate formulations were proposed, usually with one of two constraints in mind: ‘physical’ surrogates, presenting smooth boiling curve which resulted in the formulation of blends with six up to fourteen components; or ‘chemical’ surrogates focused on H/C ratio and hydrocarbon classes, then ranging from one up to six compounds. Table

3.3 presents the composition of three well known surrogates formulated with this approach (Utah/Yale, Aachen and Drexel/S5) as well as post-2007 surrogates that will be detailed in the following section.

The six-component Utah/Yale surrogate has two aromatic species in order to match jet fuel's volatility and smoke point; the simple, binary Aachen surrogate is focused on kerosene's overall H/C ratio and autoignition characteristics but also has similar heat of combustion and molecular weight; and the Drexel/S5 surrogate was formulated to mimic JP-8's low temperature reactivity even though it has lower H/C ratio (1.807) and higher molecular weight (159.2 g/mol).

These surrogates were proposed by different groups aiming particular emulations and were tested in different experiments thus their experimental results are less likely to provide valuable information to each other. Considering such scenario, the formation of the Surrogate Fuels Working Group and its collaboration with the US Air Force provided some common ground for the investigation of surrogates in the United States with the adoption of reference fuel samples. The ensuing section presents the experimental and modeling results, subdivided according to these fuel samples.

Table 3.3: Summary of the composition of surrogate mixtures for jet fuels

Compound	Utah/Yale volume %	Aachen weight %	Drexel/S5 volume %	MURI 1 mol. %	MURI 2 mol. %	Humer/UCSD vol. %	UM1 mol. %	UM2 mol. %
iso-octane				33.02	29.5			
n-decane		80		42.67				
n-dodecane	30		26		40.4	60	38.44	28.97
n-tetradecane	20							
iso-cetane	10		36				14.84	14.24
methylcyclohexane (MCH)	20		14			20	23.36	
decalin			6					31.88
toluene				24.31			23.36	24.91
<i>o</i> -xylene	15					20		
1,2,4-trimethylbenzene (TMB)		20						
1,3,5-trimethylbenzene (TMB)					7.3			
n-propylbenzene	5				22.8			
tetralin	5							
$\alpha$ -methylnaphthalene			18					

Sources: Humer *et al.* - Proc. Comb. Inst. Vol. 31 (2007); Honnet *et al.* - Proc. Comb. Inst. Vol. 32 (2009); Dooley *et al.* - Combust. Flame Vol. 157 (2010); Dooley *et al.* - Combust. Flame Vol. 159 (2012a); Kim *et al.* - Combust. Flame Vol. 161 (2014)

### 3.3 EXPERIMENTS WITH REAL FUELS AND SURROGATES

The kinetics of aviation kerosene ignition and oxidation was previously reported in the literature (DAGAUT; CATHONNET, 2006). Tables 3.4-3.6 summarize the available data published after the Jet Fuel Surrogate Working Group paper (COLKET *et al.*, 2007) and comprises experimental studies with real fuels and recently proposed surrogates including test techniques and a brief report of results.

In their recommendations for the ongoing research effort, Colket *et al.* (2007) mentioned the willingness of the US Air Force to provide research quantities of ‘standard’ fuels to the academic community. These fuels were labeled ‘POSF (Properties of Sample Fuel) 4-digit number’ and were obtained from multiple conventional and alternative sources. One of these fuels was a ‘Composite Jet A’ made by mixing equal volumes of Jet A from five different US refiners and it received the designation POSF 4658. This fuel comprises 36.7 % i-alkanes, 25.6 % naphthenes, 19.0 % aromatics and 18.7 % n-alkanes by volume (average formula  $C_{10.17}H_{19.91}$ , H/C ratio of 1.957) and was widely adopted. Some authors tested it in order to propose surrogates and detailed chemical kinetics for computational modeling whilst others performed tests with both real fuel and existing surrogates to achieve different objectives. The following subsections present the recent experimental and modeling studies with POSF 4658, different samples of JP-8 and kerosenes produced from alternative sources.

#### 3.3.1 Experiments with Jet A POSF 4658

Studies with POSF 4658 kerosene included ignition delay time behind reflected shock wave and also in rapid compression machine (RCM). It can be seen from the data in Fig. 3.1 that three sets of measurements around 20 atm are in good agreement: shock tube experiments reported by Dooley *et al.* (2010), that include the negative temperature coefficient (NTC) region of the fuel; shock tube data from Stanford Vasu *et al.* (2008), Vasu *et al.* (2009) for the high temperature ignition; and RCM data also reported by Dooley *et al.* (2010) for the low temperature region.

The NTC region is the intermediate temperature range, approximately between 700-850 K, in which the reactivity of linear alkanes

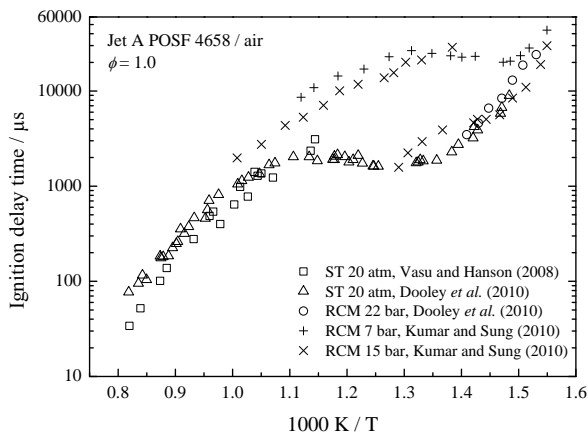


Figure 3.1: Compilation of POSF 4658 ignition delay times

decreases with increasing temperature. This phenomena occurs mainly due to a change in the equilibrium of reactions  $R + O_2 \rightleftharpoons RO_2$ , which favors  $RO_2$  at lower temperatures but shifts to favor alkyl radicals  $R$  at higher temperatures. Also governing the negative temperature coefficient behavior are radical propagation pathways at intermediate temperature, like  $HO_2$  elimination from  $RO_2$ ,  $\beta$ -scission of  $\dot{Q}OOH$ , and cyclic ether formation from  $\dot{Q}OOH$  (BATTIN-LECLERC, 2008). The RCM measurements of Kumar & Sung (2010a), Kumar & Sung (2010b) at 15 bar and 650-770 K show order-of-magnitude variations, with some ignition delays similar to shock tube data from Dooley *et al.* and others ten times longer, agreeing with RCM data at 7 bar.

While Vasu *et al.* (2008), Vasu *et al.* (2009) found good agreement in the ignition delays of the kerosene and pure n-dodecane, Dooley *et al.* (2010) obtained similar consistency with a 42.7 % n-decane, 33.0 % iso-octane, 24.3 % toluene (by mol.) surrogate (MURI 1, average formula  $C_{8.61}H_{17.27}$ , H/C ratio of 2.006). The former studies showed that ignition delays were shorter for stoichiometric cases compared with leaner ones while the latter work revealed that even though the overall ignition delays were similar, the quality of ignition between real fuel and surrogate differ markedly, with the surrogate presenting no first-stage ignition and higher post ignition pressure rise. Figure 3.2, taken from the supplementary material of Dooley *et al.* (2010) exhibits this

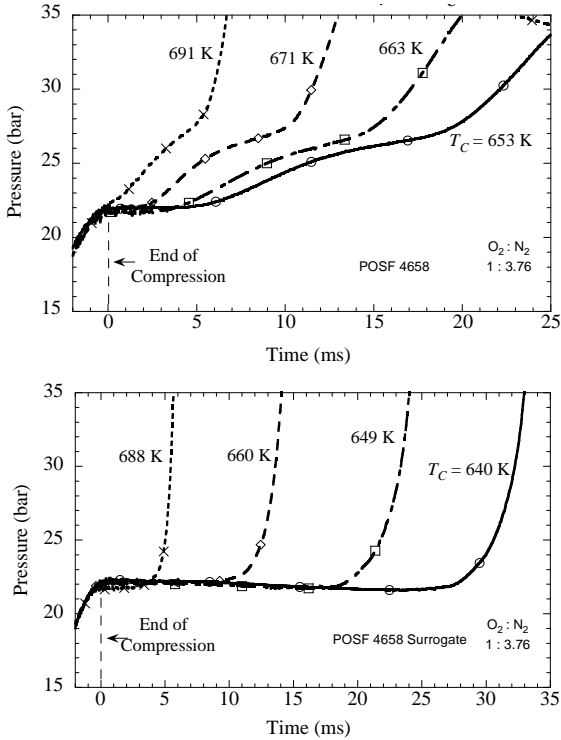


Figure 3.2: Pressure traces of RCM experiments with Jet A POSF 4658 (top), and surrogate MURI 1 (bottom), showing the absence of first-stage ignition in the latter - Source: Dooley *et al.* - Combust Flame Vol. 157 (2010)

difference in pressure-time history.

The results of Kumar & Sung (2010a), Kumar & Sung (2010b) reinforce the strong two-stage ignition and NTC behavior of the real fuels Jet A and JP-8, with first-stage ignition being sensitive to compressed temperature only while equivalence ratio seems to be determinant to second-stage, thus overall, ignition delay.

Table 3.4: Available experimental kinetics data for Jet A POSF 4658 since 2007

Technique	Fuel	Conditions	Data type and comments	Reference
Shock tube	Jet A POSF 4658, JP-8 and n-dodecane	Ignition delay times at 17-51 atm, 715-1229 K and $\phi=0.5/1$	Ignition measured by sidewall pressure and OH* emission	Vasu <i>et al.</i> (2008), Vasu <i>et al.</i> (2009)
Opposed jet burner	Jet A POSF 4658, pure components and surrogates 80%/60% n-decane 20%/40% 1,2,4-TMB (vol.)	Extinction strain rates as a function of pressure at stoichiometric fuel/oxidizer flow rates	Pressure measured by capacitance manometer; best agreement with real fuel for 60% n-decane 40% TMB surrogate	Dattarajan <i>et al.</i> (2009)
Counterflow flame	Jet A POSF 4658, Aachen and Utah/Yale surrogates	Ethylene flames doped with liquid fuels under incipiently sooting conditions, strain rate of $92 \text{ s}^{-1}$	Mole fractions profiles as function of distance to the fuel inlet; GC/MS of C <sub>7</sub> -C <sub>15</sub> alkanes, C <sub>3</sub> -C <sub>6</sub> alkanes and alkenes, C <sub>2</sub> HCs and aromatics	Jahangirian <i>et al.</i> (2009)
Flow reactor	Jet A POSF 4658 and MURI 1 surrogate 42.67% n-decane, 33.02% isooctane and 24.31% toluene (mol.)	Oxidation of stoichiometric mixtures at 12.5 atm, 500-1000 K and reaction time 1.8 s	Fuel reactivity indicated by CO, CO <sub>2</sub> concentration	Dooley <i>et al.</i> (2010)
Counterflow flame	See above	Extinction strain rates as function of fuel mole fraction for fuel/oxidizer temperatures of 500/298 K and 1 atm	Extinction strain rate calculated from flow velocities; good agreement on molar fraction basis comparison	Dooley <i>et al.</i> (2010)

Shock tube	See above	Ignition delay times for $\phi=1$ , 16-25 atm and 674-1222 K	Ignition delays measured using sidewall pressure and OH* emission	Dooley <i>et al.</i> (2010)
Rapid compression machine	See above	Ignition delay times for $\phi=1$ , 22.3 atm and 639-721 K	Ignition delays measured using sidewall pressure and OH* emission	Dooley <i>et al.</i> (2010)
Rapid compression machine	Jet A POSF 4658, Syntroleum S-8 POSF 4734 and JP-8	Ignition delay times for $\phi=0.43$ -2.29, 7-30 bar and 615-1100 K; focused on NTC and two-stage ignition	Ignition delays measured as inflection point of sidewall pressure trace; similar reactivities with S-8 > Jet A-1 > JP-8	Kumar & Sung (2010a), Kumar & Sung (2010b)
Counterflow twin flames	Jet A POSF 4658 and Syntroleum S-8 POSF 4734	Laminar flame speed and premixed extinction limits as function of equivalence ratio for unburned temperatures of 400-470 K and 1 atm	Burning velocities obtained by linear extrapolation of particle image velocimetry measurements; similar flame propagation characteristics but different extinction responses	Kumar <i>et al.</i> (2011)
Flow reactor	Jet A POSF 4658 and MURI 2 surrogate 40.4% n-dodecane, 29.5% iso-octane, 22.8% n-propylbenzene and 7.3% 1,3,5-TMB (mol.)	Oxidation of nitrogen-diluted stoichiometric mixtures at 12.5 atm, 500-1025 K and residence time 1.8 s	Reactivity indicated by CO, CO <sub>2</sub> concentration	Dooley <i>et al.</i> (2012a)
Shock tube	See above	Ignition delay times for $\phi=1$ , 17-22 bar and 666-1226 K; tailored drive gas mixtures of helium/nitrogen to study lower temperature ignition	Ignition delays measured using sidewall pressure and OH* emission	Dooley <i>et al.</i> (2012a)

Rapid compression machine	See above	Ignition delay times for $\phi=1$ , 21.7 atm and 620-710 K	Ignition delays measured as inflection point of sidewall pressure trace	Dooley <i>et al.</i> (2012a)
Shock tube	See above	Speciation of intermediates for $\phi=1$ , 18-35 atm, 901-1760 K and reaction times 1.23-3.53 ms	Concentration of CO, CO <sub>2</sub> , O <sub>2</sub> , CH <sub>4</sub> , C <sub>2</sub> H <sub>2</sub> , C <sub>2</sub> H <sub>4</sub> , C <sub>2</sub> H <sub>6</sub> , C <sub>3</sub> H <sub>6</sub> , butenes, butadienes, pentenes, hexenes, benzene and toluene by GC/MS	Dooley <i>et al.</i> (2012a)
Counterflow flame	See above	Extinction strain rates as function of fuel mole fraction for fuel/oxidizer temperatures of 500/298 K and 1 atm	Extinction strain rate calculated from flow velocities	Dooley <i>et al.</i> (2012a)
Counterflow twin flames	See above	Laminar burning velocities and premixed extinction limits as function of equivalence ratio for unburned temperatures of 400-470 K and 1 atm	Burning velocities obtained by linear extrapolation of particle image velocimetry measurements	Dooley <i>et al.</i> (2012a)
Wick-fed diffusion flame	See above	Soot volume fraction normalized by non-dimensional height	Soot fraction calculated from laser extinction data	Dooley <i>et al.</i> (2012a)
Shock tube	Jet A POSF 4658 and Jet A with JP-8 additives (MIL-T-83133D)	Ignition delay times for $\phi=0.25-1.5$ , 662-1381 K and 8-39 atm	Ignition delays measured using sidewall pressure and endwall OH* emission	Wang & Oehlschlaeger (2012)

Shock tube	Jet A POSF 4658 and MURI 2 surrogate 40.4% n-dodecane, 29.5% iso-octane, 22.8% n-propylbenzene and 7.3% 1,3,5-TMB (mol.)	Speciation of intermediates for $\phi=0.46-1.86$ , 16-27 atm, 879-1733 K and reaction times 1.34-3.36 ms	Concentration of CO, CO <sub>2</sub> , O <sub>2</sub> , CH <sub>4</sub> , C <sub>2</sub> H <sub>2</sub> , C <sub>2</sub> H <sub>4</sub> , C <sub>2</sub> H <sub>6</sub> , C <sub>3</sub> H <sub>6</sub> , butenes, butadienes, pentenes, hexenes, benzene and toluene by GC/MS	Malewicki <i>et al.</i> (2013)
Counterflow twin flames	Jet A POSF 4658, Syntroleum S-8 POSF 4734 and MURI 2 surrogate 40.4% n-dodecane, 29.5% iso-octane, 22.8% n-propylbenzene and 7.3% 1,3,5-TMB (mol.)	Laminar burning velocities as function of equivalence ratio for unburned temperatures of 350-470 K and 1-3 atm	Burning velocities obtained by linear and nonlinear extrapolation of particle image velocimetry measurements	Hui & Sung (2013)
Free-fall spherical droplet burning	Jet A POSF 4658, MURI 1 surrogate 42.67% n-dodecane, 33.02% iso-octane and 24.31% toluene and MURI 2 surrogate 40.4% n-dodecane, 29.5% iso-octane, 22.8% n-propylbenzene and 7.3% 1,3,5-TMB (mol.)	Evolution history of droplet, flame and soot shell diameters of droplets with $0.56\pm 0.04$ mm initial diameter	Diameters calculated from color and B&W video; burning rates calculated by taking the derivative of a 4th order polynomial fitted to averaged $D^2$	Liu <i>et al.</i> (2013a)
Free-fall spherical droplet burning	Jet A POSF 4658, UOP Camelina HEFA POSF 6152, UOP Tallow POSF 6308 and 50/50 blend of Jet A/Camelina HEFA (vol.)	Evolution history of droplet, flame and soot shell diameters of droplets with $0.57\pm 0.03$ mm initial diameter	Diameters calculated from color and B&W video; burning rates calculated by taking the derivative of a 4th order polynomial fitted to averaged $D^2$	Liu <i>et al.</i> (2013b)

Dooley *et al.* (2012a) employed RCM and shock tube with tailored driver gas mixtures of helium and nitrogen to study low temperature ignition of POSF 4658 and a 4-component surrogate comprising 40.4 % n-dodecane, 29.5 % iso-octane, 22.8 % n-propylbenzene and 7.3 % 1,3,5-trimethylbenzene, by mol., (MURI 2, average formula  $C_{9.92}H_{19.43}$ , H/C ratio of 1.958). As previously noted, the ignition delay times were similar, but the surrogate was unable to reproduce the two-stage ignition of the real fuel. Such results were more evident in the pressure histories of the RCM experiments thus indicating a significant difference in the reacting environments between RCM and shock tube, specially in high fuel loadings.

Flame speeds and extinction strain rates of POSF 4658 were investigated in diffusion flames employing counterflow/opposed jet burners, see Fig. 3.3. For an unburned temperature of 400 K there is a very good agreement for all data sets within 2 cm/s whilst for the 470 K data such agreement only occurs for  $\phi < 0.8$ . However this comparison could be more meaningful if data from other experiments to measure burning velocities, like constant volume reactor and cone-angle method in coflow burner, were available.

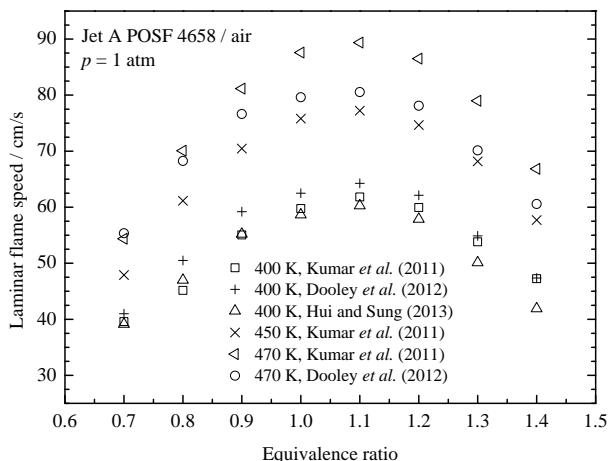


Figure 3.3: Compilation of POSF 4658 laminar flame speeds as function of equivalence ratio for different unburned gas temperatures

Dattarajan *et al.* (2009) investigated the pressure dependence of extinction strain rates of Jet A and surrogate blends comprising n-decane and 1,2,4-trimethylbenzene, motivated by the relevance of strained laminar flames to the local extinction of flamelets in turbulent combustion devices. Results show that the 60 % n-decane/40 % 1,2,4-TMB (vol.) blend closely simulates the extinction behavior of Jet A.

The authors argue that secondary radicals formed from the alkane rapidly undergo  $\beta$ -scission (elimination) to form smaller alkenes and alkyl radicals which propagate the radical pool. These alkyl radicals also react rapidly with  $O_2$  to form peroxy radicals, epoxides, olefins, OH and  $HO_2$  radicals. On the other hand, trimethylbenzene forms benzyl radicals that do not suffer elimination reactions since the ring opening and loss of aromaticity are highly endothermic. Additionally, benzyl peroxy radicals are much more unstable than alkylperoxy radicals. Hence, in blends, methyl substituted aromatics limit the amount of active alkane radicals since their C-H bond (90 kcal/mol) is much weaker than primary and secondary C-H bonds of the alkyl molecule (98.5 and 101 kcal/mol).

The results of Dooley *et al.* for the extinction of POSF 4658 and their aforementioned 3-component surrogate presented a good agreement when evaluated on a mole fraction basis but there is clear divergence in terms of mass fraction. The authors attributed this discrepancy to the different average molecular weight of surrogate and real fuel, 120.6 g/mol vs. 142 g/mol. Edwards *et al.* (2010), using the results of Dooley *et al.*, further discusses composition/property relationships of conventional and alternative jet fuels. The authors show that there is a poor correlation of the density of current jet fuels with their aromatic level while fuel density and volumetric heating values are closely correlated.

Moreover, Edwards *et al.* point out the merit of Dooley *et al.* procedure for surrogate elaboration in the context of gas phase kinetics behavior and the fact that cycloalkanes are not necessary in combustion surrogates since it is possible to replicate their behavior with molecular fragments of other hydrocarbon classes. Regardless of these encouraging results Edwards *et al.* emphasized that, in turbine engines, phenomena like droplet penetration and multi-component vaporization impact the gas phase combustion.

Kumar *et al.* (2011) compared flame speed and extinction characteristics of this Jet A and Syntroleum's Fischer-Tropsch (GtL) S-8

POSF 4734 and found that even though their burning velocities are very similar within experimental uncertainty, the alternative fuel is more resistant to stretch induced extinction, probably due to its negligible aromatic content. Such feature may have implications regarding the operation of jet engines, specially in terms of flameouts and altitude relight. In their study with MURI 2 surrogate, Dooley *et al.* (2012a) obtained extinction limits with remarkable agreement thus validating the hypothesis of using the average molecular weight as a metric for average diffusive properties of multicomponent fuels.

Wang & Oehlschlaeger (2012) employed a shock tube to measure the ignition delay times of POSF 4658 for lean,  $\phi=0.25$  and 0.5, and rich,  $\phi=1.5$  equivalence ratios, at pressure of 20 atm, in the temperature range 662-1305 K. This Jet A sample was also studied at stoichiometric condition for pressures of 8, 11, 20, and 39 atm, spanning the 674-1381 K range. The measurements showed that IDTs of POSF 4658 obtained at 20 bar and above 1000 K present a dependence on equivalence ratio that can be described using a power-law fit determined via least-squares regression with  $\tau \propto \phi^{-0.58}$ . An analogous regression for the pressure dependence of stoichiometric high temperature data yielded an expression with  $\tau \propto p^{-0.75}$ . Additionally, a blend of POSF 4658 with JP-8 additives (MIL-T-83133D) was investigated at  $\phi=1.0$ , pressure of 20 atm, and temperatures of 671-1227 K. Measurements showed no discernible influence of the additives on fuel reactivity.

Hui & Sung (2013) extended the studies of Kumar *et al.* (2011) and Dooley *et al.* (2012a) by measuring the laminar flame speed of POSF 4658, the 4-component MURI 2 surrogate as well as the individual components at 2 and 3 atm in a premixed, twin flame setup. It was shown that preheat temperature affects burning velocities mostly through adiabatic flame temperature, with peak velocity occurring in slightly rich conditions. Linear and nonlinear extrapolations were employed and the results revealed that all laminar flame speeds decrease with increasing pressure with an average difference of ca. 8 cm/s between 1 and 2 atm and 5 cm/s between 2 and 3 atm. All deduced overall reaction orders were smaller than 2 which is an indicative of the importance of three-body termination reactions with increasing pressure.

Low and intermediate reactivity of POSF 4658 was studied in flow reactor (DOOLEY *et al.*, 2010; DOOLEY *et al.*, 2012a). In the former study, comparisons with the MURI 1 surrogate indicated that iso-

octane and toluene are not reactive enough to represent the real fuel, thus exhibiting a clear deviation in reactivity at NTC conditions. The authors argue that these compounds were chosen because of the reliability of their kinetics models and that the richer molecular structural palette contained in the real fuel allows it to become oxidized at these intermediate temperatures ( $< 800$  K). In the latter work a comparison involving POSF 4658 and both MURI surrogates indicated that the changing in aromatic components from MURI 1 (toluene) to MURI 2 (n-propylbenzene + 1,3,5-TMB) resulted in no discernible improvement in reproducing real fuel's smooth transition from NTC chemistry to high temperature radical chain branching mechanism. Therefore, the role of n-alkanes in the radical pool generation is of paramount importance to the low and intermediate reactivity of fuels.

Unconventional experiments with POSF 4658 included measurement of mole fraction profiles in ethylene flame doped with jet fuel (JAHANGIRIAN *et al.*, 2009), concentration of intermediates in shock tube (DOOLEY *et al.*, 2012a; MALEWICKI *et al.*, 2013), soot fraction measured by laser extinction in wick-fed diffusion flame (DOOLEY *et al.*, 2012a) and evolution history of free-fall spherical droplet burning (LIU *et al.*, 2013a; LIU *et al.*, 2013b). Jahangirian *et al.* compared mole fraction profiles in an ethylene counterflow flame perturbed by trace amounts of POSF 4658, Aachen and Utah/Yale surrogates. Results showed that even though the surrogates' ability to reproduce larger alkenes and aromatics was only moderate the Aachen blend had an advantage due to its very simple composition. The performance of both surrogates in predicting alkene formation is better for smaller molecules, probably because there are many more pathways to produce them thus the original fuel alkane is less important. The measurement of benzene and toluene profiles illustrated the soot propensity since benzene is a crucial intermediate in the formation of naphthalene from alkanes whilst toluene is a byproduct of the growth of n-alkylbenzenes to naphthalene via benzyl radicals.

Two studies report speciation of intermediates in a heated single pulse shock tube (DOOLEY *et al.*, 2012a; MALEWICKI *et al.*, 2013). The measurements revealed the ability of the MURI 2 surrogate in emulating the formation of small molecular weight intermediates like methane and ethylene. The agreement for heavier species like toluene and isobutene is affected but this is an expected result of the limited palette of initial components and the specificity of the formation pathways for

such intermediates. These high temperature ( $> 900$  K) experiments were important to support the conceptual foundations of the surrogate formulation procedure developed in the MURI research effort.

The procedure is based on the hypothesis that a surrogate fuel must provide the same ‘distinct chemical functionalities’ e.g. n-alkyls, iso-alkenyls and benzyl-like radicals, formed after the initial reaction of the real fuel. Such assumption relaxes the need to reproduce initial fuel molecular composition to obtain comparable combustion kinetics behavior. The selection of the pure components and their proportions in the surrogate is defined with an *a priori* property matching method that involves the evaluation of four property targets: derived cetane number (DCN), H/C ratio, average molecular weight and threshold sooting index (TSI).

While the aforementioned studies encompassed gas phase combustion only, the works of Liu *et al.* (2013a), Liu *et al.* (2013b) involved the multiphase combustion of a free-falling spherical droplet. The experiment is carried out in an instrumentation package where the droplet is supported by very small ( $14\mu\text{m}$ ) diameter silicon carbide fibers. The package free-falls over a 7.6 m distance thus providing 1.2 s of low gravity. The fuels investigated included both MURI surrogates, POSF 4658 as well as UOP’s HEFAs made from camelina (POSF 6152) and tallow (POSF 6308). Results showed that the burning rate of all fuels is quite similar during initial droplet heating until reaching a quasi-steady period in which Jet A burning rate is noticeably lower. Such effect is probably associated to the presence of high boiling point compounds in the conventional fuel.

### 3.3.2 Experiments with other conventional fuels

Other studies with conventional fuel were performed with several samples of JP-8 (POSF 3773, 4177 and 6169), see Tab. 3.5. Colket *et al.* (2007) reported studies of POSF 3773 and a 50 % n-decane, 25 % n-butylcyclohexane and 25 % n-butylbenzene (vol.) surrogate in flow reactor, single cylinder engine and opposed-jet flame. Comparisons with previously proposed surrogates indicated that blends with trimethylbenzene were the only ones less reactive than JP-8, probably due to radical scavenging phenomena. Humer *et al.* (2007) employed a counterflow burner to study ignition and extinction of JP-8, Jet A and vari-

ous surrogates with n-decane, n-dodecane, methylcyclohexane (MCH), toluene and *o*-xylene. The surrogate comprising 60 % n-dodecane, 20 % MCH and 20 % *o*-xylene (vol.) exhibited the best agreement with the real fuels.

Numerical simulations, employing a reaction mechanism from the CRECK Modeling Group at Politecnico di Milano which comprises 7878 reactions between 283 species, indicated limitations of the aromatic subscheme regarding *o*-xylene chemistry and stabilized benzyl-like radicals and their roles on reactivity and polycyclic aromatic hydrocarbon (PAH) formation. The combined analysis of different surrogates revealed that replacing toluene with *o*-xylene had very little influence on extinction conditions whilst changing from n-decane to n-dodecane resulted in a significant improvement of the extinction characteristics.

Natelson *et al.* (2008) examined the low and intermediate temperature reactivities of JP-8 POSF 3773 and a 2:1:1 n-decane, n-butylcyclohexane and n-butylbenzene blend (vol.), that matches real fuel H/C ratio, in the pressurized flow reactor at Drexel University. The surrogate fuel was considerably more reactive than the real fuel and formulation adjusts to decrease its reactivity would place it further from matching JP-8 composition, e.g. greater fraction of n-butylbenzene would result in a fuel with more than 25% aromatics, beyond the limit defined in specifications. The authors suggested that improving the performance of this blend could be achieved by the use of high molecular weight iso-paraffin like iso-cetane, but such compounds usually are not readily available and are expensive.

In their following work Natelson *et al.* (2010) studied the POSF 3773 and surrogates comprising n-decane, n-butylcyclohexane and n-butylbenzene in 2:1:1 (for jet fuel) and 1:1:1 (for diesel) blends by volume in a single cylinder engine. The main objective was to assess if the low temperature chemistry verified in previous flow reactor experiments is relevant to engine conditions. Results revealed that the effect of each surrogate's heat capacity is negligible regarding in-cylinder pressure rise. Therefore both surrogates were more reactive than JP-8, with the 1:1:1 blend better emulating real fuel ignition delays for 14:1 and 15:1 compression ratios while for 16:1 both surrogates predicted delays about 1 ms shorter. The 1:1:1 blend was also more sensitive to the increment in compression ratio which indicates a greater role of preignition oxidation chemistry in its ignition.

Honnet *et al.* (2009) performed experimental and numerical stu-

dies of JP-8 (POSF 4177) and the Aachen surrogate in a counterflow burner, measuring critical conditions of autoignition, extinction and also volume fractions of soot. Results were compared with calculations employing a detailed (900 reactions comprising 122 species) kinetics model assembled from validated mechanisms of Aachen surrogate's components, i.e., n-decane and 1,2,4-TMB. For extinction, the Aachen surrogate is slightly more reactive than JP-8, extinguishing at higher strain rates for similar fuel mass fraction, with discrepancies increasing for higher strain rates. For autoignition, the reactivity trend is the same with computed results overpredicting temperature at autoignition. Regarding soot formation, the soot volume fraction decreases and the agreement between fuels increase with increasing strain rate whilst computed values showed peak soot formation closer to the stagnation plane.

Katta *et al.* (2010), Katta *et al.* (2011) investigated JP-8, n-dodecane, MCH and toluene oxidation in a co-flow burner and compared the flame images with CFD results, where the fuel was specified as either the Utah/Yale surrogate or a 77 % n-dodecane and 23 % *m*-xylene by volume blend designated SERDP surrogate. In the former work a semi-detailed (1538 reactions with 161 species) kinetics model was employed and the computations were unable to yield an anchored flame, with Utah surrogate flame anchored closer to the burner than SERDP flame, probably due to different molecular weights affecting fuel stream momentum. In the latter a detailed kinetics mechanism (5652 reactions and 206 species) was incorporated into the CFD code and calculations resulted in an upstream shift of the flame base, from 7.7 to 4.0 mm ahead of the burner rim.

Table 3.5: Available experimental kinetics data for different JP-8 samples since 2007

Technique	Fuel	Conditions	Data type and comments	Reference
Flow reactor	JP-8 POSF 3773 and surrogate 50% n-decane, 25% n-butylbenzene, 25% n-butylcyclohexane (vol.)	Oxidation at constant pressure of 0.8 MPa, temperature of 600–800 K, equivalence ratio of 0.3 and residence time of 120 ms.	Fuel reactivity in the NTC region indicated by CO production; surrogate significantly more reactive than JP-8	Colket <i>et al.</i> (2007)
Single cylinder engine	See above	Autoignition at an inlet temperature of 500 K, compression ratio of 15 and equivalence ratio of 0.23	Ignition indicated by pressure rise as a function of crank angle; surrogate ignited more easily than JP-8	Colket <i>et al.</i> (2007)
Opposed-jet flame	See above	Ignition temperature as function of fuel/nitrogen ratio at constant strain rate of 200 s <sup>-1</sup> ; extinction strain rate as function of fuel/nitrogen ratio	Temperature measured as that of the opposed jet of vitiated air; strain rate determined by particle image velocimetry; surrogate ignites more readily and is more resistant to extinction than JP-8	Colket <i>et al.</i> (2007)
Counterflow burner	JP-8, Jet A, pure components and surrogates with n-decane, n-dodecane, MCH, toluene and <i>o</i> -xylene	Ignition temperature as function of strain rate/fuel mass fraction at constant fuel mass fraction/strain rate of 0.3/550 s <sup>-1</sup> ; extinction strain rate as function of fuel mass fraction	Ignition observed with high-speed camera; best agreement with real fuels for 60% n-dodecane, 20% MCH, 20% <i>o</i> -xylene (vol.)	Humer <i>et al.</i> (2007)

Flow reactor	JP-8 POSF 3773, surrogates 50%/33% n-decane, 25%/33% n-butylbenzene, 25%/33% n-butylcyclohexane (vol.)	Oxidation at constant pressure of 0.8 MPa, temperature of 600–800 K, equivalence ratio of 0.3 and residence time of 120 ms.	Fuel reactivity in the NTC region indicated by CO production; surrogates significantly more reactive than JP-8	Natelson <i>et al.</i> (2008)
Counterflow flame	JP-8 POSF 4177 and Aachen surrogate	Ignition, extinction and volume fraction of soot at atmospheric pressure, oxygen mass fraction of 0.233 and fuel mass fraction around 0.4.	Fuel mass fraction as function of extinction strain rate; oxidizer temperature at autoignition as function of strain rate; surrogate more reactive than real fuel	Honnet <i>et al.</i> (2009)
Coflow burner	JP-8, n-dodecane, MCH and toluene	Flame height and shape for reactants at 493 K and fuel mass fraction of 0.4; comparisons with CFD including liftoff height, peak temperature and peak soot volume fraction	Flame height and shape measured by photograph; computations unable to predict anchored flames	Katta <i>et al.</i> (2010), Katta <i>et al.</i> (2011)
Single cylinder engine	JP-8 POSF 3773, surrogates 50%/33% n-decane, 25%/33% n-butylbenzene, 25%/33% n-butylcyclohexane (vol.)	Ignition delay with inlet conditions of 500 K, 0.1 MPa, $\phi=0.23$ , engine speed 800 RPM and compression ratios of 14-16:1	Ignition as function of pressure rise at crank angle degree; surrogates more reactive than JP-8	Natelson <i>et al.</i> (2010)
Rapid compression machine	JP-8 POSF 6169 and camelina HEFA POSF 6152	Ignition delay times at 7-10 bar, 670-750 K, oxidizer to fuel mass ratio O/F=14.6-48.6	Ignition delays measured as inflection point of sidewall pressure trace; HEFA present higher heat release during first-stage ignition than JP-8	Allen <i>et al.</i> (2012)

Allen *et al.* (2012) proposed a new method of reactive mixture preparation for autoignition studies in rapid compression machine, given that the low volatility of jet fuels hamper batch-based premixture. The approach relies on a fuel injector to load a small amount of fuel into the preheated test chamber. Employing this new technique the ignition delays of JP-8 (POSF 6169) and camelina HEFA (POSF 6152) were studied in the NTC and two-stage ignition range. Results indicated that tests at lean conditions (O/F=48.6) presented repeatability issues due to shot-to-shot variation in injector performance. Tests also revealed the HEFA to be more reactive than JP-8, as expected due to the negligible aromatic fraction of the alternative fuel.

### 3.3.3 Experiments with alternative jet fuels

Mzé-Ahmed *et al.* (2010) studied the oxidation of Sasol's synthetic kerosene (79.9 % iso-alkanes, 19.6 % n-alkanes and 0.5 % aromatics by mass) and its 50/50 mixture with Jet A-1 in a jet-stirred reactor. Concentration profiles of reactants, stable intermediates and products were measured and a detailed (6228 reactions and 2006 species) kinetics model including low temperature chemistry was proposed, based on previous mechanisms for n-decane, gasoline, kerosene and diesel surrogates. Measurements of stable intermediates like CH<sub>2</sub>O and C<sub>2</sub>H<sub>4</sub> indicated that the synthetic kerosene was more reactive than the conventional fuel, producing more ethylene and propene by  $\beta$ -scission. At low temperatures the high reactivity of n-alkanes is responsible for the radical pool while iso-alkanes consume OH radicals and reduce chain branching, with  $\beta$ -scissions playing a minor role in fuel decomposition. In fuel-rich conditions, NTC and maximum concentration of intermediates increase thus resulting in reduction of the radical pool.

Kick *et al.* (2012) carried out burning velocity measurements as function of equivalence ratio 1.0–1.4 at 1 atm and unburned temperature of 473 K using the cone-angle method. Among the fuels studied were Sasol's fully synthetic jet fuel (CtL) and a FT GtL fuel. Experimental data was compared with calculations employing a detailed chemical kinetics model containing 4642 reactions and 1075 species. Rate of production analysis revealed that flame speeds are mostly sensitive to the main chain branching reaction between H and O<sub>2</sub> as well as the reaction between CO and OH that governs heat release.

Comparisons with previously measured Jet A-1 flame speeds revealed a good agreement for slightly rich flames but the peak value, near 80 cm/s, for synthetics occur around  $\phi=1.1$  while for conventional fuel the maximum ca. 90 cm/s speed is at stoichiometric condition. These results indicate that the synthetic fuels tested are mainly composed by iso-alkanes.

Employing the same *a priori* combustion property matching technique to formulate surrogates, Dooley *et al.* (2012b) experimentally studied the oxidation of Syntroleum S-8 (POSF 4734) synthetic fuel, a proposed surrogate for S-8 comprising 51.9 % n-dodecane and 48.1 % iso-octane by mol and a surrogate for a lightly branched alkane (2-methylheptane) comprising 46.8 % n-decane and 53.2 % iso-octane by mol. The low-temperature (<800 K) reactivities of S-8 and its surrogate were quite similar while between 800-900 K the real fuel was noticeably more reactive. The authors also compared surrogate's experimental reactivity with different kinetics models with the Milano model being able to closely reproduce flow reactor results even though its ignition delay predictions were overpredicted by 30-50 %.

Hui *et al.* (2012) investigated ignition delay times, laminar burning velocities and premixed extinction limits of several alternative jet fuels like Syntroleum's S-8 (POSF 4734) and R-8 (POSF 5469), Shell's FT GtL (POSF 5172), Sasol's IPK (POSF 5642) and UOP's HEFAs from camelina (POSF 6152) and tallow (POSF 6308). Even though the same facilities were used before to study Jet A and S-8 in the NTC region, the experimental conditions in this work were out of the NTC range. Rapid compression machine results showed that all alternative fuels presented higher reactivity than Jet A, with GtL and camelina HEFA being consistently the more reactive, not presenting any sign of two-stage ignition. On the other hand IPK presented longer first-stage ignition delay, probably due to its highly branched alkane fraction. Flame speeds and extinction stretch rates were very similar for all fuels including Jet A, with camelina HEFA being slightly more reactive than others.

Table 3.6: Available experimental kinetics data for alternative jet fuels since 2007

Technique	Fuel	Conditions	Data type and comments	Reference
Jet stirred reactor	Sasol IPK (79.9% i-alkanes, 19.6% n-alkane and 0.5% aromatics by mass); 50/50 blend Sasol/Jet A-1	Oxidation at 10 atm, 560-1030 K, $\phi=0.5-2.0$ , residence time of 1 s	Reactivity measured by concentration profiles of reactants, stable intermediates and products; synthetic kerosene more reactive than Jet A-1	Mz�-Ahmed <i>et al.</i> (2010)
Coflow burner	Sasol fully synthetic jet fuel and blends of FT GtL with 1-hexanol and naphthenic cut	Burning velocity of premixed flames as function of equivalence ratio for 1.0 atm and unburned temperature of 473 K	Flame shape measured by photograph and velocity determined by cone angle method	Kick <i>et al.</i> (2012)
Flow reactor	Syntroleum S-8 POSF 4734 and surrogate n-dodecane and iso-octane (mol.)	Oxidation of nitrogen-diluted stoichiometric mixtures at 12.5 atm, 500-1050 K and residence time 1.8 s	Reactivity indicated by CO, CO <sub>2</sub> concentration	Dooley <i>et al.</i> (2012b)
Shock tube	See above	Ignition delay times for $\phi=1$ , 20 bar and 667-1223 K; tailored drive gas mixtures of helium/nitrogen to study lower temperature ignition	Ignition delays measured using sidewall pressure and OH* emission	Dooley <i>et al.</i> (2012b)

Counterflow flame	See above		Extinction strain rates as function of fuel mole fraction for fuel/oxidizer temperatures of 500/298 K and 1 atm	Extinction strain rate calculated from flow velocities	Dooley <i>et al.</i> (2012b)
Rapid compression machine	Syntroleum S-8 POSF 4734, Shell GtL POSF 5172, Sasol IPK POSF 5642, UOP Camelina HEFA POSF 6152, UOP Tallow POSF 6308 and Syntroleum R-8 POSF 5469		Ignition delay times for $\phi=1$ , 21.7 atm and 620-710 K	Ignition delays measured as inflection point of sidewall pressure trace	Hui <i>et al.</i> (2012)
Counterflow twin flames	See above		Laminar burning velocities and premixed extinction limits as function of equivalence ratio for unburned temperatures of 400-470 K and 1 atm	Burning velocities obtained by linear extrapolation of particle image velocimetry measurements	Hui <i>et al.</i> (2012)
Shock tube	Syntroleum S-8 POSF 4734, Shell GtL POSF 5172 and Sasol IPK POSF 5642		Ignition delay times for $\phi=1.0$ , 651-1323 K and 20 atm	Ignition delays measured using sidewall pressure and endwall OH* emission; reactivity in the NTC range (750<T<900 K): GtL > S-8 > IPK	Wang & Oehlschlaeger (2012)
Counterflow flame	Sasol IPK POSF 7629, Shell SPK POSF 5729, UOP Tallow HEFA POSF 6308, Camelina HEFA POSF 7720 and JP-8 POSF 6169		Extinction strain rates as function of fuel mole fraction for fuel/oxidizer temperatures of 500/300 K and 1 atm	Extinction strain rate calculated from flow velocities	Won <i>et al.</i> (2013)

Heated spherical chamber	See above	Critical flame initiation radius and laminar burning velocity as function of equivalence ratio at 450 K, 1 atm and 17% O <sub>2</sub> (mol.)	Flame propagation visualized by high speed Schlieren imaging for flame radius less than 25 mm	Won <i>et al.</i> (2013)
Flow reactor	See above	Oxidation of nitrogen-diluted stoichiometric mixtures at 12.5 atm, 500-1000 K and residence time 1.8 s	Reactivity indicated by CO, CO <sub>2</sub> concentration	Won <i>et al.</i> (2013)
Jet stirred reactor	Shell GtL SPK and surrogate 57.7% n-decane, 33.2% iso-octane and 9.1% n-propylcyclohexane (mol.)	Species profiles at 10 bar, 550-1150 K, $\phi=0.5-2.0$ and residence time of 1 s	Online quantification of CO, CO <sub>2</sub> , H <sub>2</sub> O, CH <sub>2</sub> O, CH <sub>4</sub> and C <sub>2</sub> H <sub>4</sub> ; other species by GC/MS	Dagaut <i>et al.</i> (2014)
Shock tube	See above	Ignition delay time at 16 bar, 650-1400 K and $\phi=0.5-1.0$	Ignition delays measuring peak emission of CH* at 431 nm	Dagaut <i>et al.</i> (2014)
Coflow burner	See above	Burning velocity of premixed flames as function of equivalence ratio for 1.0 atm and unburned temperature of 473 K	Flame shape measured by photograph and velocity determined by cone angle method	Dagaut <i>et al.</i> (2014)
Counterflow flame	2,6,10-trimethyl dodecane (farnesane), S-8 surrogate 51.9% n-dodecane and 48.1% iso-octane (mol.), farnesane surrogate 45.9% n-cetane and 54.1% iso-cetane (mol.)	Extinction strain rates as function of fuel mole fraction for fuel/oxidizer temperatures of 500/300 K and 1 atm	Extinction strain rate calculated from flow velocities	Won <i>et al.</i> (2014)

Shock tube	See above	Ignition delay times for $\phi=1$ and 20 atm	Ignition delays measured using endwall pressure and OH* emission; S-8 surrogate more reactive than farnesane and its surrogate below 870 K	Won <i>et al.</i> (2014)
Rapid compression machine	JP-5, JP-8, HRJ-5, HRJ-8, Shell GtL, Sasol IPK, Sasol solvents LPA-142, LPA-210, LINPAR 1416-V and 50/50 mixtures	Ignition delays measured at temperatures 625–1000 K, pressure of 20 bar, $\phi=0.5-1.0$	Cycloparaffins produce more olefins thus decreasing reactivity; excess oxygen can directly react with aromatics at lean conditions	Valco <i>et al.</i> (2015)
Shock tube	See above	Ignition delays measured at temperatures 625–1000 K, pressure of 20 bar, $\phi=0.5-1.0$	Cycloparaffins produce more olefins thus decreasing reactivity; excess oxygen can directly react with aromatics at lean conditions	Valco <i>et al.</i> (2015)

---

Wang & Oehlschlaeger (2012) employed a shock tube to measure the ignition delay times of Syntroleum's S-8 (POSF 4734), Shell's FT GtL (POSF 5172) and Sasol's IPK (POSF 5642), spanning the temperature range 651-1323 K, at 20 atm and  $\phi=1.0$ . The reactivity of these fuels was indistinguishable for temperatures higher than 1000 K, being also equivalent to POSF 4658 reactivity at this condition. For temperatures below 900 K, i.e., in the NTC region, ignition delay times were inversely correlated to the derived cetane number of these three fuels. Therefore, IPK (POSF 5642, DCN=31.3) presented the longest IDTs, ca. 3 ms at 800 K, while S-8 (POSF 4734, DCN=58.7) and GtL (POSF 5172, DCN=61.0), at this temperature, had ignition delays of 1.5 ms and 1.0 ms, respectively.

This Jet A sample was also studied at stoichiometric condition for pressures of 8, 11, 20, and 39 atm, spanning the 674-1381 K range. The measurements showed that IDTs of POSF 4658 obtained at 20 bar and above 1000 K present a dependence on equivalence ratio that can be described using a power-law fit determined via least-squares regression with  $\tau \propto \phi^{-0.58}$ . An analogous regression for the pressure dependence of stoichiometric high temperature data yielded an expression with  $\tau \propto p^{-0.75}$ . Additionally, a blend of POSF 4658 with JP-8 additives (MIL-T-83133D) was investigated at  $\phi=1.0$ , pressure of 20 atm, and temperatures of 671-1227 K. Measurements showed no discernible influence of the additives on fuel reactivity.

Won *et al.* (2013) employed the *a priori* property matching technique to establish combustion characteristics of a conventional JP-8 (POSF 6169) and four alternative fuels: Sasol IPK (POSF 7629), Shell SPK (POSF 5729), camelina HEFA (POSF 7720) and tallow HEFA POSF (6308). High temperature combustion properties were gauged by measuring the radical index evaluated from extinction limits of diffusion flames in counterflow burner and critical flame radius in outwardly propagating premixed flames. Low to intermediate temperature reactivities were compared in high pressure flow reactor. As previously noted the highly branched nature of Sasol's IPK result in the absence of low temperature reactivity while Shell's SPK and camelina HEFA presented extensive reactivity between 500 and 750 K.

Dagaut *et al.* (2014) employed jet stirred reactor, shock tube and coflow burner to study Shell's GtL SPK oxidation. A proposed surrogate comprising n-decane, iso-octane and n-propylcyclohexane was also tested in shock tube and coflow burner to provide additional data

for a detailed chemical kinetics model with 8217 reactions including 2185 species. Comparisons with previous results for Jet A-1 revealed that, under cool flame conditions, the oxidation of conventional fuel is faster than GtL, leading to larger formation of stable intermediates like  $\text{CH}_2\text{O}$  and  $\text{CO}$  and significantly less methane, ethylene and propene. This is expected since GtL contains larger fractions of paraffins that produce simple olefins by  $\beta$ -scission whilst methane is formed due to higher iso-alkane content. The detailed model predictions were in good agreement except for too long ignition delay times thus implying that the n-decane sub-model needs improvements.

Won *et al.* (2014) investigated the combustion behavior of 2,6,10-trimethyldodecane, a synthetic fuel candidate species also known as farnesane, by measuring shock ignition delays at 20 atm and extinction limits for strained laminar diffusion flames at 1 atm in a counterflow burner. Farnesane has DCN and H/C ratio very similar to those of Syntroleum S-8 (POSF 4734) thus, as expected, the high temperature combustion characteristics were virtually identical. However, the shock tube data revealed an unexpected difference in reactivity in the NTC region, with farnesane ignition delays being twice as long as those of S-8 surrogate below 870 K. Following a chemical functional group analysis the authors argue that for fuels with DCN larger than 50 the methylene to methyl ratio ( $\text{CH}_2/\text{CH}_3$ ) may be used as an additional target to more appropriately reproduce low temperature phenomena.

Valco *et al.* (2015) studied the autoignition behavior of 21 fuels including JP-5, JP-8, camelina-derived HRJ-5 and HRJ-8, Shell GtL, Sasol IPK, Sasol solvents LPA-142, LPA-210, LINPAR 1416-V and 50/50 mixtures of JP-5/HRJ-5, JP-8/HRJ-8, JP-5/Shell, JP-5/Sasol and so on. Experiments were carried out in shock tube and rapid compression machine at compressed temperatures between 625–1000 K, compressed pressure of 20 bar and under stoichiometric and lean conditions. Based on the chemical composition of each fuel a corresponding ignition behavior was inferred, for example, fuels with higher naphthenic content present reduced reactivity at low-to-intermediate temperatures given the propensity of its alkyl peroxy radicals to undergo  $\beta$ -scission and form olefins. Also noted was a decreased inhibitive influence of aromatics at low-temperature, lean conditions. In the presence of excess oxygen, aromatics can directly react with  $\text{O}_2$  to form peroxy radicals and bridged structures, which fragment into smaller species, thus accelerating radical production.

### 3.3.4 Additional research

Despite all the aforementioned experimental and modeling investigations, there was also considerable effort in more general, theoretical terms. As part of the studies that led to the formulation of the ‘distinct chemical functionalities’ approach, Won *et al.* (2011), Won *et al.* (2012) applied a scaling analysis to assess the quantitative contributions from mass transport, chemical energy and chemical kinetics potentials to the extinction limits of diffusion flames. The authors argue that, per molecule, potential energy, which controls flame temperature, and rate of mass diffusion are related to molecule size.

Moreover, it was inferred that extinction measurements of diffusion flames could be useful to validate kinetics models since they are governed, in a coupled manner, by kinetics, transport and thermal effects. The authors define a ‘transport-weighted enthalpy’ as the product of enthalpy of combustion per unit mole and the inverse of the square root of fuel molecular weight and a ‘radical index’ that quantifies the ability of fuels to produce OH radicals. These concepts were fundamentally evaluated with numerical computations and laser-induced fluorescence experiments and their use in a combined metric yielded a universal correlation to predict extinction limits (WON *et al.*, 2012).

Further studies with this focus, Won *et al.* (2013), included the evaluation of another near-limit metric, the critical flame initiation radius in outwardly propagating premixed flames. In summary, a larger critical radius indicates a slower rate of radical population growth. The combination of these tools with the previously stated *a priori* property matching technique and pressure flow reactor results indicated that the four property targets considered might need an amendment to include a measurable of hot ignition transition.

Kim *et al.* (2014) employed a model-based optimizer to develop two surrogates to emulate fuel properties affecting gas phase ignition and spray development of Composite Jet A POSF 4658. Besides three of the four target properties defined in the MURI studies (excluding TSI), the authors included lower heating value (LHV), density, viscosity, surface tension and distillation curve, with different assigned weights, defined by trial and error and ranging from 0.5 to 10.0, for the optimization properties. While the proposed surrogate UM1 has the four chemical, temperature-independent targets with a 10.0 weight and the physical ones with 0.5, the UM2 surrogate relaxes LHV requirement

from 10.0 to 2.0 and sets viscosity with a 10.0 weight.

Thus UM1 surrogate is a 38.44 % n-dodecane, 14.84 % iso-cetane, 23.36 % MCH and 23.36 % toluene (mol.) whilst UM2 is a 28.97 % n-dodecane, 14.24 % iso-cetane, 31.88 % decalin and 24.91 % toluene (mol.). The UM2 blend has lower H/C ratio and higher molecular weight but its estimated distillation process was significantly smoother than that of UM1. The ignition delay time of both surrogates was computed using a detailed kinetics mechanism (Model Fuels Consortium, Diesel ID161, 16936 reactions and 4014 species) and compared with POSF 4658 experiments.

The surrogate predictions in both high and low temperatures were consistently longer by a factor of two to three while in the NTC regime the calculations were within the 1 ms disagreement of the two compared experimental datasets. Comparisons with data at 20 and 40 atm revealed that the measured ignition delays slightly decrease with pressure but without changes in the temperature range of NTC whereas the kinetics modeling show significant decrease in ignition delay times and a notable shift of the NTC regime toward higher temperature.

### 3.4 CLOSING REMARKS

This chapter provided an overview of recent experimental and modeling studies with conventional and alternative jet fuels as well as recently proposed surrogates. It is important to stress that this is by no means an exhaustive review of all studies regarding the oxidation of transport-relevant hydrocarbons but a compilation of works that build upon the Jet Fuel Working Group paper (COLKET *et al.*, 2007). Many noteworthy conclusions can be drawn from this review.

This work focused on gas-phase combustion of Jet A/A-1, JP-8 and several alternative/synthetic jet fuels made from coal, natural gas as well as vegetable oils and animal fats. The experimental studies employed well-established techniques like ignition behind shock waves, oxidation in flow reactors and counterflow burners but also included some unconventional measurements like speciation of intermediates in shock tube and low-gravity spherical droplet burning, the latter experiment allowing the study of multiphase combustion.

Most experiments were developed within a framework of ‘standard fuel samples’ provided by the US Air Force, with the major hur-



This molecule may suffer addition of a second  $O_2$  to form  $\dot{O}OQOOH$  and also another intramolecular isomerization that results in an dihydroperoxy alkyl radical  $HOO\dot{P}OOH$ . In the NTC region the  $\dot{Q}OOH$  can also undergo propagation reactions producing cyclic ethers, alkenes and  $\beta$ -scission products. The cleavage of  $O-O$  bonds leads to the formation of a carbonyl radical  $O\dot{Q}O$  and two  $OH$  radicals in the so-called degenerate chain branching, which populates the radical pool at low temperatures. The instability of the secondary  $O_2$  addition and subsequent isomerization, with the formation of a cyclic intermediate, combined with the slow decomposition of  $H_2O_2$  at these temperatures is the one of the reasons behind the occurrence of negative temperature coefficient behavior. The occurrence of NTC is also linked to a change in the equilibrium of reactions  $R + O_2 \rightleftharpoons RO_2$ , which favors  $RO_2$  at lower temperatures but shifts to favor alkyl radicals  $R$  at higher temperatures. Thus, at low temperatures, the oxidation of hydrocarbons is governed by the initial concentration of fuel, which limits the formation of  $HO_2$ , and the addition of molecular oxygen to alkyl radicals. At intermediate temperatures the decomposition of  $H_2O_2$  into  $2OH$  is the rate controlling step while at the high temperature regime the branching reaction  $H + O_2 \rightarrow O + OH$  is the dominant reaction.

The process described above occurs with linear alkanes due to the absence of steric hindrance to hamper intramolecular isomerization and also because a linear paraffin has more  $C-H$  bonds in secondary carbons (higher methylene to methyl ratio) than its branched isomers. Taken together, these characteristics indicate that the identity of the linear and less-branched alkanes is of paramount importance to the formation of real fuel's radical pool. One of the major challenges in surrogate development is how to mimic real fuel's low temperature reactivity, that usually results from the interaction of hundreds of lightly-branched alkane isomers, using binary mixtures of linear and highly branched paraffins.

However, for synthetic fuels with negligible aromatic content, such task is somewhat simpler, given the apparent linearity in the combination of branched and non-branched alkanes and the current state of the chemical kinetics of representative molecules like n-dodecane and iso-octane. While the mechanism of aliphatic oxidation at low and intermediate temperatures is reasonably well developed, that of aromatics still has major gaps.

Many experiments have shown that, in the absence of some alkane fraction, a pure aromatic fuel is virtually unreactive below 900 K. In conventional fuel there is a rich palette of aromatics, from species with methyl substituents like toluene and xylene to others with long alkyl chains, whose kinetics behavior has aromatic and aliphatic character simultaneously. On the other hand the aromatic role in soot formation is partially elucidated and can be qualitatively assessed in kerosene-doped ethylene flames, showing that benzene is the crucial intermediate between alkanes and naphthalene whilst toluene is formed due to the growth of n-alkylbenzenes to naphthalene.

Without further experimental data regarding the role of aromatics in combustion, theoretical approaches showed very promising results, like the ‘distinct chemical functionalities’ hypothesis developed in the MURI research effort. The authors argue that the initial composition of a real fuel and its surrogate is not so important as their ability to populate the radical pool with similar amounts of OH, n-alkyl, iso-alkenyl and benzyl-like radicals that, on their turn, govern heat release and flame propagation.

Laminar flame speed and extinction strain rate measurements in counterflow flames were also performed with real fuels and surrogates. In these one-dimensional, high temperature tests it is possible to evaluate the impact of hydrocarbon’s transport properties on phenomena like extinction and relight. The use of metrics like transport-weighted enthalpy allows the estimation of diffusive properties of the real fuel and, in association with physical/chemical property matching procedure, it becomes very useful to the determination of surrogates for gas-phase combustion.

The synthetic, coal-to-liquid kerosene developed by Sasol has a very high fraction of branched alkanes thus being consistently less reactive than other alternative fuels made from natural gas and renewable feedstocks. The alternative fuels have negligible aromatic content which increases their gravimetric energy content and reduces soot and unburned hydrocarbon emissions though the specifications demand the addition of some conventional fuel to provide a minimum amount of aromatics that adjusts fuel density and assures seal swelling. The specifications consider synthetic fuels similar to mildly and severely hydrotreated fractions, which lack heterocompounds and alkenes, thus the blending with some conventional fuel also provide some trace amounts of components that may positively affect fuel lubricity and material

compatibility.

Regarding surrogates, most of the recently proposed mixtures comprise the same aliphatic hydrocarbons, which are n-dodecane and iso-octane. As to the role and identity of cycloalkanes and aromatics, some authors argue that naphthenes are not necessary in terms of chemical kinetics whilst others reinforce their significant fraction and importance in the real fuel, specially in terms of viscosity and distillation features but also regarding olefin formation. Even though the role of aromatics in terms of emissions and physical properties is well understood, the details of their oxidation pathways deserve more attention given that an aromatic compound, like indane or tetralin, have methyl substituents, long alkyl substituents, fused rings etc.

Besides remarkable progress in experimental and theoretical studies of liquid fuel's oxidation many questions remain open. Nevertheless the ability of some surrogates to reproduce O<sub>2</sub> consumption, CO formation, ignition delay and small olefin production, it is not evident how the specificity of the formation pathways for larger n-alkenyl radicals affects the remaining species and flame features. In summary, it is not known how the use of a handful of pure hydrocarbons, thereby only one isomer of each component, affects the formation of more complex intermediates and their subsequent consumption or involvement in soot formation and growth.

Another issue, pointed out in the MURI works, is the adequate representation of the transition from NTC regime to high temperature ignition. The authors argue that none of the *a priori* evaluated properties (DCN, H/C ratio, molecular weight and TSI) seems to correlate with the occurrence of this transition. The use of some theoretical tool analogous to the radical index and transport-weighted enthalpy may help improving the understanding of the mechanism behind this effect.

Even though there is a lot of further studies to perform with the aforementioned facilities there is also room for different experimental setups like refined techniques with the free-fall droplet combustion and measurements in optically accessible single cylinder research engines, both experiments where fuel evaporation plays an important role. From this state-of-the-art review, next chapter presents the direction taken in this work and describes the experimental facilities used.



## 4 EXPERIMENTS

### 4.1 INTRODUCTION

The preceding chapter provided an overview of recent advances in jet fuel’s experimental and modeling research, which encompasses experiments with ‘standard fuel samples’ from conventional and alternative sources as well as newly formulated chemical surrogates. Some of the important contributions of these studies can be summarized as follows:

- While the conventional, oil-derived jet fuel comprises hundreds of different aliphatic and aromatic hydrocarbons, its alternatives, either produced from natural gas, coal or renewable feedstocks, present much less variability in terms of isomers and have negligible aromatic content;
- Given the availability of facilities, most of the research studies were conducted to study gas-phase combustion of evaporated jet fuel and chemical surrogates, therefore addressing ‘property’ and ‘development’ targets. The shift towards ‘application’ targets demands new considerations and experimental approaches;
- The formulation of a chemical surrogate can rely on the assessment of a handful of conventional, normalized fuel properties like derived cetane number, mean molecular weight and H/C ratio;
- The different reactivities of linear and branched alkanes in low temperature ignition conditions are well understood but their interactions with aromatic species in the formation of the radical pool requires further investigation.

Within this scenario a two-part investigation was carried out. Initially a high pressure shock tube study of a Jet A-1 fuel sample was carried out by our collaborators at the IVG - University of Duisburg-Essen, followed by chemical kinetics modeling performed by the author. These results, combined with data from rapid compression machine experiments conducted at the Karlsruhe Institute of Technology, were presented at the 36th International Symposium on Combustion and published in the Proceedings of the Combustion Institute (DE TONI *et al.*, 2017).

The second part of the investigation comprised an experimental and numerical study of the low temperature reactivity and thermal ignition of fuel surrogates. The experiments were conducted by the author at the Combustion Chemistry Centre (C3) at the National University of Ireland, Galway. The following section will detail the Jet A-1 study.

## 4.2 EXPERIMENTS WITH JET A-1 AT IVG - UDE

The shock tube (ST) is a laboratory device which is extensively used to study unsteady, short-duration phenomena in the fields of aerodynamics, physics and chemistry (CANCINO, 2009). Given the high stagnation enthalpies and temperatures that can be obtained, the shock tube is a paramount tool in the study of gas-phase chemical kinetics. In essence, a ST consists of a long tubular reactor divided in two sections by one or more diaphragms. The low pressure section, also known as driven section, is filled with test gas i.e. the fuel/oxidant mixture. The high pressure, or driver, section is filled with inert gases like helium, argon and nitrogen.

During operation, the diaphragm is burst and the highly compressed gas flows into the low pressure section, with a shock wave being propagated through the test gas while a correspondent rarefaction wave travels through the driver gas. Figure 4.1 presents the axial pressure and temperature distributions before and after the bursting of the diaphragm.

Figure 4.1 shows the longitudinal pressure and temperature distributions at (a)  $t = 0$  and for two subsequent moments, (b) and (c) showing  $p$  and  $T$  conditions before the incident shock wave reaches the endwall, and (d) and (e) showing their axial distributions after the reflected wave passes through the test gas. It can be noticed that incident and reflected shock waves produce two increments of temperature and pressure in the test gas.

Successive longitudinal time-pressure profiles that indicate the shock front position can be plotted in a distance-time diagram as shown in Figure 4.2. At initial time, the rupture of the diaphragm is followed by a series of compression waves that rapidly collapse into a normal shock wave. The shock wave propagates at supersonic speed in the low pressure section, setting up the fluid downstream to it in motion

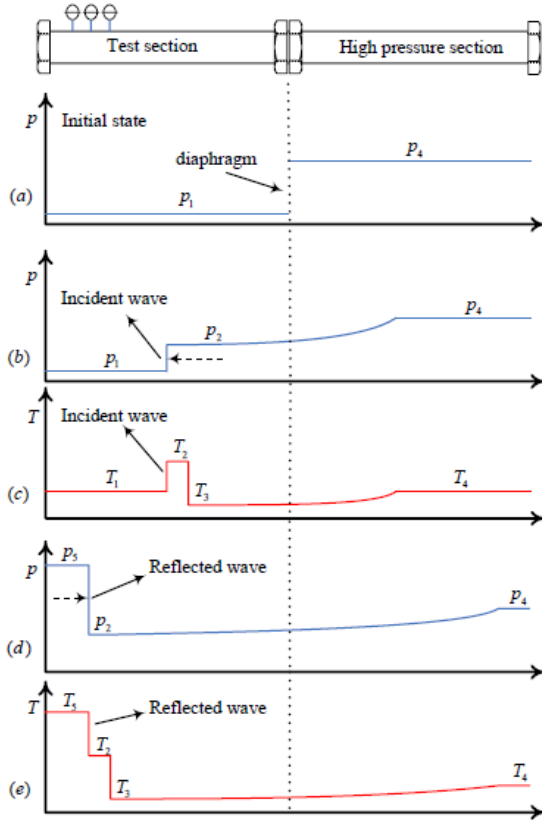


Figure 4.1: Operation of a shock tube, (a) initial condition, (b) and (c) propagation of incident shock wave, (d) and (e) propagation of reflected shock wave. Source: Cancino (2009)

towards the endwall with a velocity  $U_{iw}$ .

Upstream from the incident wave, the contact surface between the driven and driver gases moves at a velocity  $U_{cs}$ . The difference between  $U_{iw}$  and  $U_{cs}$  controls the available test time,  $\Delta t_{ms}$ , which is the interval between the passing of the reflected wave and the arrival of the contact surface. During this interval, the test gas is expected to achieve homogeneous, high temperature and pressure conditions of interest, known as  $T_5$  and  $p_5$ .

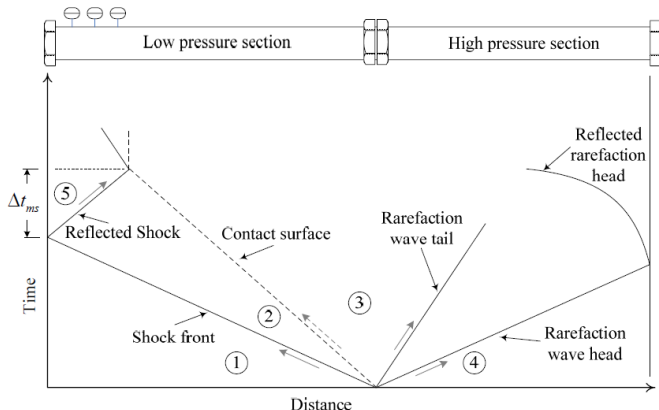


Figure 4.2: Distance-time diagram in shock tube. (1) unshocked gas, (2) shocked gas by incident shock, (3) expanded driver gas, (4) unexpanded driver gas, (5) shocked gas by reflected shock. Source: Cancino (2009)

#### 4.2.1 Facility at IVG - UDE

The high pressure shock tube at IVG - University of Duisburg-Essen is composed by a tubular section of 12.5 m divided by a diaphragm into a driver section of 6.1 m and a driven section of 6.4 m in length. The device is instrumented at the low pressure section with pressure and chemiluminescence sensors in order to capture the incident and reflected shock waves as well as pre-ignition and ignition events.

Shock speeds were determined by using the signals of three piezoelectric pressure transducers placed over the last 1.0 m of the shock tube and extrapolated to the endwall. Shock attenuations were typically 0.7 %/m to 2.5 %/m. The measured shock velocities were compared to the initially estimated values of incident shock waves and differences of about  $\pm 0.3$  % were found.

Using the SHOCK routine of CHEMKIN (REACTION DESIGN, 2009), uncertainties of about  $\pm 0.3$  % in the incident wave speed yield variations in the calculated  $T_5$  of about  $\pm 25$  K and variations in the calculated ignition delay time of about  $\pm 7.5$  %, in agreement with the experimental uncertainties found in the literature for shock tube

experiments (VASU *et al.*, 2009; OEHLSCHLAEGER *et al.*, 2009). In this work, the estimated uncertainties (CANCINO *et al.*, 2009) in the ignition delay time are in the range of  $\pm 7.5\%$  to  $\pm 10\%$ .

Pressure data were recorded with a time resolution of  $0.1\ \mu\text{s}$  and the ignition delay times were determined by extrapolating the steepest increase of the  $\text{CH}^*$  chemiluminescence emission signal, at  $431.5\ \text{nm}$ , to its zero level on the time axis as shown in Fig 4.3. To also determine the delay times of the first-stage ignition (cool flame),  $\text{CH}_2\text{O}^*$  chemiluminescence was simultaneously detected in the  $400\text{--}450\ \text{nm}$  wavelength range. The experiments were carried out with synthetic air containing  $79.5\%$   $\text{N}_2$  and  $20.5\%$   $\text{O}_2$ . As driver gas, tailored mixtures of  $5\text{--}20\%$  Ar in He were used to adjust its acoustic properties according to Palmer & Knox (1961) and Oertel (1966) to ensure long test times.

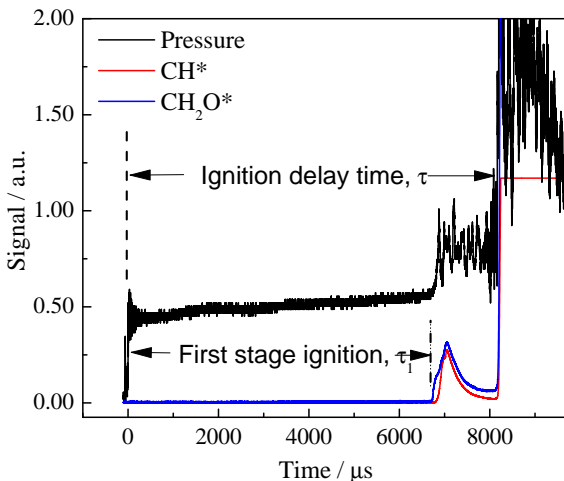


Figure 4.3: Determination of the ignition delay time from the  $\text{CH}^*$  and  $\text{CH}_2\text{O}^*$  chemiluminescence signals.

Shock tube simulations were conducted using the closed perfectly stirred reactor module of CHEMKIN-PRO (REACTION DESIGN, 2009) under constant volume and setting the temperature and pressure behind the reflected shock wave ( $T_5$ ,  $p_5$ ) as initial conditions. Ignition delay times for these simulations were defined as the instant at which the maximum value of the time derivative of OH concentration occurs.

### 4.2.2 Fuel and mixture preparation

The jet fuel examined in this investigation was the Brazilian commercial Jet A-1 fuel provided by Petrobras, also known as QAV1 “Querosene de Aviação 1”. Table 4.1 summarizes the main properties of this fuel sample.

Table 4.1: Properties of the studied Jet A-1 fuel - QAV1

Property	Value	ASTM Standard
Density, 15 °C, kg/m <sup>3</sup>	818.5	D4052
Kinematic viscosity, 20 °C, cSt	4.518	D7042
Total C mass. %	86.45	D5373
Total H mass. %	13.55	D5373
Molar mass, g/mol	160	GC/MS
Paraffins, % vol.	79.4	D1319
Olefins, % vol.	0.8	D1319
Aromatics, % vol.	19.8	D1319
Derived cetane number	41.9	D6890

It must be stressed out that the composition information provided by the ASTM D1319 test does not distinguish aliphatic hydrocarbons, linear or branched, from naphthenics nor does it provide data regarding the substituted or unsubstituted nature of aromatics. Given this limited knowledge, the chemical composition of the QAV1 was assumed as C<sub>11</sub>H<sub>21</sub>, following the practice of Vasu *et al.* (2008), thus resulting in a stoichiometric air/fuel ratio of 16.25.

Gas mixtures were prepared by injecting liquid Jet A-1 into a vacuumed, heated (125 °C) stainless steel mixing vessel. The total amounts of fuel and synthetic air were controlled manometrically to ensure the desired equivalence ratio. The mixture was stirred for 120 min to ensure homogeneity before it was filled in the test section of the shock tube.

## 4.3 EXPERIMENTS WITH SURROGATES AT C3 - NUI GALWAY

### 4.3.1 *Rapid compression machine*

A rapid compression machine (RCM) is a laboratory device that simulates the compression stroke of a single engine cycle, which allows the study of autoignition phenomena in an environment similar to a reciprocating engine but under somewhat idealized conditions. The RCM used in this study is a clone of the original Shell Thornton Research Centre machine (AFFLECK; THOMAS, 1968) that was donated to NUI Galway and it has a twin-opposed piston configuration which allows a fast compression time of ca. 15.7 ms. The pistons are pneumatically driven and hydraulically decelerated and stopped by controlled venting of hydraulic oil, with a stroke of 168 mm (each side) and a combustion chamber bore of 38.2 mm (1.5 inch). Creviced piston heads are used to contain the boundary layer thus suppressing the formation of a roll-up vortex that affects temperature homogeneity in the compressed mixture (SUNG; CURRAN, 2014). Figure 4.4 shows a photograph of the rapid compression machine facility without the heating system.



Figure 4.4: Rapid compression machine at C3 - National University of Ireland, Galway.

The piston heads used in this study were high compression ratio heads with an approximate compression ratio of 13:1. Compressed gas temperature was varied using a heating system comprising double-

stranded heating tapes (Flexelec, 1250 W) and a set of six thermocouples installed along the piston sleeves and reaction chamber. Different proportions of the inert gases nitrogen and carbon dioxide were employed to vary the heat capacity of the fuel/diluent mixture in order to obtain compressed temperatures around 650 K.

Pressure-time profiles were measured using a pressure transducer (Kistler 603B) and transferred via an amplifier (Kistler 5018) to a PC oscilloscope (Picoscope 4424) and recorded digitally on a computer using the Picolog software. For these RCM experiments, the ignition delay time is defined as the time from the peak pressure at the end of compression to the maximum rate of pressure rise during the ignition event. The ignition delay is reported as function of compressed gas temperature,  $T_c$ , which is calculated by Gaseq (MORLEY, 2004) using the initial temperature,  $T_i$ , pressure,  $p_i$ , compressed gas pressure,  $p_c$  and mixture composition.

The calculation on Gaseq employs an adiabatic compression/expansion routine which uses the temperature dependence of the ratio of specific heats,  $\gamma$ , according to

$$\ln\left(\frac{p_c}{p_i}\right) = \int_{T_i}^{T_c} \frac{\gamma}{\gamma-1} \frac{dT}{T} \quad (1)$$

while assuming frozen chemistry during compression. Figure 4.5 presents a typical RCM pressure trace for an experiment showing two-stage ignition. Estimated uncertainty limits of the RCM measurements are  $\pm 2\%$  in mixture composition,  $\pm 5$  K in compressed gas temperature,  $\pm 0.1$  bar in compressed pressure and  $\pm 15\%$  in ignition delay time.

Rapid compression machine simulations must account for the compression stroke and the effect of heat loss after top dead center, due to the relatively long duration of these processes. The basic premise for RCM simulation is known as “adiabatic core hypothesis” (SUNG; CURRAN, 2014), which assumes that the effect of heat loss to the reaction chamber during compression is limited to a thin boundary layer along the wall. Therefore the core of the gas mixture remains unaffected and even though the compression is not truly adiabatic the core is assumed to be compressed isentropically. After the end of compression the boundary layer heat loss is such that the core gas experiences an effective volumetric expansion, even though the geometric volume remains constant. As such the experimental pressure trace can be used to calculate a time-dependent “effective volume” for the core region.

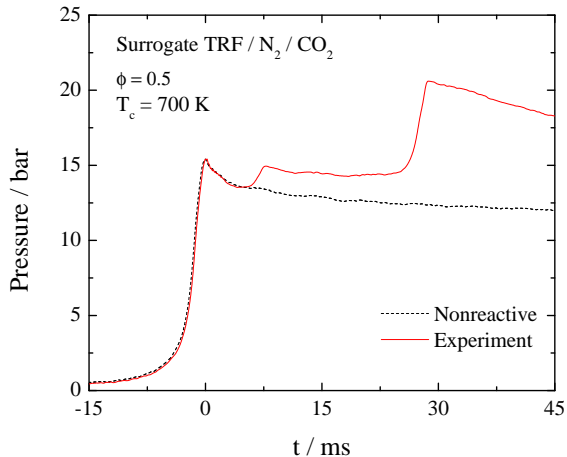


Figure 4.5: Typical RCM pressure trace showing both reactive and nonreactive pressure profiles, with the reactive profile exhibiting two-stage ignition.

In order to prepare for the simulation of a given reactive mixture in a RCM experiment that includes these facility effects, a non-reactive experiment is first carried out using a mixture with the same heat capacity, initial pressure, and initial temperature as the reactive one, typically by replacing  $O_2$  with  $N_2$  given their similar heat capacities. This measured pressure time history is directly converted into a volume history using the mixture specific heat ratio and the adiabatic core relation. An in-house Python routine was employed to compute and tabulate a volume history according to

$$V(t) = V_i \left( \frac{p(t)}{p_i} \right)^{\frac{1}{\gamma}} \quad (2)$$

It is important to note that this approach is unable to account for the heat release due to exothermic reactions. Mittal *et al.* (2010) assessed the validity of this zero-dimensional modeling for IDT prediction under conditions of two-stage ignition and NTC behavior. Based on comparison of CFD and zero-D simulations over the entire NTC regime of n-heptane the authors observed that zero-D calculations predicted first-stage ignition delays accurately but lead to a higher pres-

sure rise in the first-stage, consequently a shorter total ignition delay. Further study and discussion about these drawbacks is important but it is beyond the scope of the present investigation.

### 4.3.2 High pressure shock tube

The high pressure shock tube at C3-NUI Galway consists of a stainless steel tube of 8.76 meters in length, with an internal diameter of 6.3 cm. A double-diaphragm section divides the shock tube into a 3 meters long driver section and 5.73 m driven section. Aluminum plates were used as diaphragms in all experiments, with thickness varying from 1.0-1.4 mm depending on the desired  $T_5$ . The driver gas used was helium, with the eventual addition of nitrogen to achieve tailored driver gas conditions which allow for longer test times (CAMPBELL *et al.*, 2015). Figure 4.6 shows a photograph of the high pressure shock tube facility.

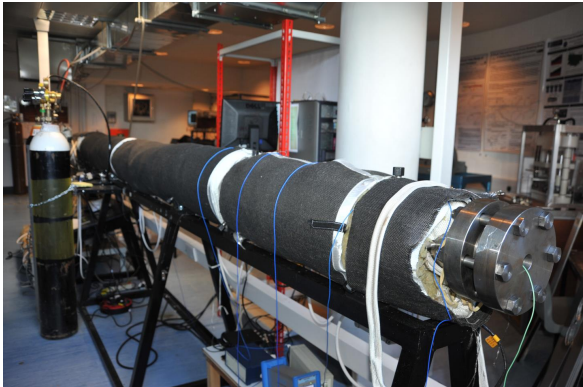


Figure 4.6: High pressure shock tube at C3 - National University of Ireland, Galway.

The diagnostic system consists of two digital oscilloscopes (TiePie Handyscope HS4) and six pressure transducers (PCB model 113A24) which measure the incident shock wave velocity at five locations separated by known distances, with the shock velocity extrapolated to the endwall. This extrapolated velocity was used to calculate the conditions,  $T_5$  and  $p_5$ , behind the reflected shock wave using the

equilibrium routine of Gaseq.

The pressure at the endwall was monitored using a pressure transducer (Kistler 603B) and the ignition delay time was defined as the interval between the rise in pressure due to the arrival of the incident shock wave at the endwall and the subsequent maximum rate of pressure rise. Experiments exhibiting significant pre-ignition pressure rise ( $\geq 5$  %/ms) were excluded from the study in order to avoid any non-ideal effects, thus allowing the acquired data to be accurately simulated by assuming constant volume, homogeneous adiabatic conditions. Estimated uncertainty limits of the measurements are 1 % in reflected shock temperature  $T_5$ ,  $\pm 2$  % in mixture composition and  $\pm 15$  % in ignition delay time.

### 4.3.3 Fuel surrogates and mixture preparation

Given the literature review presented in the preceding chapters and the facilities' configuration at the C3, especially the heating system (tanks, valves, manifolds and facilities), a series of experiments was devised using two different fuel surrogates. The composition of the tested surrogates is presented in Table 4.2.

Table 4.2: Surrogate compositions, in % mol., investigated at C3 - NUI Galway

Surrogate	n-heptane	n-decane	i-octane	toluene
MURI 1		42.7	33.0	24.3
TRF	42.7		33.0	24.3

Surrogate MURI 1, also known as POSF 4658 surrogate, was chosen given its extensive testing and comparison with a representative jet fuel sample, as well as the availability of a validated chemical kinetics mechanism (DOOLEY *et al.*, 2010). The tests performed in this study expand its validation data to different i.e. lower pressure, 15 bar, and lean equivalence ratio, 0.5. However, the low vapor pressure of n-decane, below 2 mbar at 25 °C, requires a preheating of tanks, manifolds and facility to 70 °C, in order to avoid fuel condensation. Therefore the available preheating temperature range for RCM experiments was limited to 70-105 °C, corresponding to compressed gas temperatures of 650-700 K.

Surrogate TRF is a lighter version of MURI 1, replacing n-decane with n-heptane, which has higher vapor pressure, 60.9 mbar at 25 °C, thus offering a broader range of preheating temperature, hence compressed temperature, to work with. Using the correlations taken from Morgan *et al.* (2010) this TRF mixture has an estimated RON/MON of 62/59. Detailed chemical kinetics models for this composition are available, including a model developed by Cancino *et al.* (2011) and an unpublished model from C3.

The pure hydrocarbon fuels were acquired from TCI UK (n-heptane, n-decane) and Sigma-Aldrich (iso-octane, toluene) with purity  $\geq 99.0\%$ . Liquid mixtures were prepared by volume and blended with a magnetic stirrer during 90 minutes. As these surrogate fuels are liquid at room temperature, the reactive test mixtures were prepared by a direct injection method. The heated mixing tanks were vacuumed to 0.1 mbar then fuel was injected using a gas-tight syringe (SGE Analytical Science, 5 ml) and its partial pressure was measured using a MKS pressure transducer and digital readout. The injection was followed by the addition of oxygen and nitrogen/carbon dioxide to achieve the desired final pressure and composition.

Mixtures were stirred for approximately one hour before the experiments. In order to ensure that fuel condensation had not happened between the tank and test chamber, in situ testing using an infrared laser system similar to that of Mével *et al.* (2012) was performed. Figure 4.7 exhibits a schematic of the laser diagnostic setup.

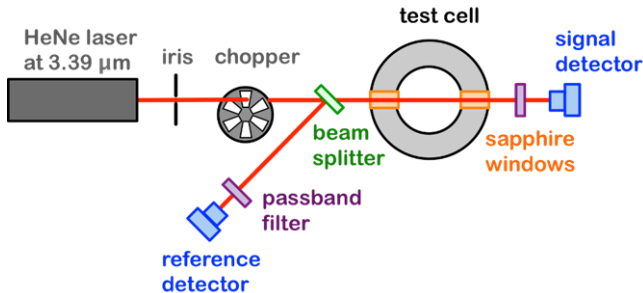


Figure 4.7: Schematic of the infrared laser diagnostic setup.

The light source is a 2 mW HeNe laser emitting at 3.39 μm, which passes through an optical chopper (ThorLabs, with MCF1F10

blade) operating at 300 Hz thus creating an on-off signal. A beam splitter (ThorLabs CM1-BP145B4) was used to send part of the light beam to a reference detector (ThorLabs PDA20H-EC), which is used to account for laser intensity variation and high frequency noise, while the remaining laser travels through the RCM chamber and reaches an equal detector after it. Each detector is fitted with a narrow pass band filter that selects the wavelength at which the HeNe laser line interacts with the C-H bond absorption line.

The ratio of the incident laser intensity,  $I^0$ , to the transmitted one,  $I$ , at a given frequency can be related to the fuel concentration  $C_f$  using the Beer-Lambert's law:

$$I = I^0 \exp(-LC_f\sigma_v) \quad (3)$$

where  $L$  is the path length through the gas mixture and  $\sigma_v$  is the absorption cross section at the frequency  $v$ . Given the use of a reference detector the absorption cross section can be expressed as follows:

$$\sigma_v = -\frac{1}{LC_f} \ln \left( \frac{I_{sig} I_{ref}^0}{I_{det} I_{sig}^0} \right) \quad (4)$$

where the subscripts *sig* and *ref* denote signal and reference. Thus the absorption cross section corresponds to the slope of:

$$-\frac{A}{L} = f(C_f) \quad (5)$$

with  $A$  corresponding to

$$A = \ln \left( \frac{I_{sig} I_{ref}^0}{I_{det} I_{sig}^0} \right) \quad (6)$$

Estimated uncertainties in the laser absorption measurements are 0.1 mbar in pressure,  $\pm 2$  K in temperature and 0.2 mm in path length, with a total uncertainty of  $\approx 2\%$  in measured fuel concentration.

## 4.4 RESULTS

Experiments with the Brazilian Jet A-1 sample were conducted at IVG - UDE between June and August/2013, spanning the 700-1250 K range for lean,  $\phi=0.3$ , and stoichiometric compositions at 15 and 30 bar. Experiments with MURI 1 and TRF surrogates were carried out at the C3 - NUI Galway facilities between January and July/2016, with conditions covering the 650-1300 K range for lean,  $\phi=0.5$ , and stoichiometric compositions at 15 bar. The ensuing subsections present tables and Arrhenius plots of shock tube measurements with Jet A-1, the pressure-time histories of rapid compression machine experiments, followed by tables and Arrhenius plots including both RCM and ST data of the surrogates tests.

### 4.4.1 Measurements of IDT for Jet A-1

The shock tube ignition delay times for stoichiometric and lean,  $\phi = 0.3$ , Jet A-1 mixtures are presented in Figure 4.8 and Table 4.3.

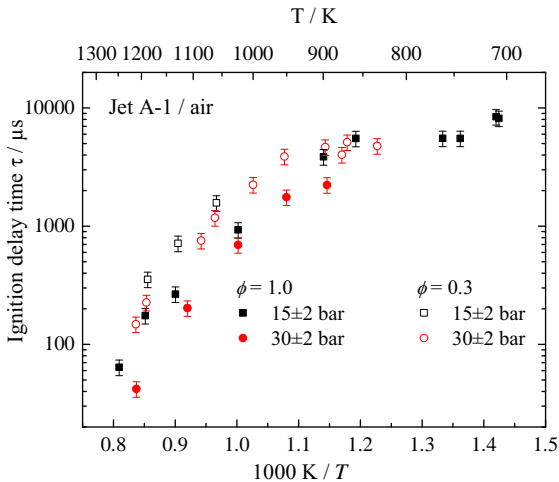


Figure 4.8: Shock tube measurements of ignition delay times for Jet A-1.

Table 4.3: Measured ignition delay times in ST for stoichiometric and lean Jet A-1/air mixtures

$\phi$	$T_5/\text{K}$	$\pm\Delta T_5/\text{K}$	$p_5/\text{bar}$	$\tau_1/\mu\text{s}$	$\tau_{ign}/\mu\text{s}$
0.3	1169.0	2	14.1	–	355
0.3	1105.4	4	15.2	–	716
0.3	1034.3	8	16.3	–	1574
0.3	879.3	–	14.1	–	N.I.
0.3	794.9	–	14.7	–	N.I.
0.3	1195.6	1	29.6	–	148
0.3	1171.8	1	28.9	–	226
0.3	1061.5	4	27.5	–	755
0.3	1036.8	6	25.9	–	1179
0.3	974.5	11	28.1	–	2242
0.3	928.5	18	24.8	–	3889
0.3	874.9	20	27.7	–	4671
0.3	854.6	17	30.4	–	4025
0.3	848.4	22	25.5	–	5142
0.3	814.8	19	31.5	–	4777
1.0	1235.7	1	16.8	–	64
1.0	1174.3	1	14.9	–	175
1.0	1110.6	1	16.1	–	266
1.0	998.1	5	15.7	–	931
1.0	876.9	17	14.7	–	3865
1.0	838.4	23	15.3	–	5528
1.0	750.0	21	13.1	–	5535
1.0	734.3	20	14.9	–	5533
1.0	704.3	30	16.3	7045	8428
1.0	702.1	29	16.2	6829	8176
1.0	1194.5	1	31.0	–	42
1.0	1087.2	1	30.5	–	203
1.0	998.0	3	30.5	–	695
1.0	925.7	8	29.4	–	1759
1.0	872.6	10	29.0	–	2233

Stoichiometric, high-temperature data at 15 bar is very similar to Jet A POSF 4658 IDTs reported by Wang & Oehlschlaeger (2012), but comparisons of shock tube data at intermediate temperatures indicate that QAV1 has ignition delay times a factor-of-two longer than POSF 4658. As mentioned before, Wang & Oehlschlaeger (2012) also reports data for Syntroleum’s S-8 (POSF 4734), Shell’s FT GtL (POSF 5172) and Sasol’s IPK (POSF 5642), with the latter having intermediate temperature IDTs somewhat comparable with our present results, even though the data with this synthetic fuel is sparse. For instance, at

20 atm, the IPK sample had an IDT of 3.332 ms at 805 K and 2.686 ms at 869 K, while QAV1, at 15 bar, had ignition delay times of 5.528 ms at 838 K and 3.865 ms at 877 K.

The measurements are curve-fitted to an equation of the form  $\tau = A \exp(B/T) p^{-x} \phi^{-y}$  where  $x$  and  $y$  are the pressure and stoichiometry exponents, respectively. Multiple linear regression analysis were performed using  $\ln(\tau)$  as dependent variable and  $(1/T)$ ,  $\ln(p)$  and  $\ln(\phi)$  as independent variables and identified the values of  $x = 0.89$  and  $y = 0.79$ . For the temperature and pressure dependence, the expression

$$\tau/\mu s = 10^{2.06 \pm 0.22} \exp\left(\frac{14510 \pm 490}{T/K}\right) (p/\text{bar})^{-0.89 \pm 0.12} (\phi)^{-0.79 \pm 0.06} \quad (7)$$

was determined from a curve-fit for the temperature range 925–1195 K. A weak NTC seems to occur between 750 and 850 K for stoichiometric, 15 bar tests.

#### 4.4.2 Measurements of IDT for MURI 1 surrogate

Figure 4.9 presents the pressure-time histories for the stoichiometric RCM experiments while Fig. 4.10 shows the lean,  $\phi=0.5$ , measurements.

One can notice that both sets of data present a two-stage ignition behavior, something that the original MURI experiments in RCM, taken at compressed pressure of 22 bar and reported by Dooley *et al.* (2010), did not show. The authors argued that “the emulation of two-stage POSF 4658 ignition would appear to be extremely challenging and will likely require a surrogate of more structurally diverse chemical fragments than those generated by a simple mixture of n-decane, *iso*-octane and toluene”. This aforementioned two-stage ignition presented by POSF 4658, previously shown in Fig. 3.2, is reported by them as “pseudo-first-stage” given the absence of an interval between ignition events during which the measured pressure history shows a plateau.

It must be pointed out that: a) their measurements were taken in synthetic air while the present experiments employed synthetic air/carbon dioxide mixtures; b) the facilities are quite different, with their data being obtained in the single-piston UConn RCM, which has a compression time between 25–35 ms, compared to ca. 16 ms of the NUIG facility. Regarding the mixture’s composition, carbon dioxide

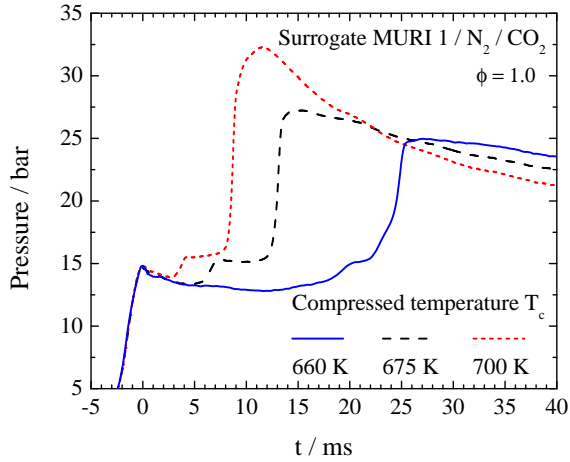


Figure 4.9: Pressure-time histories of stoichiometric MURI 1 autoignition in RCM.

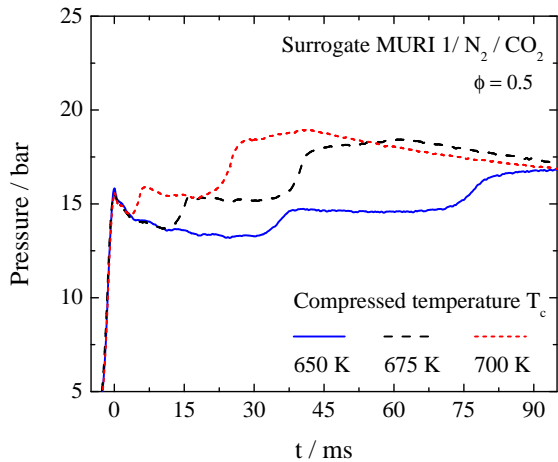


Figure 4.10: Pressure-time histories of lean MURI 1 autoignition in RCM.

does not undergo dissociation into CO and O in temperatures lower than 1000 K, hence its chemical kinetic effect is likely negligible. In

respect to the difference in compression times, Sung & Curran (2014) noted that shorter compression times, which result in significant pressure rise in the last milliseconds of the compression stroke, are desirable in order to minimize the extent of chemical induction processes during compression. This seems to be the case with our observations.

Regarding the overall pressure-time histories, at stoichiometric conditions Fig. 4.9 the interval between first stage and total ignition is much shorter, under 5 ms, than for the lean cases Fig. 4.10, over 15 ms. Also noteworthy is that the pressure increase due to the main ignition event is quite significant for stoichiometric conditions which is not the case for lean mixtures, where both first stage and main ignition pressure increases are small.

Under the conditions presented in both figures it is noticeable that ignition delay times decrease with increasing compressed temperatures, implying that the temperature range is lower than the onset of negative temperature coefficient (NTC) regime. For compressed temperatures above 700 K the pressure trace during compression was not equal to its nonreactive counterpart, therefore indicating the occurrence of kinetic phenomena before top dead center. Table 4.4 presents the detailed RCM measurements.

Table 4.4: Measured ignition delay times in RCM for stoichiometric and lean MURI 1/air/CO<sub>2</sub> mixtures

$\phi$	$T_c$ /K	$p_c$ /bar	$\tau_{ign}$ /ms
1.0	661	15.60	24.60
1.0	659	15.54	25.80
1.0	671	16.17	12.82
1.0	676	16.88	10.70
1.0	674	14.59	12.81
1.0	675	14.67	12.94
1.0	699	14.89	8.63
1.0	701	15.10	8.48
0.5	675	15.82	38.70
0.5	674	15.57	39.60
0.5	697	15.68	24.60
0.5	697	15.60	24.40
0.5	721	15.90	12.20
0.5	722	15.60	11.50

In order to complement the low-to-intermediate temperature data obtained in the RCM, a series of shock tube tests were conducted. Figure 4.11 shows the experimental measurements at both facilities

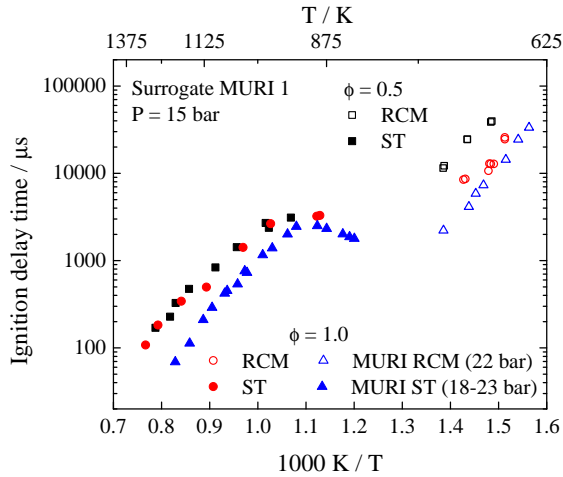


Figure 4.11: Measured ignition delay times for surrogate MURI 1.

Table 4.5: Measured ignition delay times in ST for stoichiometric and lean MURI 1/air mixtures

$\phi$	$T_5/\text{K}$	$p_5/\text{bar}$	$\tau_{ign}/\mu\text{s}$
1.0	1304.0	14.51	108
1.0	1261.7	14.72	183
1.0	1188.9	15.50	343
1.0	1119.7	14.96	497
1.0	1031.6	15.45	1416
1.0	974.0	15.25	2650
1.0	890.9	13.73	3225
1.0	885.9	13.76	3295
0.5	1270.1	13.90	170
0.5	1222.9	15.19	228
0.5	1206.0	13.53	327
0.5	1166.8	15.11	474
0.5	1096.5	14.49	835
0.5	1045.7	14.45	1423
0.5	984.0	14.03	2700
0.5	977.7	15.59	2372
0.5	935.8	14.97	3112

in an Arrhenius plot as well as original, stoichiometric MURI data,

for comparison and Table 4.5 presents the detailed experimental shock tube data.

It is noticeable that the RCM data shows a marked difference in reactivity between stoichiometric and lean cases, with the latter being around three times longer. The original RCM data of Dooley *et al.* (2010) follows a similar trend, with their data taken at pressures 50 % higher being around half as long as our results.

However, the equivalence ratio effect is not observable in the shock tube data, which is quite similar for both series of measurements. Comparison with original MURI data, taken at slightly higher pressures, shows a similar behavior close to the end of the NTC regime, around 900 K, but at higher temperatures the present ignition delay data is significantly longer.

#### 4.4.3 Measurements of IDT for TRF surrogate

Ignition delay times were measured for the TRF surrogate and Figure 4.12 presents the pressure-time histories for its stoichiometric RCM experiments while Table 4.6 shows the detailed measurements.

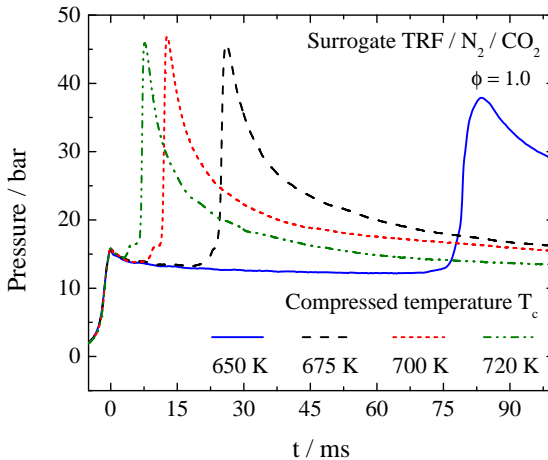


Figure 4.12: Pressure-time histories of stoichiometric TRF surrogate autoignition in RCM.

Table 4.6: Measured ignition delay times in RCM for stoichiometric TRF/air/CO<sub>2</sub> mixtures

$\phi$	$T_c$ /K	$p_c$ /bar	$\tau_{ign}$ /ms
1.0	646	15.43	73.70
1.0	647	15.45	79.20
1.0	644	15.17	76.80
1.0	674	16.00	22.80
1.0	672	15.78	24.10
1.0	671	15.74	24.80
1.0	698	15.88	11.90
1.0	698	15.90	12.00
1.0	722	15.85	6.90
1.0	721	15.70	6.52
1.0	721	15.67	6.53
1.0	778	15.51	4.00
1.0	778	15.44	3.91

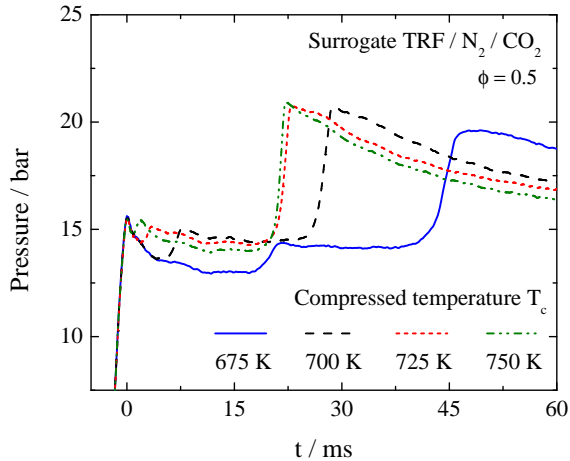


Figure 4.13: Pressure-time histories of lean TRF surrogate autoignition in RCM.

One can notice that stoichiometric TRF pressure histories exhibit a much sharper pressure peak during the ignition event when compared to stoichiometric MURI data, Fig. 4.9. This difference is associated to the composition of each surrogate, hence the total amount

of fuel, and their rate of consumption up to the main ignition event. Also noticeable is the occurrence of a small pre-ignition event, especially above 675 K, instead of a clear first-stage ignition as shown in Fig. 4.9. Figure 4.13 shows the pressure-time histories for the lean mixture experiments and Table 4.7 presents the detailed measurements.

Table 4.7: Measured ignition delay times in RCM for lean TRF/air/CO<sub>2</sub> mixtures

$\phi$	T <sub>c</sub> /K	p <sub>c</sub> /bar	$\tau_{ign}$ /ms
0.5	674	15.61	43.50
0.5	674	15.62	44.10
0.5	699	15.50	29.20
0.5	699	15.49	27.20
0.5	700	15.55	26.90
0.5	725	15.44	22.50
0.5	725	15.47	22.00
0.5	726	15.53	21.20
0.5	752	15.50	20.60
0.5	752	15.51	21.30
0.5	752	15.51	20.20
0.5	757	15.53	13.00
0.5	761	15.91	13.10
0.5	761	15.89	12.60
0.5	780	15.89	14.10
0.5	779	15.88	13.97
0.5	810	16.05	15.10
0.5	810	16.15	15.20
0.5	834	15.65	14.50
0.5	834	15.63	14.27

In Fig. 4.13 one can see a distinct pressure plateau between ignition events and also notice the onset of NTC region given the IDT at 725 and 750 K. Further data points were obtained for lean mixtures up to 834 K but for this intermediate temperatures the repeatability of compressed pressure was inferior, with no discernible first-stage ignition, even though the main ignition remained consistent. Table 4.8 shows the detailed shock tube measurements while Figure 4.14 presents an Arrhenius plot showing both shock tube and rapid compression machine data. As noted earlier, the equivalence ratio effect is very clear on the RCM experiments, with lean ignition delays being around twice as long as stoichiometric ones for temperatures below 675 K, with the difference increasing with temperature as the lean mixtures approaches

Table 4.8: Measured ignition delay times in ST for stoichiometric and lean TRF/air mixtures

$\phi$	$T_5/\text{K}$	$p_5/\text{bar}$	$\tau_{ign}/\mu\text{s}$
1.0	1267.8	15.20	113
1.0	1218.9	15.26	195
1.0	1167.0	14.54	312
1.0	1134.4	15.11	531
1.0	1080.0	15.04	931
1.0	1048.9	14.74	1171
1.0	1024.0	14.83	1848
1.0	999.0	14.76	1717
1.0	945.0	14.61	2919
0.5	1252.7	14.86	137
0.5	1194.6	14.65	279
0.5	1170.2	14.52	375
0.5	1130.2	14.24	674
0.5	1089.4	14.48	936
0.5	1048.9	13.93	1496
0.5	1036.3	14.36	1740
0.5	990.3	14.46	2670

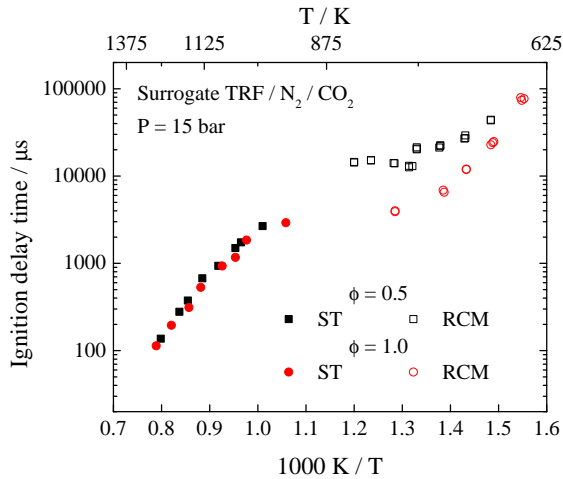


Figure 4.14: Measured ignition delay times for surrogate TRF

a plateau of reactivity associated with NTC phenomena.

It must be stressed out that the ‘gap’ between RCM measurements around 760 K is due to different blend of nitrogen/carbon dioxide used to attain the higher temperature data. The shock tube data is also similar to the MURI data, with the stoichiometric mixture showing slightly shorter ignition delays.

Having presented the experimental facilities and the ignition delay time measurements obtained, the ensuing chapter will detail the chemical kinetics modeling of this data as well as a comparative sensitivity analysis between two mechanisms for the TRF surrogate.

## 5 MODELING AND ANALYSIS

The previous chapter presented the measurements of ignition delay time for a commercial jet fuel sample and for two different, three-component surrogates. This chapter presents the chemical kinetics modeling of the obtained ignition delay data. The ensuing subsections detail the kinetics models employed and the comparisons between experiments and calculations.

### 5.1 MURI MECHANISM

The MURI mechanism published by Dooley *et al.* (2010) was assembled by the authors “to help interpret our experimental observations”. This detailed mechanism, comprising 6633 reactions among 1599 species, combines three individual kinetic models developed at Princeton University and Lawrence Livermore National Laboratory (LLNL) for toluene, C<sub>5</sub> to C<sub>10</sub> n-alkanes and C<sub>5</sub> to C<sub>8</sub> iso-alkanes. The C<sub>0</sub> to C<sub>4</sub> submodel adopted was the one for the toluene submechanism, which consists of the H<sub>2</sub>/O<sub>2</sub> model of Li *et al.* (2007), C<sub>1</sub> chemistry of Zhao *et al.* (2008), C<sub>2</sub> to C<sub>4</sub> submechanism of Healy *et al.* (2008) and the alkenyl submodel of Laskin *et al.* (2000).

Dooley *et al.* acknowledged that a detailed assessment and validation of the mechanism was not carried out and that the model should closely reproduce their flow reactor data while predicting ignition delays up to a factor-of-two longer. Cross reactions involving high molecular weight fuel radicals are not included, therefore, fuel components only interact through their respective influence on the small species population. Battin-Leclerc (2008), on her review of kinetic models for surrogates, argued that “cross-term” reactions are usually negligible in the oxidation of hydrocarbon mixtures but in the presence of aromatic components some of these reactions involving resonance-stabilized radicals could be important, at least to explain the formation of minor products.

### 5.1.1 Modeling of Jet A-1 ignition delays

In order to perform simulations of Jet A-1 data, two surrogate mixtures were proposed. The composition of these surrogates and corresponding *a priori* targets, previously discussed in Section 3.3.1, are presented in Table 5.1.

Table 5.1: Composition of proposed Jet A-1 surrogates for autoignition simulations and related *a priori* targets.

	Surrogate A	Surrogate B
n-decane, % mol.	33.5	65.4
iso-octane, % mol.	36.5	14.0
toluene, % mol.	30.0	20.6
Derived cetane number, by regression	42.0	56.5
$[\text{CH}_2/\text{CH}_3] \times [\text{CH}_2+\text{CH}_3]$ mass fraction	1.304	2.462

Surrogate ‘A’ was based on regression analysis of derived cetane number, as employed by Dooley *et al.* (2010). Since several mixtures of these three hydrocarbons can produce the same DCN, the mixture chosen as surrogate ‘A’ was the one with similar volume fraction of aromatics hence 30.0 % toluene by mol i.e. 20.5 % by volume.

Surrogate mixture ‘B’ was formulated considering the experimental evidence (SHAFER *et al.*, 2006; MOSES, 2008; DRYER *et al.*, 2012) that linear and weakly-branched alkanes are the statistical ‘mode’ of hydrocarbon isomers present in liquid fuels and this preponderance can be related to a methylene-to-methyl ( $\text{CH}_2/\text{CH}_3$ ) ratio that globally correlates with the low-temperature reactivity. Therefore, surrogate ‘B’ was formulated regarding the ASTM D1319 composition and adding this molecular group composition  $[\text{CH}_2/\text{CH}_3] \times [\text{CH}_2+\text{CH}_3]$  metric (WON *et al.*, 2014) while relaxing the DCN matching criteria. Figure 5.1 shows the comparison between experimental and numerical results of surrogate ‘B’.

The numerical IDT prediction based on the composition of surrogate ‘A’ was about 60 % higher than the IDT values predicted by surrogate ‘B’ leading to a larger deviation compared to the experiments therefore only modeling with surrogate ‘B’ is presented. As mentioned before, an overestimation of IDT for both surrogates is expected since this chemical kinetics model consistently overestimated IDT of

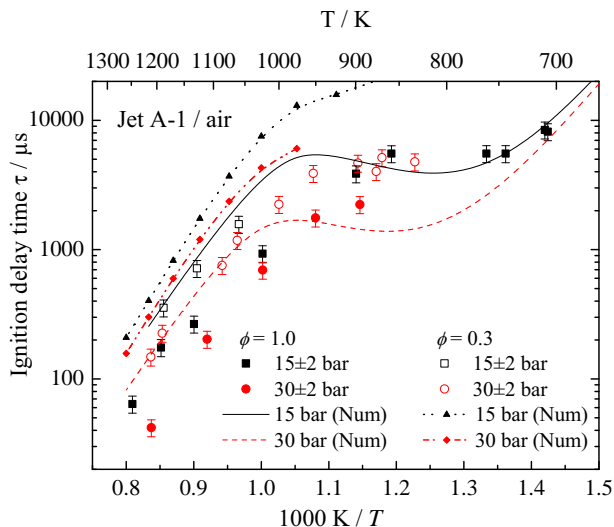


Figure 5.1: Comparison of measured Jet A-1/air and simulated surrogate ‘B’ ignition delay times.

the original experiments of Dooley *et al.* (2010), in which the *a priori* target-matching criteria was carried out for all four targets.

The computed IDTs of surrogate ‘A’ presented a significant overestimation, corroborating our expectation that the strategy of DCN matching with adjusted volume of aromatics is not enough to characterize ignition behavior. Among the likely causes for this lack of agreement is, as aforementioned, the limited information provided by the ASTM D1319 composition evaluation which does not distinguish aliphatics (linear and branched) from naphthenics nor does it provide data regarding the substituted or unsubstituted nature of the aromatics. Such information would be helpful to use another MURI target i.e. the overall H/C ratio.

On the other hand, surrogate ‘B’ computations predicted IDTs very close to the experimental values for low-to-intermediate temperatures (700–900 K) at 15 bar and stoichiometric mixtures. In this temperature range the combustion chemistry is quite complex, with the transition from low-temperature,  $O_2$  addition mechanism to the degenerate chain branching reaction involving  $HO_2$  and  $H_2O_2$ . The

agreement between experiment and computations for other conditions was qualitative, with lean mixtures having longer IDTs than stoichiometric ones and an increase in pressure resulting in shorter ignition delays. The faster ignition of surrogate ‘B’ compared to ‘A’ is due to the higher fraction of n-decane that offers sixteen secondary hydrogen sites (methylene) where molecular oxygen can promote an H-abstraction. The other alkane in the formulation, iso-octane, has only two such sites and they are shielded against O<sub>2</sub> attack by the methyl substituents in both adjacent carbons.

In the low-to-intermediate temperatures, surrogate ‘B’ has enough secondary hydrogen sites to present reactivity similar to the real fuel. However, in the transition from the NTC region to high temperature, n-decane is mostly gone while toluene, after an initial H-abstraction at the methyl substituent, forms a resonance-stabilized benzylic radical. Therefore, the surrogate ability to reproduce the real fuel’s intermediate-to-high temperature reactivity is limited by the absence of sufficient methylene units in the compounds other than n-decane. Dooley *et al.* also argue that the model shows an elongated NTC behavior, which is likely due to an under-emphasis of  $\beta$ -scission reactions of the alkyl radicals thus leading to increased low temperature chemistry processes instead of high temperature chain branching. This behavior is also noticeable in the present simulations.

### 5.1.2 Modeling of surrogate MURI 1 ignition delays

Figures 5.2 and 5.3 present selected comparisons between measured and calculated pressure-time histories for rapid compression machine experiments.

One can notice that under both stoichiometry conditions the mechanism is able to reproduce the trend of decreasing ignition delay around 50 % with a temperature increase of 15–25 K. Also, the computed first-stage pressure rises are higher than the experimental ones, as noted by Mittal *et al.* (2010). The stoichiometric calculations were able to show a brief first-stage ignition which was promptly followed by the hot ignition event while the lean equivalence ratio calculations reproduced quite well the interval between first-stage and overall ignition. In terms of ignition delay agreement the mechanism is around a factor-of-two slower than the experiments, as Dooley and coauthors

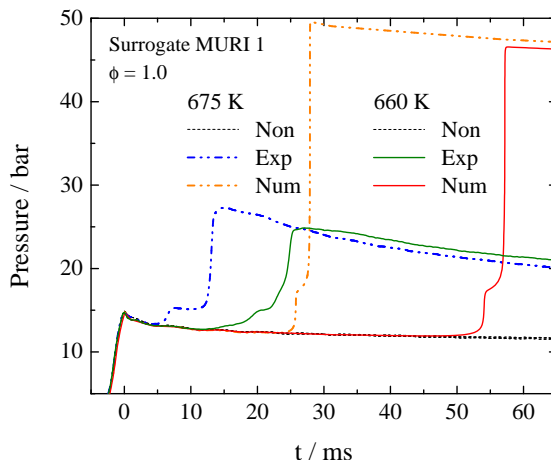


Figure 5.2: Measured and calculated pressure time histories for stoichiometric MURI ignition delays. Nonreactive pressure histories in black, solid lines represent compressed temperature of 660 K, dashed lines 675 K

reported originally.

Figure 5.4 presents the Arrhenius plot comparing experiments and calculations. As mentioned in Chapter 4, shock tube simulations use constant volume, perfectly stirred reactor conditions, thus these simulations are labelled “Const Vol”, while rapid compression machine calculations employ the effective volume history in order to account for heat loss and facility effects and are labelled “Fac Eff”.

As noted in the original MURI data (DOOLEY *et al.*, 2010), Fig. 5.4 shows that computed ignition delays for RCM experiments are consistently longer than the measurements. However, while this behavior was also presented in the original shock tube study, here the model actually reproduces the experimental ST data for temperatures close to 1125 K at both stoichiometric and lean conditions. The main disagreement occurs at temperatures between 875–1000 K, where, for example, the IDT for a lean experiment at 950 K is overestimated by a factor-of-three.

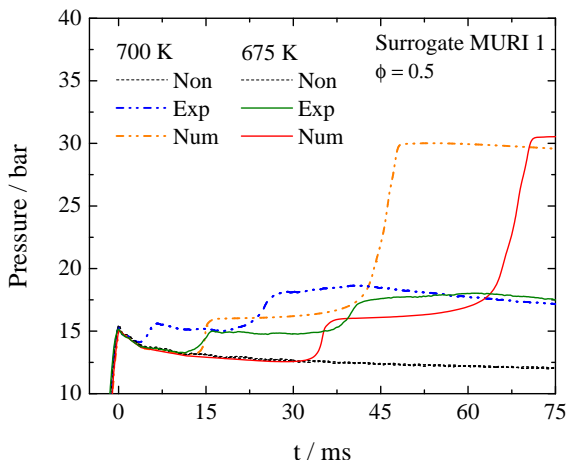


Figure 5.3: Measured and calculated pressure time histories for lean MURI ignition delays. Nonreactive pressure histories in black, solid lines represent compressed temperature of 675 K, dashed lines 700 K

## 5.2 MECHANISMS FOR TRF SURROGATE

Mixtures of n-heptane, iso-octane and toluene, generally known as toluene reference fuels (TRF) have been extensively studied as surrogates for gasoline (PITZ *et al.*, 2007; ANDRAE; HEAD, 2009; SMALLBONE *et al.*, 2010; KUKKADAPU *et al.*, 2013). In this work two detailed chemical kinetics models were employed to simulate TRF experiments: a multi-component gasoline surrogate mechanism by Cancino *et al.* (2011) and an unpublished version of the “Galway Mech”, a continuously work-in-progress model developed at the Combustion Chemistry Centre at NUI Galway in partnership with LLNL and the Clean Combustion Research Center at the King Abdullah University of Science and Technology (KAUST) in Saudi Arabia.

The detailed chemical kinetics model of Cancino and coauthors comprises 5242 elementary reactions among 1130 species. The model was assembled by merging the primary reference fuels (PRF) mechanism of Curran *et al.* (1998), the ethanol oxidation model of Cancino *et al.* (2009), the toluene submodel from Andrae *et al.* (2007) and the diisobutylene chemistry of Metcalfe *et al.* (2007).

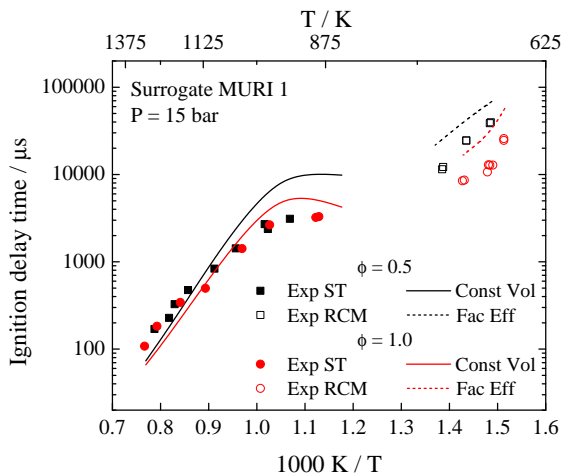


Figure 5.4: Experimental and computed ignition delay times for surrogate MURI. Solid lines represent constant volume (ST) simulations, dashed lines show simulation with facility effects (RCM).

The detailed Galway Mech comprises 6224 reactions among 1537 species. This model is based on the extensively validated AramcoMech 2.0 which was developed in a hierarchical way at the C3-NUI Galway employing their “consistent reaction rate rule” approach. The core  $\text{H}_2/\text{O}_2$  and up to  $\text{C}_4$  mechanism includes validation against ignition delay times in RCM and ST, intermediate species measured in flames, jet-stirred and plug-flow reactors for a series of fuels including hydrogen, syngas, methane, methanol, formaldehyde, ethane, ethylene, acetylene, ethanol, acetaldehyde, dimethyl ether and propene. The n-heptane submodel was reported by Zhang *et al.* (2016) while the iso-octane and aromatic chemistry have been under development in collaboration with LLNL and KAUST. The following figures present selected comparisons between measured and calculated pressure time histories employing both mechanisms.

Figure 5.5 shows that, at stoichiometric conditions, both mechanisms are able to produce a short first-stage ignition promptly followed by the hot ignition event thus reproducing the overall behavior of the experimental pressure history, with the NUIG model yielding shorter ignition delay times than Cancino’s. In the temperature range shown

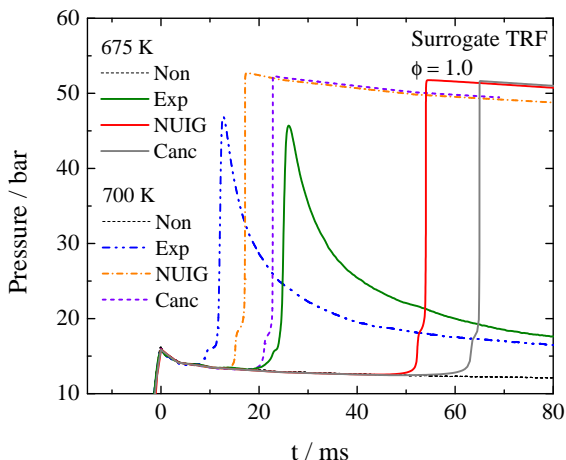


Figure 5.5: Measured and calculated pressure time histories for stoichiometric TRF ignition delays. Nonreactive pressure histories in black, solid lines represent compressed temperature of 675 K, dashed lines 700 K

an increase of 25 K in compressed temperature reduces the experimental ignition delay by roughly 50% while the models predict a decrease of 65–70% over the same range. Therefore the models overestimate the IDT by a factor of 2.5–3 at 675 K and by 1.5–2 at 700 K.

In Fig. 5.6, one can see that the models produce a pressure plateau, between first-stage and overall ignition, similar to the experiment but slightly shorter, which is likely due to the overestimation of the first-stage pressure rise previously pointed out by Mittal *et al.* (2010). For these lean conditions the overestimation of IDT is lower than for stoichiometric cases, with the models actually reproducing the ignition delay at 750 K. This condition will be further investigated by means of a sensitivity analysis in the following section. Figures 5.7 and 5.8 present the comparison of experiments and simulations in an Arrhenius plot.

Figure 5.7 presents the comparison between experiments and simulations at stoichiometric condition. For the low temperature range the best agreement occurs for temperatures of 720–770 K, with ignition delay times below this range being overpredicted. Regarding the intermediate and high temperature conditions both mechanisms follow

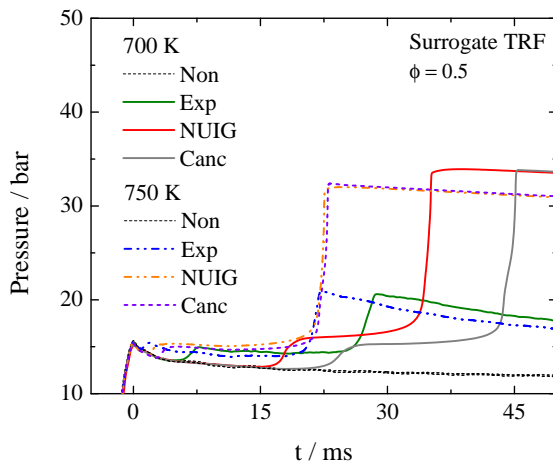


Figure 5.6: Measured and calculated pressure time histories for stoichiometric TRF ignition delays. Nonreactive pressure histories in black, solid lines represent compressed temperature of 700 K, dashed lines 750 K

the experiments closely, with the NUIG model showing a slightly better agreement with its slower predictions.

For the lean equivalence ratio data presented in Fig. 5.8, one can notice trends similar to those of stoichiometric data. For low temperature the best agreement occurs around 750 K with a factor-of-two overestimation of IDT happening at lower temperatures. Given the availability of pressure-time histories above 750 K, i.e. in the NTC region, it is possible to note that the Cancino model shows a plateau of reactivity when simulated under RCM conditions while for NUIG's mechanism the predictions show a clear NTC behavior. For the high temperature data the mechanism of Cancino shows strong agreement between 1000–1125 K, with an overall good agreement for both mechanisms.

In order to elucidate which elementary reactions are governing the different predictions of these two mechanisms for TRF a sensitivity analysis was performed at the RCM condition at which both models yield the same overall ignition delay time. This analysis is the topic of the ensuing section.

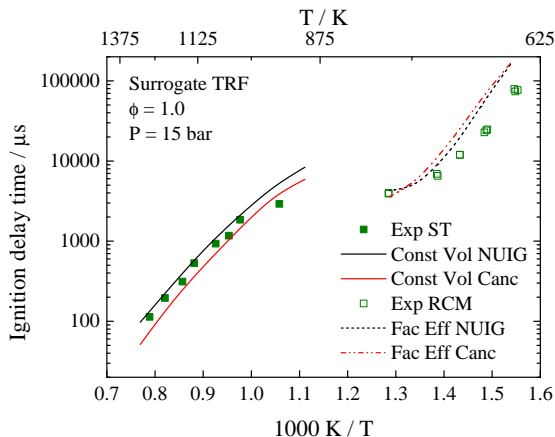


Figure 5.7: Experimental and computed ignition delay times for surrogate TRF at stoichiometric condition. Solid lines represent constant volume (ST) simulations, dashed lines show simulation with facility effects (RCM).

### 5.3 SENSITIVITY ANALYSIS

Sensitivity analysis is a computational tool that provides the relative importance of reaction parameters in respect to a selected target. It can be used also for optimization of detailed kinetics models since it gives information about the more sensitive, thus important, reactions in a kinetics scheme. The methodology can be applied to the time-evolution of the chemical species of a reactive system as the one in the autoignition of reactive mixtures in perfectly stirred reactors.

The choice of appropriate target depends on the objective of the analysis. This target has to be one of the dependent variables involved, such as temperature, species concentration or reaction rate. Independent variables cannot be defined as targets for sensitivity analysis, therefore it is not possible to perform a sensitivity analysis on ignition delay time. In this case an indirect approach is necessary e.g. setting a chemical species or set of reactions known to affect fuel depletion and temperature increase as targets.

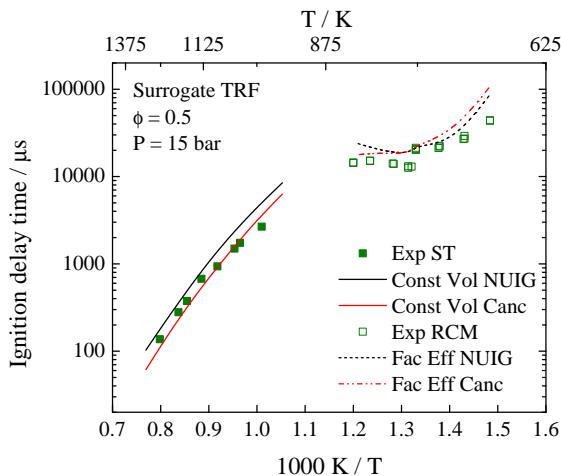


Figure 5.8: Experimental and computed ignition delay times for surrogate TRF at lean condition. Solid lines represent constant volume (ST) simulations, dashed lines show simulation with facility effects (RCM).

### 5.3.1 Sensitivity analysis of RCM ignition delay

The sensitivity coefficients in a sensitivity analysis performed by the corresponding module of CHEMKIN-PRO are obtained for each time-step of the transient solution. It is common to find in the literature (SIVARAMAKRISHNAN *et al.*, 2005; ANDRAE *et al.*, 2008) results of sensitivity analysis on temperature or chemical species in the form of bar graphs showing results at a specific elapsed time, like at ignition time, or at a specific fuel conversion. Typically the critical reactions at ignition time are identified and their original Arrhenius parameters are modified or optimized in order to show better agreement with experimental data.

Although these analysis at a single elapsed time e.g. ignition point may provide useful results, plenty of information is lost since the ignition event depends on all the kinetic events that occurred during the ignition delay. Cancino (2009) developed a computational tool for the post-processing of CHEMKIN's output files to account for the response of the sensitivity analysis of all reactions at every time-step during the ignition delay period, in a procedure called "overall analysis".

This overall analysis classified the three most sensitive reactions positively and negatively affecting a given species e.g. OH at each solution time-step thus gathering information about six reactions at a time. Once the classification was over, the routine calculated the amount of the ignition delay interval in which each reaction remained in the three tiers. Cancino successfully employed this tool in the optimization of his ethanol kinetics model (CANCINO *et al.*, 2009).

Here an in-between approach to sensitivity analysis was taken to study the differences between Cancino and NUIG models. The experimental condition investigated is lean equivalence ratio  $\phi=0.5$  and compressed temperature of 750 K. The corresponding experimental and computed pressure time histories are show in Figure 5.9.

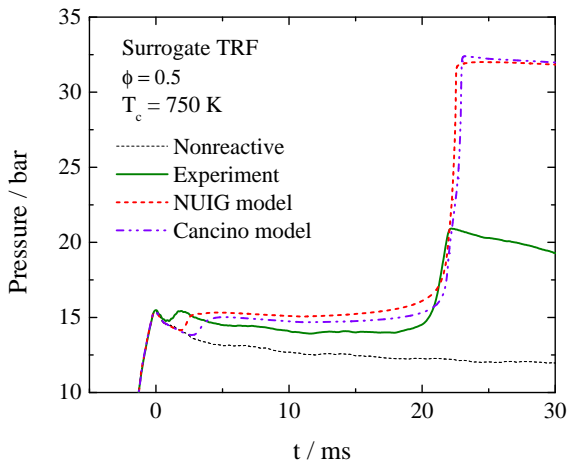


Figure 5.9: Measured and calculated pressure time histories for lean TRF ignition delay at compressed temperature of 750 K.

The normalized sensitivity coefficients computed by CHEMKIN-PRO were analyzed at five time-steps along the ignition delay interval: a) at the first inflection point of the pressure profile after compression i.e. when the mechanism starts to compute a pressure higher than the nonreactive profile; b) at an instant approximately halfway during the first-stage ignition; c) at the time-step in which the temperature is 825 K; d) at the instant in which the temperature is 850 K; e) at the last time-step before the onset of the hot ignition event.

As one can notice, the overall ignition delay time is virtually the same for experiment and simulations but the first-stage ignition delay is longer by about 1 ms from experiment to NUIG's prediction and from the latter to Cancino's prediction. In order to elucidate the different elementary reactions controlling the evolution of the reactive system a sensitivity analysis was carried out for seventeen species in Cancino model and eighteen species in NUIG model. These species are listed in Table 5.2

Table 5.2: Nomenclature of the species included in the sensitivity analysis, Cancino / NUIG

Oxygen	n-heptane	iso-octane	toluene
O <sub>2</sub>	NC7H16	IC8H18 / IC8	C6H5CH3
O	C7H15-1	AC8H17 / IC8-1R	C6H5CH2
OH	C7H15-2	BC8H17 / IC8-3R	absent / C6H4CH3
HO <sub>2</sub>	C7H15-3	CC8H17 / IC8-4R	
H <sub>2</sub> O <sub>2</sub>	C7H15-4	DC8H17 / IC8-5R	

The investigated species include molecular oxygen, the original hydrocarbon fuels, usually denoted as 'RH', their respective 'R' radicals resulting from the first H-abstraction, the dominant H-abstrating species O, OH and HO<sub>2</sub> as well as H<sub>2</sub>O<sub>2</sub> due to the importance of its decomposition into two OH radicals, which is a dominant chain branching reaction. Before looking into the sensitivity coefficients it is interesting to observe the fuel depletion during the ignition delay, as shown in Figure 5.10.

It is interesting to note the rapid depletion of n-heptane and iso-octane in NUIG's model, the latter being faster than Cancino's n-heptane consumption. After the end of compression NUIG's model takes a little under 2 ms to show the onset of first-stage ignition and during the next millisecond n-heptane is depleted to around 30% of its initial concentration, iso-octane to below 40% while more than 70% of toluene remains. For Cancino's model the first-stage onset occurs around 2.7 ms after the end of compression and in the following millisecond n-heptane is consumed to 40%, iso-octane to 60% and around 80% of toluene is still present.

Figure 5.11 shows the reactions with the higher sensitivity coefficients regarding the concentration of OH at the onset of first-stage pressure rise. Negative coefficients represent reactions related to consumption of OH, positive ones represent production of OH.

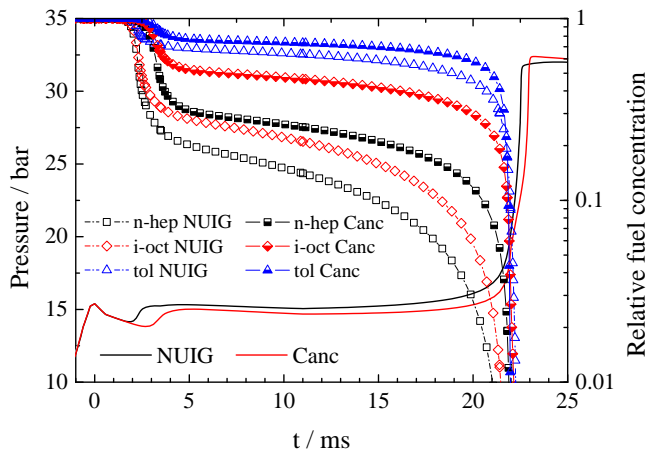


Figure 5.10: Computed pressure time histories and fuel depletion for lean TRF ignition delay at compressed temperature of 750 K. Open symbols denote NUIG's model, half-filled symbols indicate Cancino's model.

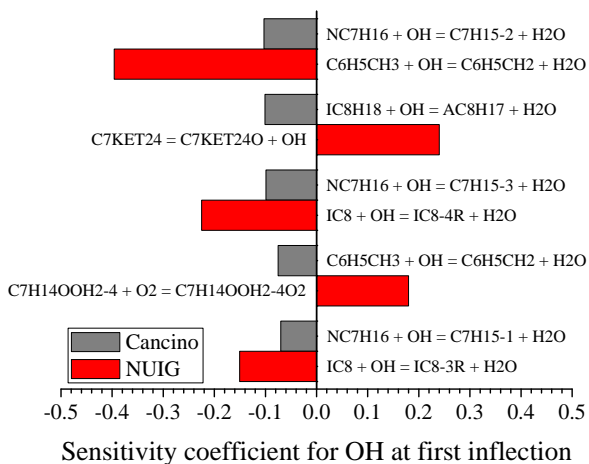


Figure 5.11: Sensitivity coefficients for the OH radical at the onset of first stage pressure rise, 1.8 ms for NUIG, 2.7 ms for Cancino.

For the Cancino model all the most sensitive reactions are H-abstractions from fuel by OH, with three of them being reactions with the most reactive fuel molecule, n-heptane, which is the expected initiation step for such reactive system. For the NUIG model, however, not only the coefficients are significantly larger but none of the reactions directly involves n-heptane. Two of the reactions producing OH involve products of the low-temperature oxidation of n-heptane i.e. the decomposition of the ketohydroperoxide C7KET24 and the O<sub>2</sub> addition to the hydroperoxy alkyl radical (QOOH) C7H14OOH2-4, while the OH-consuming channels are those of toluene and iso-octane.

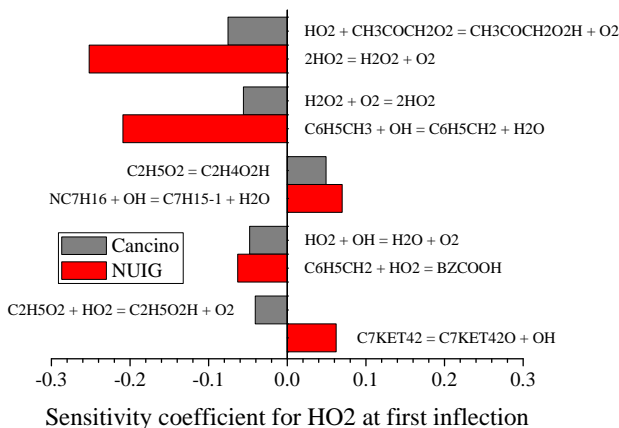


Figure 5.12: Sensitivity coefficients for HO<sub>2</sub> at the onset of first stage pressure rise, 1.8 ms for NUIG, 2.7 ms for Cancino.

Figure 5.12 shows the coefficients for hydroperoxyl radical HO<sub>2</sub> concentration at this time-step. Cancino's model shows hydroperoxyl radical only interacting with small molecular weight species i.e. HO<sub>2</sub> losing its hydrogen atom to other peroxides like acetyl (CH<sub>3</sub>COCH<sub>2</sub>O<sub>2</sub>), and ethyl peroxide (C<sub>2</sub>H<sub>5</sub>O<sub>2</sub>), and also OH, thus reforming O<sub>2</sub>. Other sensitive reaction is the conversion of two hydroperoxyl radicals into molecular oxygen and hydrogen peroxide H<sub>2</sub>O<sub>2</sub>, which is known for its marked negative temperature coefficient (HIPPLER *et al.*, 1990). For NUIG's model this latter reaction is the most sensitive and one of the two directly depleting HO<sub>2</sub>, the other being the interaction with benzyl radical to form benzyl hydroperoxide (BZ-

COOH = C<sub>6</sub>H<sub>5</sub>CH<sub>2</sub>OOH). Also promoting hydroperoxyl depletion, though indirectly, is H-abstraction by OH from toluene. The remaining reactions indirectly yield HO<sub>2</sub>: H-abstraction from n-heptane by OH and the decomposition of ketohydroperoxide C7KET42. Figure 5.13 shows the coefficients for n-heptane concentration at this time-step.

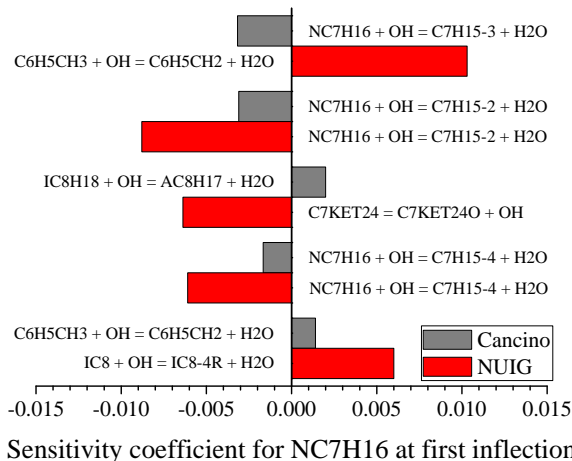


Figure 5.13: Sensitivity coefficients for n-heptane at the onset of first stage pressure rise, 1.8 ms for NUIG, 2.7 ms for Cancino.

One promptly notes that the magnitude of these coefficients is much smaller than those for OH radical due to fuel's high concentration i.e. the denominator of the sensitivity coefficient is large. Regarding the mechanism of Cancino, the three OH-sensitive reactions consuming n-heptane, Fig. 5.11, are the ones producing the alkyl radicals '-2', '-3' and '-1'. In the n-heptane sensitivity the represented reactions are the ones producing alkyl radicals '-3', '-2' and '-4'. For the NUIG mechanism the sensitive reactions consuming n-heptane produce the alkyl radicals '-2' and '-4', with the other reaction promoting heptane consumption being the decomposition of C7KET24. Once again the most sensitive reaction for the NUIG model is the formation of the resonance-stabilized benzylic radical C6H5CH2.

Figure 5.14 presents the sensitivity coefficients for iso-octane at this time-step. As noted for the n-heptane analysis, iso-octane coefficients are also small, to the point that Cancino's model only shows

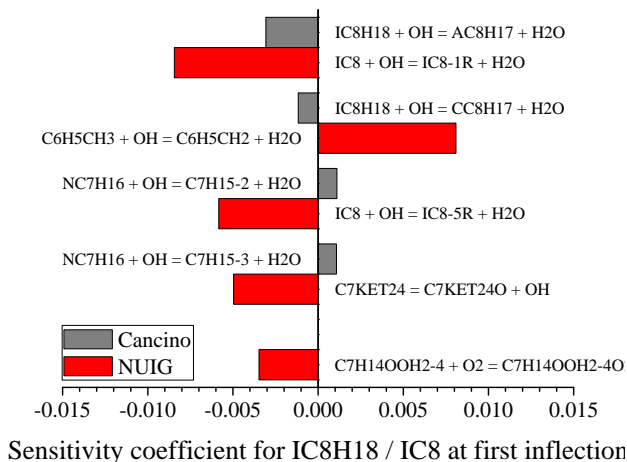


Figure 5.14: Sensitivity coefficients for iso-octane at the onset of first stage pressure rise, 1.8 ms for NUIG, 2.7 ms for Cancino.

four sensitive reactions for this species. The two most sensitive are H-abstractions by OH from the parent fuel yielding iso-octyl radicals while the remaining two are H-abstractions by OH from n-heptane, which result in reduced iso-octane consumption. In NUIG's mechanism the sensitive reactions are also H-abstractions from iso-octane by OH while the other reactions are the decomposition of the ketohydroperoxide C7KET24 and the O<sub>2</sub> addition to the n-heptane derived QOOH, all of them depleting iso-octane. The formation of benzylic radical is once again prominent in its radical scavenging role. The sensitive reactions for toluene are very similar therefore will not be shown here.

A few time-steps later, during the first-stage pressure rise the sensitive reactions for OH are quite different as can be seen in Figure 5.15. One can see that, during the first stage pressure rise, reactions mostly affecting OH concentration are not interactions with high molecular weight hydrocarbons but rather with formaldehyde (CH<sub>2</sub>O), yielding formyl radical and water. Also important is the decomposition of methyl hydroperoxide (CH<sub>3</sub>O<sub>2</sub>H) that yields methoxy radical (CH<sub>3</sub>O) and OH. These two reactions are the intermediate steps in the oxidation of CH<sub>3</sub> to CO i.e. CH<sub>3</sub> → CH<sub>3</sub>O → CH<sub>2</sub>O → HCO → CO. The mechanism of Cancino also shows the decomposition of acetyl hydro-

peroxide ( $\text{CH}_3\text{COCH}_2\text{O}_2\text{H}$ ) and ethyl hydroperoxide ( $\text{C}_2\text{H}_5\text{O}_2\text{H}$ ), both species that appeared in Fig. 5.12, to be sensitive. The NUIG model analysis indicates the importance of benzyl hydroperoxide ( $\text{BZCOOH} = \text{C}_6\text{H}_5\text{CH}_2\text{OOH}$ ) decomposition into alkoxy benzyl and OH.

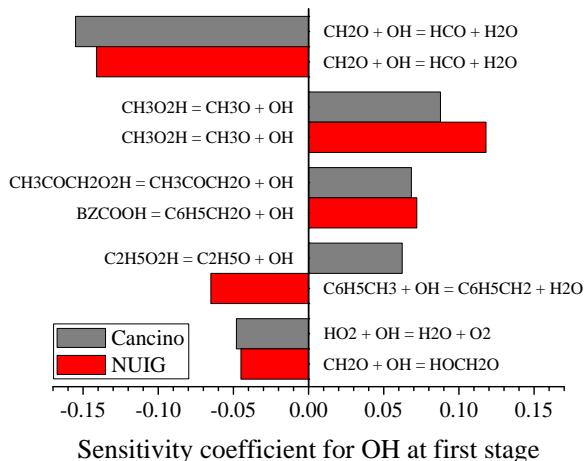


Figure 5.15: Sensitivity coefficients for OH during the first stage pressure rise, 2.3 ms for NUIG, 3.4 ms for Cancino.

Figure 5.16 shows the sensitivity coefficients for  $\text{HO}_2$  at this instant. For both mechanisms the most sensitive reaction is the conversion of two  $\text{HO}_2$  into  $\text{H}_2\text{O}_2$  and molecular oxygen, followed by hydroperoxyl interaction with methyl peroxide. Among the sensitive reactions contributing, though indirectly, to the formation of  $\text{HO}_2$  is H-abstraction by OH from formaldehyde and the decompositions of  $\text{CH}_3\text{O}_2\text{H}$  and  $\text{BZCOOH}$ .

Even with the strong consumption of n-heptane during the first millisecond after the pressure inflection point, the sensitivity coefficients of the reactions affecting this fuel's concentration are smaller than 0.01, as shown in Fig. 5.13. This is also the case for the reactions involving iso-octane and toluene. As one would expect the reactions of fuel-derived alkyl radicals present significant sensitivity as can be seen in Figure 5.17 for heptyl radicals.

It must be stressed out that Fig. 5.17 does not show the most sensitive reaction for each of the four heptyl radicals, which is their

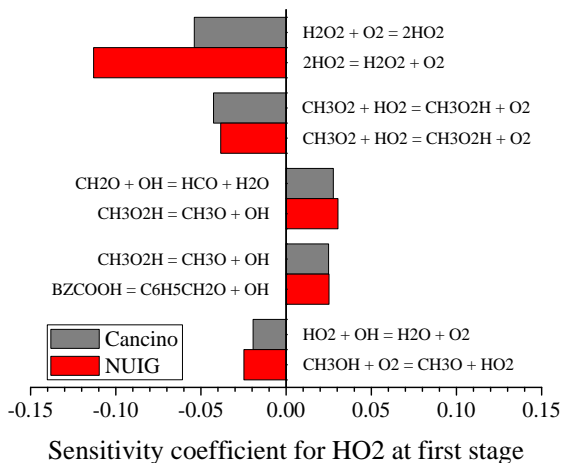


Figure 5.16: Sensitivity coefficients for  $\text{HO}_2$  during the first stage pressure rise, 2.3 ms for NUIG, 3.4 ms for Cancino.

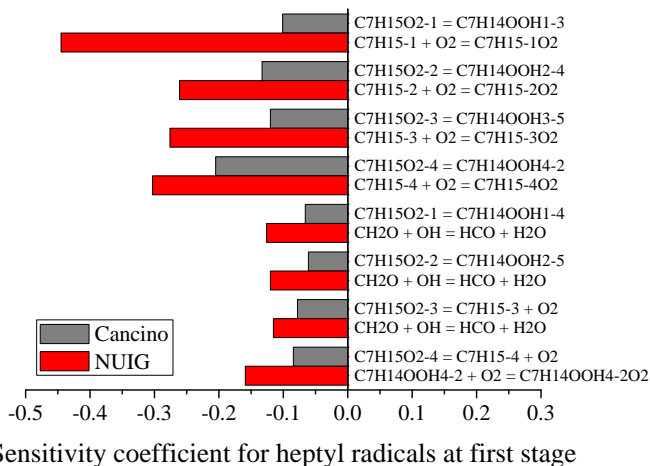


Figure 5.17: Sensitivity coefficients for the four heptyl radicals during the first stage pressure rise, 2.3 ms for NUIG, 3.4 ms for Cancino.

respective formation from n-heptane, but rather the second and third most sensitive reactions i.e. the most important alkyl consuming channels. Among this reduced set, the most sensitive reaction for Cancino's model is an internal H-abstraction through a six-membered transition state forming hydroperoxyalkyl C7H14OOH4-2. This particular molecule is formed from the theoretically less abundant C7H15-4 alkyl radical, which was not present in the OH-sensitivity of Fig. 5.11. Other sensitive reactions are the three analogous six-membered ring internal H-abstractions (1-3, 2-4, 3-5), two internal H-abstractions through less-favored seven-membered transition state (1-4, 2-5), and O<sub>2</sub> additions to heptyl radicals '-3' and '-4'.

For NUIG's mechanism the O<sub>2</sub> addition to 1-heptyl radical is the most sensitive reaction, followed by the corresponding O<sub>2</sub> additions to radicals '-4', '-3' and '-2', in this order. The remaining reactions are an O<sub>2</sub> addition to QOOH and the OH interaction with formaldehyde, the latter being the third most sensitive reaction for heptyl isomers '-1', '-2' and '-3'. So, thus far, the sensitive reactions indicate that Cancino's model slower formation of 'R' radicals is followed by a faster formation of RO<sub>2</sub> then a slower isomerisation to QOOH while the trend for NUIG's mechanism seems the opposite, with O<sub>2</sub> addition to alkyl radicals being the sensitive step. Figure 5.18 presents the sensitive reactions depleting octyl radicals.

One can notice that the most sensitive reaction for both mechanisms is the decomposition of *tert*-iso-octyl, which is formed by abstraction of iso-octane's only tertiary hydrogen, into iso-butene and *tert*-butyl. For NUIG's model the remaining reactions are O<sub>2</sub> additions to iso-octyl isomers, the decomposition of iso-octyl peroxide into IC8D3 (2,4,4-trimethyl-2-pentene) and HO<sub>2</sub>, and the OH interaction with formaldehyde. For Cancino's model the second most sensitive reaction is the decomposition of an iso-octyl radical into iso-butene and iso-butyl, followed by the reaction between formaldehyde and OH, and internal H-abstractions among octyl peroxides. For toluene-derived radicals the important reaction at this time-step occurs between benzyl radical C<sub>6</sub>H<sub>5</sub>CH<sub>2</sub> and HO<sub>2</sub>, with the mechanism of Cancino reporting the products as C<sub>6</sub>H<sub>5</sub>CH<sub>2</sub>O and OH while in NUIG's model this reaction produces BZCOOH.

A few time-steps later, during the pressure plateau between first stage and main ignition, reactive mixture temperature reaches 825 K, around 3.1 ms after the end of compression for NUIG's prediction and

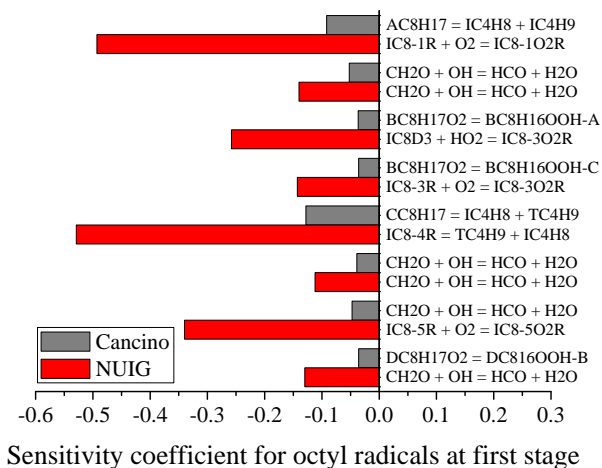


Figure 5.18: Sensitivity coefficients for the four octyl radicals during the first stage pressure rise, 2.3 ms for NUIG, 3.4 ms for Cancino.

4.9 ms for Cancino's. Figure 5.19 presents the OH-sensitive reactions at this condition.

The graph shows that the reaction of OH with formaldehyde is an important hydroxyl-consuming channel for both mechanisms, being the most sensitive reaction for Cancino's model and the second most for NUIG's. The decomposition of methyl hydroperoxide ( $\text{CH}_3\text{O}_2\text{H}$ ) yielding methoxy radical ( $\text{CH}_3\text{O}$ ) and OH is the most sensitive reaction for NUIG's model while the decomposition of  $\text{H}_2\text{O}_2$  into 2 OH is the second most sensitive for Cancino's. Looking at the remaining reactions and their signs, Cancino's mechanism shows  $\text{H}_2\text{O}_2$  decomposition, which is the governing intermediate temperature chain-branching reaction, as sensitive at this temperature while the other reactions involving H/O/ $\text{C}_1$  species are OH-consuming. For NUIG's mechanism both OH-consuming channels are interactions with formaldehyde while OH formation reactions are decompositions of  $\text{C}_2/\text{C}_3$  species.

In Figure 5.20 one can notice that the most sensitive reaction for each mechanism remains the same noted in Fig. 5.16 i.e. the conversion of 2  $\text{HO}_2$  into hydrogen peroxide and molecular oxygen, but the sensitivity coefficient is significantly higher. For Cancino's model the other reactions include some ketone decompositions that slightly promote the

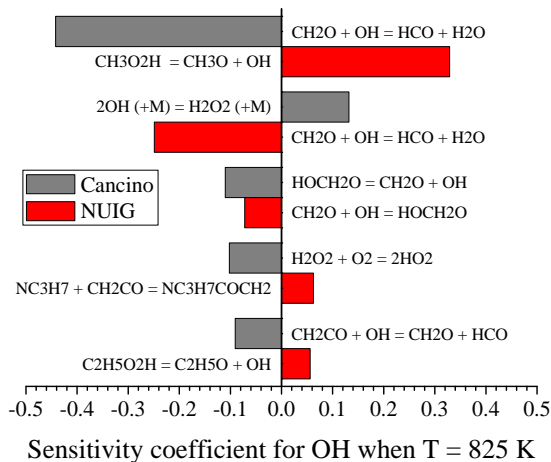


Figure 5.19: Sensitivity coefficients for OH when temperature T = 825 K, 3.1 ms for NUIG, 4.9 ms for Cancino.

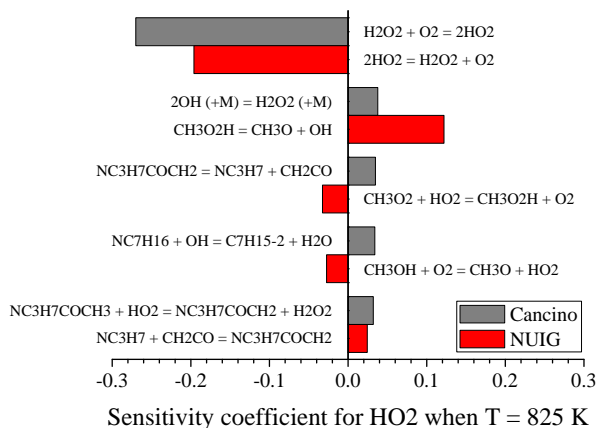


Figure 5.20: Sensitivity coefficients for HO2 when temperature T = 825 K, 3.1 ms for NUIG, 4.9 ms for Cancino.

formation of HO<sub>2</sub> while the remaining reactions for NUIG's model are methoxy, methanol and methyl peroxide interactions with the radical

pool. Figure 5.21 shows the reactions affecting the n-heptane derived ‘R’ radicals at this time-step.

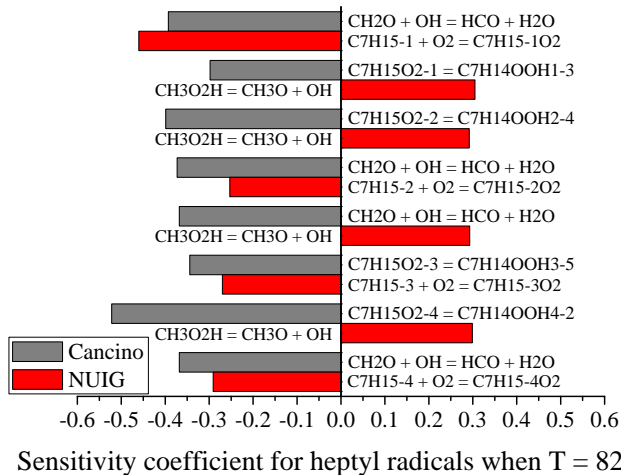


Figure 5.21: Sensitivity coefficients for the four heptyl radicals when temperature  $T = 825$  K, 3.1 ms for NUIG, 4.9 ms for Cancino.

As aforementioned, the most sensitive reaction for each of these heptyl radicals is their formation from the parent fuel by H-abstraction thus Fig. 5.21 presents the second and third most sensitive reactions. Here one can notice that the mechanism from NUIG shows the decomposition of  $\text{CH}_3\text{O}_2\text{H}$  affecting the concentration of heptyl radicals by means of yielding OH that will attack the parent fuel. The other reactions for this model are the  $\text{O}_2$  additions to heptyl radicals also present in Fig. 5.17. For Cancino’s, the sensitive coefficients are much larger than during the first-stage time-step and the internal H-abstraction forming heptyl hydroperoxide  $\text{C}_7\text{H}_{14}\text{OOH}\text{-4-2}$  remains the most sensitive reaction. The remaining reactions are the analogous six-membered ring internal H-abstractions (1-3, 2-4, 3-5) and the reaction between  $\text{CH}_2\text{O}$  and OH, which appeared in NUIG’s sensitivity at the previous condition, Fig. 5.17.

In Fig. 5.22 the sensitive coefficients for octyl radicals are shown. As pointed out in the previous graph, coefficients for Cancino’s model are much larger than those at the first-stage time-step. Regarding octyl

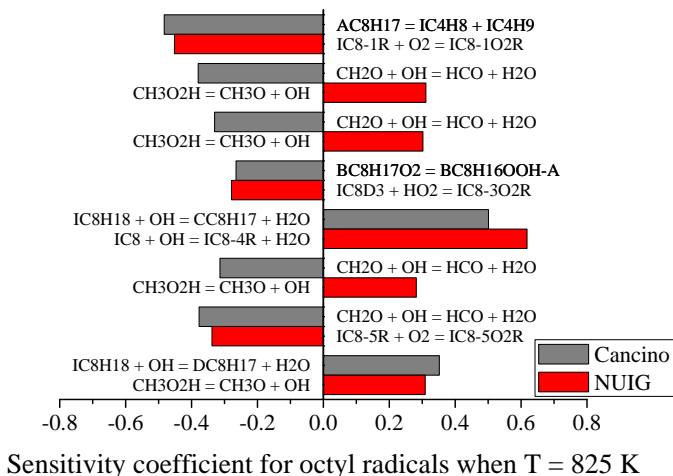


Figure 5.22: Sensitivity coefficients for the four octyl radicals when temperature  $T = 825$  K, 3.1 ms for NUIG, 4.9 ms for Cancino.

radical consumption, Cancino's mechanism indicates the decomposition of AC8H17 into iso-butene and iso-butyl as the most sensitive reaction, followed by the reaction between formaldehyde and OH, and internal H-abstraction producing hydroperoxy alkyl radical BC8H16OOH-A. At this condition the formation of octyl radicals CC8H17 and DC8H17 from the parent fuel are also sensitive. For NUIG model the most sensitive reaction is H-abstraction of iso-octane's only tertiary hydrogen to form IC8-4R. The remaining reaction with positive coefficient is the decomposition of methyl hydroperoxide ( $\text{CH}_3\text{O}_2\text{H}$ ) yielding methoxy radical ( $\text{CH}_3\text{O}$ ) and OH. Reactions with negative coefficients are  $\text{O}_2$  additions to octyl isomers '-1R' and '-5R', and decomposition of IC8-3O2R into IC8D3 and  $\text{HO}_2$ .

The sensitive reactions for toluene-derived radicals at this time-step are the same as aforementioned, between benzyl radical  $\text{C}_6\text{H}_5\text{CH}_2$  and  $\text{HO}_2$ , with the mechanism of Cancino reporting the products as  $\text{C}_6\text{H}_5\text{CH}_2\text{O}$  and OH while in NUIG's model this reaction produces BZCOOH.

Several time-steps later the temperature of the reactive mixture reaches 850 K, around 8.5 ms after the end of compression for NUIG's prediction and 15.3 ms for Cancino's. This interval between predictions

is quite significant and its cause is not *a priori* evident. The most likely explanation is that the model of Cancino presents stronger sensitivity to the endothermic reaction  $\text{HO}_2 + \text{HO}_2 \rightarrow \text{H}_2\text{O}_2 + \text{O}_2$ . Figure 5.23 presents the OH-sensitive reactions at this instant.

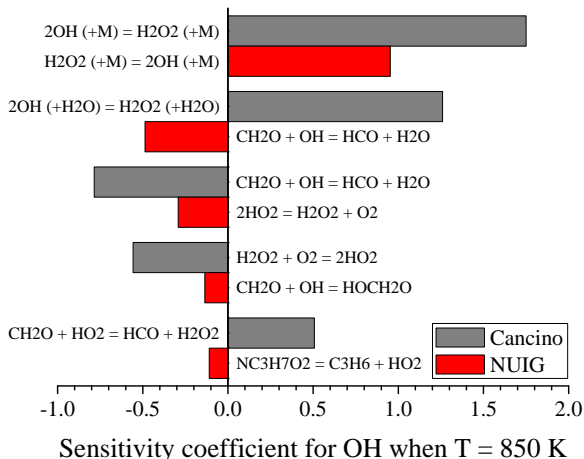


Figure 5.23: Sensitivity coefficients for OH when temperature  $T = 850$  K, 8.5 ms for NUIG, 15.3 ms for Cancino.

The graph shows that, at this temperature, the intermediate chain branching decomposition of hydrogen peroxide is the dominant reaction for both mechanisms. It is interesting to note that Cancino's model has an explicit elementary reaction for water as a third body and its coefficient is quite significant compared to NUIG's overall reaction. Reactions involving formaldehyde, OH,  $\text{HO}_2$ , and  $\text{H}_2\text{O}_2$  comprise the remaining of the sensitive subset.

The sensitivity coefficients for  $\text{HO}_2$  at this condition are shown in Figure 5.24. Compared to the sensitivity evaluated at 825 K, Cancino's model indicates that  $\text{HO}_2$  concentration is no longer sensitive to ketone decompositions but only to core H/O/ $\text{C}_1$  reactions. In fact, the sensitivity data of all species analyzed, listed in Tab. 5.2, for 850 K up to the main ignition event comprise the same set of reactions: H-abstraction by OH from formaldehyde; conversion of two hydroperoxyl radicals into hydrogen peroxide and molecular oxygen; and the chain-branching decomposition of hydrogen peroxide yielding two hydroxyl

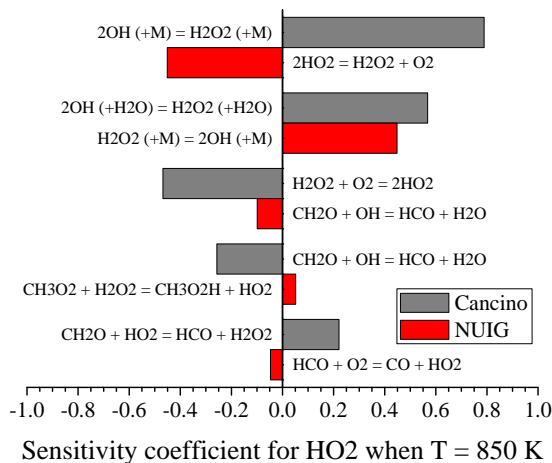


Figure 5.24: Sensitivity coefficients for  $\text{HO}_2$  when temperature  $T = 850$  K, 8.5 ms for NUIG, 15.3 ms for Cancino.

radicals. The latter reaction extensively populates the radical pool with OH, resulting in the final consumption of the remaining parent fuels.

Other reactions with marked sensitivity are unimolecular decompositions of octyl radicals, the same reactions noted at first-stage pressure rise, Fig. 5.18. It is interesting to note that, from this 850 K instant, Cancino's model predicts the temperature to increase to around 915 K in 5.5 ms until the occurrence of main ignition while for NUIG's mechanism the temperature increases to 965 K during 12.5 ms. Figure 5.25 outlines the most sensitive reactions at each condition analyzed, in terms of positive or negative contribution to the mixture reactivity.

In summary, the sensitive analysis carried out suggests that, for NUIG's model, the autoignition of this surrogate mixture is governed by two processes: the rate of  $\text{O}_2$  additions to alkyl radicals; and the competition between the decomposition of  $\text{CH}_3\text{O}_2\text{H}$  into methoxy radical and OH, the decomposition of  $\text{H}_2\text{O}_2$ , and the radical scavenging role of benzyl radical. For the mechanism of Cancino the reactions determining overall reactivity are internal H-abstractions  $\text{RO}_2 \rightleftharpoons \dot{\text{Q}}\text{OOH}$ , followed by the competition between  $\text{H}_2\text{O}_2$  decomposition and its reaction with molecular oxygen yielding two  $\text{HO}_2$ .

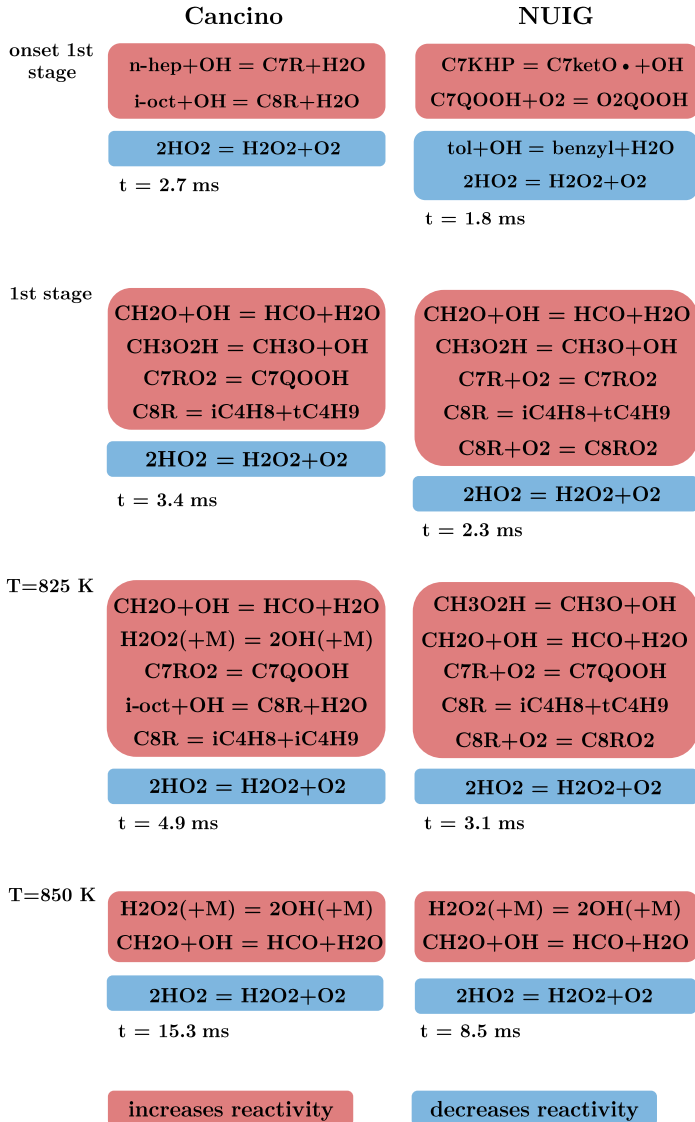


Figure 5.25: Summary of the most sensitive reactions during TRF's ignition delay, in rapid compression machine, at 15 bar, 750 K and  $\phi=0.5$ . Reactions in red promote reactivity, reactions in blue decrease reactivity.



## 6 CONCLUSIONS AND RECOMMENDATIONS

The present thesis aimed at analyzing the autoignition behavior of jet fuel and fuel surrogates, yielding contributions regarding the use of alternative aviation fuels produced from renewable feedstocks. Based on a thorough literature review of experimental studies with commercial fuels and proposed surrogates, an experimental and chemical kinetics modeling study was carried out, focusing on the evaluation of negative temperature coefficient (NTC) phenomena and two-stage ignition behavior.

First, ignition delay time measurements of a Brazilian commercial Jet A-1 fuel sample (QAV1) were performed in a high pressure shock tube spanning a temperature range from 700 K to 1250 K, pressures of 15 bar and 30 bar and fuel/air equivalence ratios of 0.3 and 1.0. Two-stage ignition was detected in stoichiometric tests around 700 K and 15 bar. Between 750 and 850 K, the ignition data showed a weak NTC behavior, i.e., a reactivity plateau, in which the ignition delay times were ca. 5.5 ms. In comparison with other conventional jet fuel, the NTC region of Jet A POSF 4658, measured at 20 atm, spanned the 750-900 K range, with IDTs of approximately 2 ms (WANG; OEHLISCHLAEGER, 2012). In the case of an alternative aviation fuel, Syntroleum's S-8 POSF 4734, ignition data also obtained at 20 atm showed NTC behavior between 725-950 K, with IDTs around 1.3 ms (DOOLEY *et al.*, 2012b).

An expression fitting the QAV1 high temperature measurements was obtained and a detailed chemical kinetics modeling of the autoignition was carried out using the three-component MURI 1 (n-decane, iso-octane, toluene) mechanism from Dooley *et al.* (2010). Based on Dooley's proposed approach of *a priori* target matching, a first surrogate mixture used to simulate QAV1 autoignition was formulated considering information provided by ASTM standards, i.e., volumetric fraction of paraffins, olefins, and aromatics, and derived cetane number (DCN). A second surrogate mixture, employing a methylene-to-methyl metric (WON *et al.*, 2014) instead of DCN, was also proposed. Computation with this latter blend (65.4 % n-decane, 14.0 % iso-octane, 20.6 % toluene, by mol) predicted ignition delay times very close to the experimental values for low-to-intermediate temperatures (700-900 K) at 15 bar and stoichiometric condition. The agreement between experiment and computations for other conditions was qualitative.

Considering our results with QAV1 and literature data, one can notice that, even with knowledge of the elementary reactions governing NTC behavior, its extent is not, as of today, associated or correlated to any *a priori* fuel property target. The methylene-to-methyl metric, proposed by Won *et al.* (2014) is a “constraining macroscopic measure of the low temperature, alkylperoxy radical dominated kinetic reactivity of large paraffinic fuels” which, in association with derived cetane number (DCN), provide an insight into the ignition propensity of fuel samples. However, these parameters were explored by Won *et al.* using pure aliphatic fuels and surrogates. Further studies are necessary to include the antagonistic effect of aromatic species into similar targets.

The second part of the investigation comprised an experimental and computational study of the low temperature reactivity and thermal ignition of jet fuel surrogates. The experiments, employing both rapid compression machine and shock tube facilities, were conducted at the Combustion Chemistry Centre (C3) at the National University of Ireland, Galway. The surrogates investigated were a literature jet fuel surrogate (MURI 1) and a lighter version of MURI 1 called surrogate TRF, which is similar to a low-octane gasoline. The experimental conditions spanned temperatures between 650 to 1300 K, equivalence ratios of 0.5 and 1.0, and pressure of 15 bar.

For the MURI 1 experiments, both stoichiometric and lean data presented a two-stage ignition behavior, a feature that the original MURI data in RCM, taken at compressed pressure of 22 bar and reported by Dooley *et al.* (2010), did not show. Regarding the overall pressure-time histories, at stoichiometric conditions the interval between first stage and total ignition was much shorter, under 5 ms, than for the lean cases, over 15 ms. Also noteworthy was that the pressure increase due to the main ignition event was quite significant for stoichiometric conditions, which was not the case for lean mixtures, where both first stage and main ignition pressure increases were small.

Also, the RCM data showed a marked difference in reactivity between stoichiometric and lean cases, with the latter being around three times longer. The original MURI RCM data followed a similar trend, with their data taken at pressures 50 % higher being around half as long as our results. However, the equivalence ratio effect was not observable in our shock tube data, which was quite similar for both series of measurements. Comparison with original MURI data, taken at slightly higher pressures, showed a similar behavior close to the end of

the NTC regime, around 900 K, but at higher temperatures the present data was significantly slower.

For RCM modeling with MURI 1 mechanism, one can notice that under both equivalence ratio conditions the mechanism was able to reproduce the trend of decreasing ignition delay around 50% with a temperature increase of 15–25 K in the low temperature region. Also, the computed first-stage pressure rises were higher than the experimental ones, as noted by Mittal *et al.* (2010). The stoichiometric calculations were able to show a brief first-stage ignition which was promptly followed by the hot ignition event while the lean equivalence ratio calculations reproduced quite well the interval between first-stage and overall ignition. In terms of ignition delay agreement the mechanism was around a factor-of-two slower than the experiments, as Dooley and coauthors reported originally.

Comparisons of both RCM and ST measurements with original MURI data revealed that RCM data showed a similar trend i.e. the computed ignition delays were consistently longer than the measurements. However, while this behavior was also presented in the original shock tube study, here the model actually reproduced the experimental ST data for temperatures close to 1125 K at both stoichiometric and lean conditions. The main disagreement occurred at temperatures between 875–1000 K, where, for example, the IDT for a lean experiment at 950 K was overestimated by a factor-of-three.

Regarding RCM experiments with surrogate TRF, one can notice that stoichiometric TRF pressure histories exhibited a much sharper pressure peak during the ignition event when compared to stoichiometric MURI data. This difference occurs due to the composition of each surrogate, hence the total amount of fuel, and their rate of consumption up to the main ignition event. Also noticeable was the occurrence of a small pre-ignition event, especially above 675 K, instead of a clear first-stage ignition. Considering data from both facilities, the equivalence ratio effect was very clear on the RCM experiments, with lean ignition delays being around twice as long as stoichiometric ones for temperatures below 675 K, with the difference increasing with temperature as the lean mixtures approach a plateau of reactivity associated with NTC phenomena. The shock tube data was also similar to the MURI data, with the stoichiometric mixture showing slightly shorter ignition delays.

Computations of the TRF data were performed with two detailed

chemical kinetics models: an alcohol-containing gasoline model developed at LabCET (CANCINO, 2009) and an unpublished mechanism by C3 - NUI Galway. For stoichiometric RCM data both mechanisms were able to produce a short first-stage ignition promptly followed by the hot ignition event thus reproducing the overall behavior of the experimental pressure history, with the NUIG model yielding shorter ignition delay times than Cancino's. For lean equivalence ratio  $\phi=0.5$ , both models produced a pressure plateau between first-stage and overall ignition similar to the experiment but slightly shorter, which is likely due to the overestimation of the first-stage pressure rise previously pointed out by Mittal *et al.* (2010). For these lean conditions the overestimation of IDT was lower than for stoichiometric cases, with the models actually reproducing the ignition delay at 750 K.

Simulations of both RCM and ST data at stoichiometric condition showed that the best agreement occurs for temperatures of 720–770 K, with ignition delay times below this range being overpredicted. Regarding the intermediate and high temperature conditions both mechanisms follow the experiments closely, with the NUIG model showing a slightly better agreement with its slower predictions. For the lean equivalence ratio computations, one can notice trends similar to those of stoichiometric data. For low temperature the best agreement occurs around 750 K with modest overestimation of IDT happening at lower temperatures. Given the availability of pressure-time histories above 750 K, i.e. in the NTC region, it was possible to note that the Cancino model showed a plateau of reactivity when simulated under RCM conditions while for NUIG's mechanism the predictions showed a clear NTC behavior. For the high temperature data the mechanism of Cancino showed strong agreement between 1000–1125 K, with an overall good agreement for both mechanisms.

In order to elucidate which elementary reactions were governing the predictions of these two mechanisms for TRF, a sensitivity analysis was performed at the RCM condition at which both models yield the same overall ignition delay time, i.e., lean equivalence ratio  $\phi=0.5$  and compressed temperature of 750 K. The normalized sensitivity coefficients computed by CHEMKIN-PRO were analyzed at five time-steps along the ignition delay interval for seventeen/eighteen species in Cancino/NUIG model. The obtained coefficients suggests that, for NUIG's model, the autoignition of this surrogate mixture is governed by two processes in different moments during the induction time. At first the

reactivity is controlled by the rate of  $O_2$  additions to alkyl radicals; and later on there is a competition between OH-production and consumption: the decomposition of  $CH_3O_2H$  into methoxy radical and OH combined with the decomposition of  $H_2O_2$  into two OH; and the radical scavenging role of benzyl radical. For the mechanism of Cancino the reactions determining overall reactivity are internal H-abstractions  $RO_2 \rightleftharpoons QOOH$ , followed by the competition between  $H_2O_2$  decomposition and its reaction with molecular oxygen yielding two  $HO_2$ .

In summary, this autoignition study is, to the author's knowledge, the first time that these measurements and simulations have been performed for Brazilian Jet A-1 aviation fuel. The accompanying experiments and simulations with fuel surrogates provided further insights regarding the occurrence of negative temperature coefficient behavior and two-stage ignition phenomena of jet fuel surrogates. The sensitivity analysis showed that reactivity-governing reactions for ignition at intermediate temperatures are those involving alkyl peroxy radicals  $RO_2$ , hydroperoxyalkyl radicals  $QOOH$ , formaldehyde  $CH_2O$  as well as the core H/O species OH and  $H_2O_2$ .

## 6.1 RECOMMENDATIONS

The present investigation was limited by the low vapor pressure of the heavier fractions of jet fuel as well as that of fuel relevant hydrocarbons like n-dodecane, n-butylbenzene and  $\alpha$ -methylnaphthalene. Oxidation studies of these molecules are quite difficult with batch-based mixture preparation due to the high preheating temperatures necessary to ensure that no condensation occurs on the tank, gas lines and experiment. Continuous flow facilities like the perfectly stirred reactor and pressurized flow reactor provide a somewhat easier approach to the evaporation issue, with the use of heated carrier gas, usually nitrogen, and by employing a syringe pump to meter the fuel.

Further experimental and theoretical investigations of aromatic species heavier than toluene are crucial to improve their chemical kinetics submodel. Hydrocarbons like 1,2,4-trimethylbenzene and n-butylbenzene have substituents that allow the formation of strain-favored transition states for  $RO_2 \rightleftharpoons QOOH$  isomerizations, which contribute to intermediate temperature reactivity. Also important to the formulation of more suitable fuel surrogates is a better characteriza-

tion of real fuel samples by ASTM standards, gas chromatography and mass spectroscopy. Further information regarding the linear, branched or cyclic nature of the alkanes as well as the aromatics' substituents can provide clearer targets regarding fuel's H/C and CH<sub>2</sub>/CH<sub>3</sub> ratios.

## BIBLIOGRAPHY

- ACHTEN, W. M. J.; VERCHOT, L.; FRANKEN, Y. J.; MATHIJS, E.; SINGH, V. P.; AERTS, R.; MUYS, B. Jatropha bio-diesel production and use. **Biomass and Bioenergy**, v. 32, p. 1063–1084, 2008.
- AFFLECK, W.; THOMAS, A. An opposed piston rapid compression machine for preflame reaction studies. **Proceedings of the Institution of Mechanical Engineers**, v. 183, p. 365–387, 1968.
- ALLEN, C.; TOULSON, E.; EDWARDS, T.; LEE, T. Application of a novel charge preparation approach to test the autoignition characteristics of JP-8 and camelina hydroprocessed renewable jet fuel in a rapid compression machine. **Combustion and Flame**, v. 159, p. 2780–2788, 2012.
- ANDERSON, B.; BEYERSDORF, A.; HUDGINS, C.; PLANT, J.; THORNHILL, K.; WINSTEAD, E. **Alternative Aviation Fuel Experiment (AAFEX)**. Hampton, Virginia, 2011.
- ANDRAE, J.; BJÖRNBOM, P.; CRACKNELL, R.; KALGHATGI, G. Autoignition of toluene reference fuels at high pressures modeled with detailed chemical kinetics. **Combustion and Flame**, v. 149, p. 2–24, 2007.
- ANDRAE, J.; HEAD, R. HCCI experiments with gasoline surrogate fuels modeled by a semidetailed chemical kinetic model. **Combustion and Flame**, v. 156, n. 4, p. 842–851, 2009.
- ANDRAE, J. C.; BRINCK, T.; KALGHATGI, G. T. HCCI experiments with toluene reference fuels modeled by a semidetailed chemical kinetic model. **Combustion and Flame**, v. 155, n. 4, p. 696–712, 2008.
- BATTIN-LECLERC, F. Detailed chemical kinetic models for the low-temperature combustion of hydrocarbons with application to gasoline and diesel fuel surrogates. **Progress in Energy and Combustion Science**, v. 34, p. 440–498, 2008.
- BLAKEY, S.; RYE, L.; WILSON, C. W. Aviation gas turbine alternative fuels: A review. **Proceedings of the Combustion Institute**, v. 33, p. 2863–2885, 2011.

- BOWDEN, J. N.; ERWIN, J. **Investigation of sources, properties, and preparation of distillate test fuels - NASA CR-168227.** Cleveland, Ohio, 1983.
- BUDIN, J. T.; BREENE, W. M.; PUTNAM, D. H. Some compositional properties of camelina (*Camelina sativa* L. Crantz) seeds and oils. **Journal of the American Oil Chemists Society**, v. 72, p. 309–315, 1995.
- CAMPBELL, M. F.; PARISE, T.; TULGESTKE, A. M.; SPEARRIN, R. M.; DAVIDSON, D. F.; HANSON, R. K. Strategies for obtaining long constant-pressure test times in shock tubes. **Shock Waves**, v. 25, n. 6, p. 651–665, 2015.
- CANCINO, L.; FIKRI, M.; OLIVEIRA, A.; SCHULZ, C. Thermal oxidation of ethanol: experimental and numerical analysis of ignition chemistry of ethanol–air mixtures in shock-heated gases. In: **Twenty Seventh International Symposium in Shock Waves.** Saint Petersburg, Russia: International Shock Wave Institute, 2009. v. 27, n. 1, p. 300–306.
- CANCINO, L.; FIKRI, M.; OLIVEIRA, A.; SCHULZ, C. Ignition delay times of ethanol-containing multi-component gasoline surrogates: Shock-tube experiments and detailed modeling. **Fuel**, v. 90, p. 1238–1244, 2011.
- CANCINO, L. R. **Development and application of detailed chemical kinetics mechanism for ethanol and ethanol-containing hydrocarbon fuels.** Florianópolis, Santa Catarina: Doctoral thesis, 2009.
- CHEVRON. **Alternative Jet Fuels, Addendum 1 to Aviation Fuels Technical Review (FTR-3/A1).** Houston, Texas, 2006.
- CHEVRON. **Aviation Fuels Technical Review (FTR-3).** Houston, Texas, 2006.
- COIMBRA, M. C.; JORGE, N. Characterization of the pulp and kernel oils from *Syagrus oleracea*, *Syagrus romanzoffiana*, and *Acrocomia aculeata*. **Journal of Food Science**, v. 76, n. 8, 2011.

- COLKET, M.; EDWARDS, T.; CERNANSKY, N.; DRYER, F.; EGOLFOPOULOS, F.; FRIEND, D. Development of an experimental database and kinetic models for surrogate jet fuels. In: **45th AIAA Aerospace Sciences Meeting and Exhibit**. Reno, Nevada: American Institute of Aeronautics and Astronautics, 2007.
- CORPORAN, E.; DEWITT, M. J.; BELOVICH, V.; PAWLIK, R.; LYNCH, A. C.; GORD, J. R.; MEYER, T. R. Emissions characteristics of a turbine engine and research combustor burning a Fischer-Tropsch jet fuel. **Energy & Fuels**, v. 21, p. 2615–2626, 2007.
- CORPORAN, E.; EDWARDS, T.; SHAFER, L.; DEWITT, M. J.; KLINGSHIRN, C.; ZABARNICK, S. Chemical, thermal stability, seal swell, and emissions studies of alternative jet fuels. **Energy & Fuels**, v. 25, p. 955–966, 2011.
- CURRAN, H. J.; PITZ, W.; WESTBROOK, C.; CALLAHAN, G.; DRYER, F. Oxidation of automotive primary reference fuels at elevated pressures. **Proceedings of the Combustion Institute**, v. 27, n. 1, p. 379–387, 1998.
- DAGAUT, P.; CATHONNET, M. The ignition, oxidation, and combustion of kerosene: a review of experimental and kinetic modeling. **Progress in Energy and Combustion Science**, v. 32, p. 48–92, 2006.
- DAGAUT, P.; KARSENTY, F.; DAYMA, G.; DIÉVART, P.; HADJALI, K.; MZÉ-AHMED, A.; BRAUN-UNKHOFF, M.; HERZLER, J.; KATHROTIA, T.; KICK, T.; NAUMANN, C.; RIEDEL, U.; THOMAS, L. Experimental and detailed kinetic model for the oxidation of a Gas to Liquid (GtL) jet fuel. **Combustion and Flame**, v. 161, p. 835–847, 2014.
- DATTARAJAN, S.; PARK, O.; FISHER, E. M.; GOULDIN, F. C.; BOZZELLI, J. W. Subatmospheric extinction of opposed jet diffusion flames of jet fuel and its surrogates. In: **47th AIAA Aerospace Science Meeting including The New Horizons Forum and Aerospace Exposition**. Orlando, Florida: AIAA - American Institute of Aeronautics and Astronautics, 2009.
- DE TONI, A.; WERLER, M.; HARTMANN, R.; CANCINO, L.; SCHLESSEL, R.; FIKRI, M.; SCHULZ, C.; OLIVEIRA, A.; OLIVEIRA,

- E.; ROCHA, M. Ignition delay times of Jet A-1 fuel: Measurements in a high-pressure shock tube and a rapid compression machine. **Proceedings of the Combustion Institute**, v. 36, n. 3, p. 3695 – 3703, 2017.
- DEWITT, M. J.; CORPORAN, E.; GRAHAM, J.; MINUS, D. Effects of aromatic type and concentration in Fischer-Tropsch fuel on emissions production and material compatibility. **Energy & Fuels**, v. 22, p. 2411–2418, 2008.
- DOOLEY, S.; WON, S. H.; CHAOS, M.; HEYNE, J.; JU, Y.; DRYER, F. L. A jet fuel surrogate formulated by real fuel properties. **Combustion and Flame**, v. 157, p. 2333–2339, 2010.
- DOOLEY, S.; WON, S. H.; HEYNE, J.; FAROUK, T. I.; JU, Y.; DRYER, F. L. The experimental evaluation of a methodology for surrogate fuel formulation to emulate gas phase combustion kinetic phenomena. **Combustion and Flame**, v. 159, p. 1444–1466, 2012.
- DOOLEY, S.; WON, S. H.; JAHANGIRIAN, S.; JU, Y.; DRYER, F. L.; WANG, H.; OEHLSCHLAEGER, M. A. The combustion kinetics of a synthetic paraffinic jet aviation fuel and a fundamentally formulated, experimentally validated surrogate fuel. **Combustion and Flame**, v. 159, p. 3014–3020, 2012.
- DRY, M. E. The Fischer-Tropsch process: 1950–2000. **Catalysis Today**, v. 71, p. 227–241, 2002.
- DRYER, F. L.; JU, Y.; SUNG, C.-J.; BREZINSKY, K.; SANTORO, R. J.; LITZINGER, T. A. **Generation of Comprehensive Surrogate Kinetic Models and Validation Databases for Simulating Large Molecular Weight Hydrocarbon Fuels - MURI Final Report AFRL-OSR-VA-TR-2012-1159**. Arlington, Virginia, 2012.
- EDWARDS, T. Liquid fuels and propellants for aerospace propulsion: 1903-2003. **Journal of Propulsion and Power**, v. 19, p. 1089–1107, 2003.
- EDWARDS, T.; MOSES, C.; DRYER, F. Evaluation of combustion performance of alternative aviation fuels. In: **46th AIAA/ASME/SAE/ASEE Joint Propulsion Conferences**.

- Nashville, Tennessee: American Institute of Aeronautics and Astronautics, 2010.
- EXXON MOBIL. World Jet Fuel Specifications with Avgas Supplement.** Leatherhead, United Kingdom, 2005.
- FARRELL, J. T.; CERNANSKY, N. P.; DRYER, F. L.; FRIEND, D. G.; HERGART, C. A.; LAW, C. K. Development of an experimental database and kinetic models for surrogate diesel fuels. In: **2007 SAE World Congress**. Detroit, Michigan: SAE International, 2007.
- GRAHAM, J. L.; STRIEBICH, R. C.; MYERS, K. J.; MINUS, D. K.; HARRISON III, W. E. Swelling of nitrile rubber by selected aromatics blended in an synthetic jet fuel. **Energy & Fuels**, v. 20, p. 759–765, 2006.
- GRIFFITHS, J. F. Reduced kinetic models and their application to practical combustion systems. **Progress in Energy and Combustion Science**, n. 21, p. 25–107, 1995.
- GUNSTON, B. **World Encyclopaedia of Aero Engines**. New York: Harpercollins, 1989. 192 p.
- GUNSTON, B. (Ed.). **Jane's Fighting Aircraft of World War II**. Westoning: Military Press, 1994. 318 p.
- HEALY, D.; CURRAN, H.; SIMMIE, J.; KALITAN, D.; ZINNER, C.; BARRETT, A.; PETERSEN, E.; BOURQUE, G. Methane/ethane/propane mixture oxidation at high pressures and at high, intermediate and low temperatures. **Combustion and flame**, v. 155, n. 3, p. 441–448, 2008.
- HIPPLER, H.; TROE, J.; WILLNER, J. Shock wave study of the reaction  $\text{HO}_2 + \text{HO}_2 \rightarrow \text{H}_2\text{O}_2 + \text{O}_2$ : Confirmation of rate constant minimum near 700 K. **The Journal of Chemical Physics**, v. 93, n. 3, p. 1755–1760, 1990.
- HOLLEY, A.; DONG, Y.; ANDAC, M.; EGOLFOPOULOS, F. N. Extinction of premixed flames of practical liquid fuels: Experiments and simulations. **Combustion and Flame**, v. 144, p. 448–460, 2006.

- HONG, T. D.; SOERAWIDJAJA, T. H.; REKSOWARDOJO, I. K.; FUJITA, O.; DUNIANI, Z.; PHAM, M. X. A study on developing aviation biofuel for the Tropics: Production process - Experimental and theoretical evaluation of their blends with fossil kerosene. **Chemical Engineering and Processing: Process Intensification**, v. 74, p. 124–130, 2013.
- HONNET, S.; SESHADRI, K.; NIEMANN, U.; PETERS, N. A surrogate fuel for kerosene. **Proceedings of the Combustion Institute**, v. 32, p. 485–492, 2009.
- HUBER, G. W.; IBORRA, S.; CORMA, A. Synthesis of transportation fuels from biomass: chemistry, catalysts, and engineering. **Chemical Reviews**, v. 106, p. 4044–4098, 2006.
- HUI, X.; KUMAR, K.; SUNG, C. J.; EDWARDS, T.; GARDNER, D. Experimental studies on the combustion characteristics of alternative jet fuels. **Fuel**, v. 98, p. 176–182, 2012.
- HUI, X.; SUNG, C. J. Laminar flame speeds of transportation-relevant hydrocarbon and jet fuels at elevated temperatures and pressures. **Fuel**, v. 109, p. 191–200, 2013.
- HUMER, S.; FRASSOLDATI, A.; GRANATA, S.; FARAVELLI, T.; RANZI, E.; SEISER, R.; SESHADRI, K. Experimental and kinetic modeling study of combustion of JP-8, its surrogates and reference components in laminar nonpremixed flows. **Proceedings of the Combustion Institute**, v. 31, p. 393–400, 2007.
- IATA. **IATA 2015 Report on Alternative Fuels - 10th Edition**. Geneva, Switzerland, 2016.
- JAHANGIRIAN, S.; MCENALLY, C. S.; GOMEZ, A. Experimental study of ethylene counterflow diffusion flames perturbed by trace amounts of jet fuel and jet fuel surrogates under incipiently sooting conditions. **Combustion and Flame**, v. 156, p. 1799–1809, 2009.
- KATTA, V. R.; NEWMAN-LEHMAN, T.; SESHADRI, K.; ZELINA, J.; ROQUEMORE, W. M. Performance of JP-8 surrogate models in predicting laboratory jet flames. In: **48th AIAA Aerospace Sciences Meeting including The New Horizons Forum and Aerospace Exposition**. Orlando, Florida: AIAA - American Institute of Aeronautics and Astronautics, 2010.

- KATTA, V. R.; NEWMAN-LEHMAN, T.; SESHADRI, K.; ROQUE-MORE, W. M. Lean blowout limits for JP-8 surrogates and their parent components. In: **49th AIAA Aerospace Sciences Meeting including the New Horizons Forum and Aerospace Exposition**. Orlando, Florida: AIAA - American Institute of Aeronautics and Astronautics, 2011.
- KAZAKOV, A.; CHAOS, M.; ZHAO, Z.; DRYER, F. Computational singular perturbation analysis of two-stage ignition of large hydrocarbons. **Journal of Physical Chemistry A**, v. 110, p. 7003–7009, 2006.
- KICK, T.; HERBST, J.; KATHROTIA, T.; MARQUETAND, J.; BRAUN-UNKHOFF, M.; NAUMANN, C.; RIEDEL, U. An experimental and modeling study of burning velocities of possible future synthetic jet fuels. **Energy**, v. 43, p. 111–123, 2012.
- KIM, D.; MARTZ, J.; VIOLI, A. A surrogate for emulating the physical and chemical properties of conventional jet fuel. **Combustion and Flame**, v. 161, p. 1489–1498, 2014.
- KUKKADAPU, G.; KUMAR, K.; SUNG, C.-J.; MEHL, M.; PITZ, W. J. Autoignition of gasoline and its surrogates in a rapid compression machine. **Proceedings of the Combustion Institute**, v. 34, n. 1, p. 345–352, 2013.
- KUMAR, K.; SUNG, C. J. A comparative experimental study of the autoignition characteristics of alternative and conventional jet fuel/oxidizer mixtures. **Fuel**, v. 89, p. 2853–2863, 2010.
- KUMAR, K.; SUNG, C. J. An experimental study of the autoignition characteristics of conventional jet fuel/oxidizer mixtures: Jet-A and JP-8. **Combustion and Flame**, v. 157, p. 676–685, 2010.
- KUMAR, K.; SUNG, C. J.; HUI, X. Laminar flame speeds and extinction limits of conventional and alternative jet fuels. **Fuel**, v. 90, p. 1004–1011, 2011.
- LASKIN, A.; WANG, H.; LAW, C. K. Detailed kinetic modeling of 1, 3-butadiene oxidation at high temperatures. **International Journal of Chemical Kinetics**, v. 32, n. 10, p. 589–614, 2000.

- LI, J.; ZHAO, Z.; KAZAKOV, A.; CHAOS, M.; DRYER, F. L.; SCIRE, J. J. A comprehensive kinetic mechanism for CO, CH<sub>2</sub>O, and CH<sub>3</sub>OH combustion. **International Journal of Chemical Kinetics**, v. 39, n. 3, p. 109–136, 2007.
- LIU, Y. C.; SAVAS, A. J.; AVEDISIAN, C. T. The spherically symmetric droplet burning characteristics of Jet-A and biofuels derived from camelina and tallow. **Fuel**, v. 108, p. 824–832, 2013.
- LIU, Y. C.; SAVAS, A. J.; AVEDISIAN, C. T. Spherically symmetric droplet combustion of three and four component miscible mixtures as surrogates for Jet-A. **Proceedings of the Combustion Institute**, v. 34, p. 1569–1576, 2013.
- LOHMANN, R.; JEROSZKO, R. **Broad Specification Fuels Technology Program Phase I - NASA CR-168180**. Cleveland, Ohio, 1983.
- LUMSDEN, A. **British Piston Aero Engines and Their Aircraft**. Marlborough: The Crowood Press, 2005. 336 p.
- MALEWICKI, T.; GUDIYELLA, S.; BREZINSKY, K. Experimental and modeling study on the oxidation of Jet-A and the n-dodecane/ iso-octane/ n-propylbenzene/ 1,3,5-trimethylbenzene surrogate fuel. **Combustion and Flame**, v. 160, p. 17–30, 2013.
- MAURICE, L. Q.; LANDER, H.; EDWARDS, T.; HARRISON III, W. E. Advanced aviation fuels: a look ahead via a historical perspective. **Fuel**, v. 80, p. 747–756, 2001.
- MEEKS, E.; NAIK, C.; PUDUPPAKKAM, K.; MODAK, A.; EGOLFOPOULOS, F.; TSOTSIS, T.; WESTBROOK, C. **Experimental and modeling studies of the combustion characteristics of conventional and alternative jet fuels - NASA CR-216356**. Cleveland, Ohio, 2011.
- METCALFE, W. K.; PITZ, W. J.; CURRAN, H. J.; SIMMIE, J. M.; WESTBROOK, C. K. The development of a detailed chemical kinetic mechanism for diisobutylene and comparison to shock tube ignition times. **Proceedings of the Combustion Institute**, v. 31, n. 1, p. 377–384, 2007.

- MÉVEL, R.; BOETTCHER, P.; SHEPHERD, J. Absorption cross section at 3.39  $\mu\text{m}$  of alkanes, aromatics and substituted hydrocarbons. **Chemical Physics Letters**, Elsevier, v. 531, p. 22–27, 2012.
- MINISTRY OF DEFENCE. **Defence Standard 91-91 Issue 7 Amendment 2 Turbine Fuel, Kerosine Type, Jet A-1 NATO Code: F-35 Joint Service Designation: AVTUR**. Bristol, United Kingdom, 2012.
- MITTAL, G.; RAJU, M. P.; SUNG, C.-J. CFD modeling of two-stage ignition in a rapid compression machine: Assessment of zero-dimensional approach. **Combustion and Flame**, v. 157, n. 7, p. 1316–1324, 2010.
- MORGAN, N.; SMALLBONE, A.; BHAVE, A.; KRAFT, M.; CRACKNELL, R.; KALGHATGI, G. Mapping surrogate gasoline compositions into RON/MON space. **Combustion and Flame**, v. 157, p. 1122–1131, 2010.
- MORLEY, C. **Gaseq, Version 0.76**. 2004. Disponível em: <<http://www.gaseq.co.uk>>.
- MOSES, C. A. **Comparative Evaluation of Semi-Synthetic Jet Fuels**. Alpharetta, Georgia, 2008. 49 p.
- MZÉ-AHMED, A.; HADJ-ALI, K.; DIÉVART, P.; DAGAUT, P. Kinetics of oxidation of a synthetic jet fuel in a jet-stirred reactor: experimental and modeling study. **Energy & Fuels**, v. 24, p. 4904–4911, 2010.
- NATELSON, R. H.; JOHNSON, R. O.; KURMAN, M. S.; CERNANSKY, N. P.; MILLER, D. L. Comparison of reactivity in a flow reactor and a single cylinder engine. **Experimental Thermal and Fluid Science**, v. 34, p. 928–932, 2010.
- NATELSON, R. H.; KURMAN, M. S.; CERNANSKY, N. P.; MILLER, D. L. Experimental investigation of surrogates for jet and diesel fuels. **Fuel**, v. 87, p. 2339–2342, 2008.
- OEHLSCHLAEGER, M. A.; STEINBERG, J.; WESTBROOK, C. K.; PITZ, W. J. The autoignition of iso-cetane at high to moderate temperatures and elevated pressure: Shock tube experiments and

- kinetic modeling. **Combustion and Flame**, v. 156, p. 2165–2172, 2009.
- OERTEL, H. **Stossrohre. Theorie, Praxis, Anwendungen**. New York: Wien, Springer-Verlag, 1966. 1030 p.
- PALMER, H. B.; KNOX, B. E. Contact surface tailoring in a chemical shock tube. **ARS Journal**, v. 31, p. 826–828, 1961.
- PITZ, W. J.; CERNANSKY, N. P.; DRYER, F. L.; EGOLFOPOULOS, F. N.; FARRELL, J. T.; FRIEND, D. G.; PITTSCH, H. Development of an experimental database and chemical kinetic models for surrogate gasoline fuels. In: **2007 SAE World Congress**. Detroit, Michigan: SAE International, 2007.
- REACTION DESIGN. **CHEMKIN-PRO 15083**. San Diego: Reaction Design, 2009.
- RENNINGER, N.; MCPHEE, D. **Fuel compositions comprising farnesane and farnesane derivatives and method of making and using same**. 2010. US Patent 7,846,222.
- ROSFJORD, T. **Aviation-Fuel Property Effects on Combustion - NASA CR-168334**. Cleveland, Ohio, 1984.
- SHAFER, L. M.; STRIEBICH, R. C.; GOMACH, J.; EDWARDS, T. Chemical class composition of commercial jet fuels and other specialty kerosene fuels. In: **14th AIAA/AHI Space Planes and Hypersonic Systems and Technologies Conference**. Canberra, Australia: AIAA - American Institute of Aeronautics and Astronautics, 2006.
- SIVARAMAKRISHNAN, R.; TRANTER, R. S.; BREZINSKY, K. A high pressure model for the oxidation of toluene. **Proceedings of the Combustion Institute**, v. 30, n. 1, p. 1165–1173, 2005.
- SMALLBONE, A. J.; MORGAN, N.; BHAVE, A.; KRAFT, M.; CRACKNELL, R. F.; KALGHATGI, G. Simulating combustion of practical fuels and blends for modern engine applications using detailed chemical kinetics. In: **2010 SAE World Congress**. Detroit, Michigan: SAE International, 2010.

- STARIK, A. M.; TITOVA, N. S.; TOROKHOV, S. A. Kinetics of Oxidation and Combustion of Complex Hydrocarbon Fuel: Aviation Kerosene. **Combustion, Explosion, and Shock Waves**, v. 49, p. 392–408, 2013.
- SUNG, C.-J.; CURRAN, H. J. Using rapid compression machines for chemical kinetics studies. **Progress in Energy and Combustion Science**, v. 44, p. 1–18, 2014.
- TSANG, W.; HUDGENS, J. W.; ALLISON, T. C.; BURGESS, JR., D. R.; MANION, J. A.; MATHEU, D. M. **Workshop on Combustion Simulation Databases for Real Transportation Fuels - NISTIR 7155**. Gaithersburg, Maryland, 2003.
- VALCO, D.; GENTZ, G.; ALLEN, C.; COLKET, M.; EDWARDS, T.; GOWDAGIRI, S.; OEHLSCHLAEGER, M. A.; TOULSON, E.; LEE, T. Autoignition behavior of synthetic alternative jet fuels: An examination of chemical composition effects on ignition delays at low to intermediate temperatures. **Proceedings of the Combustion Institute**, v. 35, n. 3, p. 2983 – 2991, 2015.
- VASU, S. S.; DAVIDSON, D. F.; HANSON, R. K. Jet fuel ignition delay times: Shock tube experiments over wide conditions and surrogate model predictions. **Combustion and Flame**, v. 152, p. 125–143, 2008.
- VASU, S. S.; DAVIDSON, D. F.; HANSON, R. K. High-pressure shock tube experiments and modeling of n-dodecane/air ignition. In: **Shock Waves - 26th International Symposium on Shock Waves**. Göttingen, Lower Saxony: Springer Berlin Heidelberg, 2009. v. 1, p. 293–298.
- WANG, H.; OEHLSCHLAEGER, M. A. Autoignition studies of conventional and fischer-tropsch jet fuels. **Fuel**, v. 98, p. 249–258, 2012.
- WESTBROOK, C. K. Chemical kinetics of hydrocarbon ignition in practical combustion system. **Proceedings of the Combustion Institute**, v. 28, p. 1563–1577, 2000.
- WON, S. H.; DOOLEY, S.; DRYER, F. L.; JU, Y. Radical index on extinction limits of diffusion flames for large hydrocarbon fuels. In: **49th AIAA Aerospace Sciences Meeting including the New**

- Horizons Forum and Aerospace Exposition.** Orlando, Florida: AIAA - American Institute of Aeronautics and Astronautics, 2011.
- WON, S. H.; DOOLEY, S.; DRYER, F. L.; JU, Y. A radical index for the determination of the chemical kinetic contribution to diffusion flame extinction of large hydrocarbon fuels. **Combustion and Flame**, v. 159, p. 541–551, 2012.
- WON, S. H.; DOOLEY, S.; VELOO, P. S.; WANG, H.; OEHLSCHLA-GER, M. A.; DRYER, F. L.; JU, Y. The combustion properties of 2,6,10-trimethyl dodecane and a chemical functional group analysis. **Combustion and Flame**, v. 161, p. 826–834, 2014.
- WON, S. H.; VELOO, P. S.; SANTNER, J.; JU, Y.; DRYER, F. L. Comparative evaluation of global combustion properties of alternative jet fuels. In: **51st AIAA Aerospace Sciences Meeting including the New Horizons Forum and Aerospace Exposition.** Grapevine, Texas: AIAA - American Institute of Aeronautics and Astronautics, 2013.
- WOOD, C.; MCDONNELL, V.; SMITH, R.; SAMUELSON, G. Development and application of a surrogate distillate fuel. **Journal of Propulsion and Power**, v. 5, p. 399–405, 1989.
- YETTER, R.; DRYER, F.; RABITZ, H. Some interpretive aspects of elementary sensitivity gradients in combustion kinetics modeling. **Combustion and Flame**, v. 59, n. 2, p. 107–133, 1985.
- ZHANG, K.; BANYON, C.; BUGLER, J.; CURRAN, H. J.; RODRIGUEZ, A.; HERBINET, O.; BATTIN-LECLERC, F.; B'CHIR, C.; HEUFER, K. A. An updated experimental and kinetic modeling study of n-heptane oxidation. **Combustion and Flame**, v. 172, p. 116–135, 2016.
- ZHAO, Z.; CHAOS, M.; KAZAKOV, A.; DRYER, F. L. Thermal decomposition reaction and a comprehensive kinetic model of dimethyl ether. **International Journal of Chemical Kinetics**, v. 40, n. 1, p. 1–18, 2008.

## APPENDIX A – FUNDAMENTALS OF SENSITIVITY ANALYSIS

The main purpose of the sensitivity analysis is to determine the local performance of a system of equations when there is a perturbation in a selected parameter. In a kinetics context, the response of the system is examined when the Arrhenius parameters of the kinetics mechanism are changed, for a set of boundary conditions. The response is usually measured relative to the magnitude of the changes introduced. The magnitude of the sensitivity coefficient for a particular rate constant is related to the influence on the behavior of that particular reaction hence the sensitivity analysis represents a local analysis in a reactive system.

Consider the non-linear mass conservation equation (GRIFFITHS, 1995)

$$\frac{dc_i}{dt} = f_i(\mathbf{k}, \mathbf{c}) \quad \text{where } i = 1, \dots, N \quad (1)$$

where  $\mathbf{k}$  and  $\mathbf{c}$  are the rate coefficient and species concentration vectors, respectively, and  $N$  is the number of chemical species. In order to generate a solution for this equation it is necessary to specify the component values for the vector  $\mathbf{k}$ . The concentration vector  $\mathbf{c}$  is a function of the parameter vector as well as time,  $\mathbf{c}(\mathbf{k}, t)$ . A first order sensitivity coefficient with respect to species  $\mathbf{c}_i$  may be defined as

$$\frac{\delta c_i}{\delta k_j}(\mathbf{k}, t) = \frac{\mathbf{c}_i(k_j + \Delta k_j, t) - \mathbf{c}_i(k_j, t)}{\Delta k_j} \quad (2)$$

which represents the change in the species concentration  $\mathbf{c}_i$  at time  $t$  due to a change in the  $j^{\text{th}}$  rate parameter  $k_j$ . The gradient and its second order counterpart

$$\frac{(\delta^2 c_i)}{(\delta k_j)^2} \quad (3)$$

convey quantitative information about the solution in the vicinity of the operating point. The linearized response of the sensitivity with respect to time throughout the reaction data set is given by

$$\frac{d}{dt} \left[ \frac{\delta c_i}{\delta k_j} \right] = \sum_l \mathbf{J}_{il} \frac{\delta c_i}{\delta k_j} + \frac{\delta f_i}{\delta k_j} \quad (4)$$

in which  $\mathbf{J}_{il}$  is the Jacobian matrix defined as

$$\mathbf{J}_{il} = \frac{\delta f_i}{\delta c_l} \quad (5)$$

Equation (5) must be solved by numerical integration in order to obtain deviations in  $c_i(t)$  as a result of the changes in  $k$ . If the ordinary differential equations describing the species concentration as function of time are stiff, as is typically the case in combustion systems, then the sensitivity equations are likely to be computationally expensive to solve.

Once the sensitivity coefficients have been obtained they are usually normalized using the expression (YETTER *et al.*, 1985)

$$\omega_{ij} = \frac{\delta [\ln c_i(t)]}{\delta [\ln k_j]} \quad (6)$$

The magnitude of  $\omega_{ij}$  gives the relative importance of the  $j^{th}$  reaction in influencing the concentration of species  $i$  at time  $t$ . Setting each  $k_j$  to zero and calculating the corresponding sensitivities,  $\omega_{ij}$  indicates the significance of the  $j^{th}$  reaction. If all coefficients  $\omega_{ij}$  of the  $j^{th}$  reaction are very small then the  $j^{th}$  reaction may be regarded as unimportant. In the opposite case, if one or more normalized sensitivities are large then the  $j^{th}$  reaction is said to be “governing” or “determining” for the  $i^{th}$  species.

As mentioned before and also pointed out by Kazakov *et al.* (2006) this sensitivity analysis method computes time-dependent local sensitivity coefficients for either temperature or mass fraction of specific species, making the ignition analysis indirect since it consists in perturbing a particular rate coefficient and monitoring the change in the observable of interest.